Microscopic and Macroscopic Models for Pedestrian Crowds

Inauguraldissertation
zur Erlangung des akademischen Grades
eines Doktors der Naturwissenschaften
der Universität Mannheim

vorgelegt von

Msc.-Math. Juntima Makmul
aus Phetchaburi

Mannheim, 2016

Dekan: Professor Dr. Heinz Jürgen Müller, Universität Mannheim
Referent: Professor Dr. Simone Göttlich, Universität Mannheim
Korreferent: Professor Dr. Axel Klar, Technische Universität Kaiserslautern

Tag der mündlichen Prüfung: 12. April 2016

Abstract

This thesis is concerned with microscopic and macroscopic models for pedestrian crowds. In the first chapter, we consider pedestrians exit choices and model human behaviour in an evacuation process. Two microscopic models, discrete and continuous, are studied in this chapter. The former is a cellular automaton model and the latter is a social force model. Different numerical test cases are investigated and their results are compared.

In chapter 2, a hierarchy of models for pedestrian flows is derived. We examine a detailed microscopic social force model coupled to a local visibility model on the one hand and macroscopic models including the interaction forces and a local visibility term on the other hand. Particle methods are applied to solve these models. Numerical experiments are explored and compared on the microscopic as well as on the hydrodynamic and scalar models.

Zusammenfassung

Diese Arbeit befasst sich mit mikroskopischen und makroskopischen Modellen für Fuängermengen. Im ersten Kapitel betrachten wir die Wahl eines Gebäudeausganges von Personengruppen und modellieren menschliches Verhalten bei einem Evakuierungsprozess. Zwei mikroskopische Modelle, das diskrete und das kontinuierliche Modell, werden im zweiten Kapitel vorgestellt. Das erstgenannte ist ein netzförmiges Automaten-Modell und das letztgenannte ein soziale Kraft Modell. Verschiedene numerische Testfälle werden untersucht und ihre Resultate werden verglichen.

Im zweiten Kapitel wird eine Hierarchie der Modelle für Fuängermengen abgeleitet. Wir betrachten ein detailliertes, mikroskopisches soziale Kraft Modell verbunden mit einem lokalen Sichtbarkeitsmodell auf der einen Seite und makroskopische Modelle, die Interaktionskräfte und einen Sichtbarkeitsterm enthalten, auf der anderen Seite. Partikelmethoden werden angewandt, um diese Modelle zu lösen. Numerische Experimente werden untersucht und verglichen, sowohl im Hinblick auf die mikroskopischen als auch im Hinblick auf die hydrodynamischen und scalaren Modelle.

Acknowledgements

First of all, I would like to thank my supervisor Prof. Dr. Simone Göttlich who provided an interesting topic for research, encouraged me and gave me remarkable suggestions throughout my thesis.

I would also like to thanks to Prof. Dr. Axel Klar for being co-referee.

I would like to thank Peter Schillen for his helpful discussions and insightful comments during this research.

I am very grateful for the working environments provided by the Department of Mathematics at the University of Mannheim. I like to thank my colleagues and friends in the research group with whom I had a wonderful time.

Special thanks goes to Markus Guth for his persistent help and support.

I would like to express my gratitude to my parents and relatives in Thailand for their encouragement and support during this period.

Finally, I thank the Higher Educational Strategic Scholarships for Frontier Research Network (SFR) for the financial support and for the pursuit of this research work.

Contents

Introduction

In a world with an increasing number of people there are more and more events where huge crowds gather. Sport matches, public viewings, concerts but also religious meetings or trade fairs are only some examples for this development. It is hard to manage the arrival and the well-regulated departure of this massive groups of people. One of these public events was the love parade, that took place in many different german cities once a year until 2010. After a terrible accident at Duisburg in 2010, where 21 visitors died after too many people had arrived at the acess to the event field, the love parade was stopped for the following years. A better organization of the entrance of people to the event, for example by adding more entrance ways, could have prevented that accident.

Many other crowd disasters with even more victims can be traced more than 100 years in different coutries. The disasters due to the fires in the Ringtheater in Vienna in 1881 with several hundred fatalities is one example [76]. At the Troquois Theater in Chicago 500 people died in 1903. In 1979 there was a tragedy at the concert of The Who with 11 casualties [51]. The stampede in Baghdad in 2005 with 1011 casualties, the fire at the nightclub in Brazil in 2013, where more than 200 people died, and the accident in Shanghai on New Years Eve in 2014 with 36 dead and 42 injured pedestrians are further examples. Table 1 shows a list of the major crowd disasters in the recent years.

In awareness of the large number of crowd disasters, many researchers have payed attention in studying the movements and behaviors of individuals in a crowd, especially in evacuation scenarios. Many pedestrian evacuation models have been developed to help designers in planning public building with respect to issues of safety, evacuation and navigation. The models can provide a useful guidance of the location and the form of planned buildings. It is focused on the arrangement of walkways, entrances, exits, staircases, elevators, escalators, corridors and the shape of rooms.

Date	Place	Deaths	Injured	Reason
2013	Ivory Coast, Africa	62	62	Stampede at a New Year's Eve celebration
2013	Porto Alegre, Brazil	> 200	62	Fire at nightclub
2013	Allahabad, Indian	> 36	> 31	Overcrowding
2013	Hubei, China	4	14	Crush on a staircase
2013	Shanghai, China	-	7	Stampede over Beckham
2013	Madhya Pradesh, India	50	100	Stampede and drowning after jumping off a bride
2013	Anambra, Nigeria	28	200	Church stampede
2014	Ningxia, China	14	10	Stampede at a mosque
2014	Mumbai, India	18	40	Stampede ahead of spiritual leader Syedna's funeral
2014	Abuja, Nigeria	7	> 12	Stampede during a government recruitment drive
2014	DR Congo, Africa	14	8	Stampede during a tribute festival
2014	DR Congo, Africa	15	24	Stampede at football match
2014	Shanghai, China	35	> 40	Crush at Chinese city's riverfront

Table 1: List of major crowd disasters in 2013-2014: http://www.gkstill.com /CV/ExpertWitness/CrowdDisasters.html.

The development of pedestrians dynamic models has became an interesting area in many fields of study. Presently, there are numerous simulation methods, such as social force model [33, 34, 37, 39, 40, 41], optimal-velocity model [64, 65], magnetic force model [69], cellular automata models [3, 4, 10, 81, 86] and discrete choice model [6, 7, 73].

Pedestrian models can be classified into three types: Microscopic, mesoscopic and macroscopic descriptions. In the former, the individual characteristics, such as individual interactions, direction and speed are considered. Pedestrians' behaviour is affected by all kinds of interaction factors, such as surrounding environment or building structure. The microscopic model can be further categorized into the discrete model and the continuous model.

The cellular automaton model (CA model) as a part of the discrete model was first proposed by Neumann and Burks in 1940s [66] to study biological

reproduction and crytal growth. It is composed of discrete values in space, time and state. The following four main constituents play an important role in cellular automata models [59, 68]:

1. The physical environment: It specifies the simulation domain on which the CA is applied. The space is divided into a uniform lattice of cells with system size $m \times n$. Typically, these cells are all equal in size and made from regular polygons, such as triangular, rectangular or hexagonal grid. A hexagonal grid is an appropriate choice to represent a pedestrian and the arrangement of pedestrians is quite natural. The disadvantage of this grid is, that it is quite hard to implement. Furthermore, it is not able to represent straight walls appropriately. A rectangular grid is easy to implement and it suites to represent straight walls. A triangular grid is more flexible to apply for complex shapes of obstacles, but it is not good at representing a pedestrian and straight walls.

2. The cells' states: Each cell can be in a certain state that is abstracted from a finite set of possible states. Generally, an integer represents the number of distinct possible states of a cell. States in a cell could be empty cell, occupied by a pedestrian, obstacle cell or exit cell, for example.

3. The cells' neighborhoods: For each cell neighbouring cells are defined. In general we can define the neighbourhood of a cell in different ways, but the same definition need to be applied for all cells. The two most common types of neighborhoods are the Von-Neumann and the Moore neighborhoods.

4. A local transition rule: It is the rule or function that acts to a cell and its neighbourhood to change the cell's state from one discrete time step to another (system iteration). The rule is applied consequently to all cells in a parallel update or a sequential update. By employing a parallel update, all cells are treated equally and the moves of all pedestrians are done concurrently. Accordingly, conflicts may arise when two or more pedestrians want to move to the same target cell. This could be resolved by randomly choosing one pedestrian to move. The others have to stay in their old cells. In contrast, employing a sequential update, no conflict arises. Cells are updated sequentially with a fixed order or a random order. When a pedestrian choose a destination cell, he has to check if this cell has been reserved by another pedestrian within the same time step. If not, he can reserve that cell and move to it at the

end of the iteration. If the cell is already reserved, an alternative cell has to be chosen. Since all cells are treated unequally, the sequential update is not representing a classical cellular automaton.

Due to its simplication, the application field of cellular automata are very wide spread. They are used for example in biology [23], fluid [89], traffic flow [63] and pedestrian flow [88]. By modelling pedestrian crowds, this model can reproduce pedestrian collective phenomena, such as the clogging effect [90, 91], the lane formation [75], the oscillation at bottleneck [11, 75] and the faster is slower effect [3, 90, 91].

The social force model, as a part of the continuous model, is one of the most popular choice to model dynamic behaviour of pedestrians. This model which was introduced by Helbing describes the pedestrians' movements based on Newtonian mechanics. It produces realistic movements in simulations by taking the individual characteristics into account, such as desired speed, desired destination and physical interaction factors. This model can reproduce most of the observed pedestrian collective phenomena in nature, for example the lane formation [35, 40], the stripe formation [33], the oscillations at bottlenecks [35, 40], the temporary roundabout traffic at intersections [35, 40], the faster is slower effect [35], the clogging effect [35], the herding and ignorance of available exits [35, 41] and the freezing by heating [35, 36].

Considering the macroscopic description, the state of the system is described by locally averaged quantities, specifically density, velocity and energy. This approach that is usually applied to the case of large crowd deals with group behaviour and with the crowd as a whole. Detailed human behaviour and interactions are overlooked. The macroscopic model is less computationally intensive compared to the microscopic model, since it has less details in terms of interactions among individuals and among individuals with the environment. Classically, the macroscopic models can be obtained by conservation equations interrelated to mass, linear momentum and energy. They are usually represented by partial differential equations, where the initial and/or boundary value needs to be prescribed to obtain the solution. Examples of macroscopic models used for the pedestrian flow model can be found in [17, 38, 44, 87] for first order macroscopic models (or scalar models) and in [9, 49, 48] for second order macroscopic models.

In the mesoscopic description (or kinetic description), the state of the system is expressed by a suitable probability distribution over the microscopic state of the interacting entities. This approach was first applied to

human crowd motion by Henderson [43] and consequently extended by authors [20, 32]. The mesoscopic description is used when the state of system is still identified by position and velocity of the microscopic elements. Different models are obtained by modeling interactions among individuals in different ways: Localized binary interactions as for the Boltzmann equation and long range interaction in the case of the Vlasov equation. The evolution of the distribution function is generally presented by nonlinear intergro differential equation and the distribution function is defined by the statistical distribution of individuals' positions and velocities. The macroscopic equations can be derived from the kinetic model under appropriate integrability assumptions. We refer to the references [20, 29, 32] for pedestrian flow macroscopic models which are obtained from the kinetic models.

Chapter 1 is related to the modeling of pedestrian's exit choices and behaviour during an evacuation on microscopic level. A cellular automaton model and a social force model are used for the study. We simulate evacuation processes of pedestrians in a multiple exits room with and without obstacles. In a room with multiple exits, selecting an appropriate exit to evacuate is a very important decision that pedestrians face during an evacuation. It is influenced by many factors, such as personal characters, observations and the room structure. Therefore, studying the exit choice behaviour of pedestrians is the foundation used to guide a pedestrian evacuation. To analyze the pedestrians' ability to select an exit route during the evacuation, some published papers have been reported:

Zheng et al. [99] studied the effect of the exit choice behavior on the evacuation with the influence of fire spreading. Their simulation results show that the evacuation efficiency is improved when the exit choice behavior is considered. An experiment and a simulation of pedestrian exit-selecting behaviors during a building evacuation were performed by Fang et al. [25]. According to their study, pedestrians tend to move through the closer exit when the pedestrian density is low or medium. But when the crowd is congested, people move to a distant exit to avoid a long waiting time.

Shaobo et al. [81] shows the impact of the occupant density around exits on the chosen exit route. As a result of this paper, pedestrians choose the exit according to the distance to exits on the one hand and according to the occupant density around the exits on the other hand.

Zainuddin et al. [97] introduced the cellular automata model which contains a probabilistic neural network for determining the pedestrians' ability to select an exit route. Another model of exit choice based on distance, occupant density around the exit area and visibility of the environment is proposed by Zia et al. [101].

Yong et al. [94] applied a logit-based discrete choice to study the exit choice behavior in rooms with internal obstacles and multiple exits. Many factors, influencing the exit choice behavior, are considered in this model, including the information obtained by evacuees, the tendency of following others, the visibility and familiarity of exits and the physical conditions of nearby exits.

Researches have shown that the pedestrians' emotions, such as impatience, can affect the escape route choice [21, 25, 41]. An impatient pedestrian tends to walk faster, pushes other neighbouring pedestrians and rushes towards the nearest available exit [21, 41, 56]. Zheng et al. [99] recommended that for improving an evacuation model the psychological term, such as the pedestrian's degree of impatience, should be added to make the model more realistic.

Abe [1] performed an experiment of evacuation conducted in a large super market in Japan. More than 300 people have been interviewed about their choices of escape routes after they had escaped from the building. His data collected shows that 26.3% of the evacuated pedestrians chose the opposite direction to the smoking area to escape from the fire. Therefore, the smoke density is also one important factor in a simulation domain with fire or smoke source, which influences the pedestrians' exit choice.

Our microscopic models are based on the work of Yuan et al. [95]. The exit selection of a pedestrian in our model incorporates the distance and the occupant density. It takes the degree of the pedestrian's impatience and the smoke density around the exit area into account as well. The impatience degree of an individual in our model is measured in term of changes of his actual speed. It is introduced in the research of Aik et al. [3]. We refer to [21, 35, 86] for different settings of the pedestrian's degree of impatience.

In an extend model, we study and model human behaviour in emergency situations. The smoke spreading effect models the pedestrians' movements in the way that they try to avoid high smoke density regions. Therefore, an equation for the smoke concentration is to be combined combine with the CA model and the SF model in a smart way. In our model, the concentration of smoke is assumed to obey the advection-diffusion equation. This equation is used in many applications in science and engineering for fluid motion, heat transfer, flow of gas or pollutant [8, 26, 82]. We solve it numerically and the solution is used to determine the exit choice and investigate moving rules for pedestrians under propagation of smoke. The operator splitting method, which is an efficient approach to solve problems in multi-dimensions, is applied to solve the equation. The convergence of this method to approximate the advection-diffusion equation is proved.

Human behavior in emergent cases as modelled by the unadventurous ef-

fect, the inertial effect and the group effect proposed in [95] and the flow with the stream effect introduced in [96] is presented in an extended model. Although the unadventurous effect, the inertial effect and the group effect have already been studied by [95], they didn't take the degree of the pedestrian's impatience into account. The flow with the stream effect was performed only in a room with one exit. It is worth to study it in a multiple exits room as well. These effects were described and simulated in connection with the CA model but not with the SF model. However, our ways to model these effects in the SF model are explained. We implement these effects on the CA model as well as on the SF model in a room with multiple exits, compare their numerical results and point out the differences.

We also extend the work of [95] by considering an evacuation process of pedestrians in a room with internal obstacles as well. The Eikonal equation is applied to attain the distance of each cell in the domain to an exit in presence of obstacles. We couple it into the CA model and the SF model and solve it numerically by the fast marching method [79]. Obstacles with smooth boundary, i.e. circular and rectangular obstacles, are exploited for experiments. Different arrangements of obstacles are set and their influences to the evacuation time are studied and analyzed.

In chapter 2 we present a hierarchy of models for the pedestrian flow. It ranges from a social force model [35] coupled with a local visibility model [9, 17] to macroscopic models including the interaction forces and a local visibility model. In the local visibility model, the Eikonal equation is introduced and used as the direction towards the destination in the shortest way. The pedestrians are assumed to have a global knowledge of the physical setting. They move in the direction that compromises between the shortest way and the direction with least congestion in their visual field.

The microscopic social force model comprises the local interaction between pedestrians and a non-local term which is described by a local visibility model. We scale the amplitude of the local interaction in the microscopic model applying the weak coupling assumption. A mean field equation is derived from the local interaction in the microscopic model. This proceeding is classical and similar derivations can be found in the reference [29] for pedestrian flow, for the case of swarming model presented in the reference [13] and in the reference [30] for complex material flow problem.

Then, the hydrodynamic equations, represented by density and mean velocity, are attained by integrating the mean field equation and using a monokinetic closure. The derived hydrodynamic equations still contain a non-local term due to the derivation from the mean field equation. The qualitative behaviour of the hydrodynamic model is analyzed as in [5, 9]. Finally, the

scalar model with a non-local term is derived from the hydrodynamic model via simple justifications.

For numerical experiments, particle methods are used to approximate the solutions of the microscopic and macroscopic models. The macroscopic models are considered on Lagrangian description. The integration over the interaction potential is calculated by a straight-forward integration rule. We approximate the spatial derivative of the density in the local visibility model using a smoothing particle hydrodynamic method (SPH) [28, 50]. To approximate the derivative of the mean velocity at the particle location, a corrective smoothing particle method (CPSM) [15] is applied.

Smoothed particle hydrodynamics (SPH) is a technique to approximate a function through the use of particles. It was initially developed by Lucy [58], Gingold and Monaghanto [28] to solve astrophysical problems in three-dimensional open space. Presently, applications of this method are widely used, for example in geophysics, engineering and in the computer game industry. In the SPH method, a function and/or its derivative on a particle is approximated by the values over the nearest neighbour particles in the support domain of the considered particle. The support domain is defined by the smoothing length of the smoothing function. The smoothing function is usually chosen to be an even function and should satisfy the normalization condition (i), the Delta function property (ii) and the compact condition (iii).

A corrective smoothed particle method (CSPM), which was established by Chen et al. [15], is based on the Taylor series expansion on the SPH approximation of a function. This method was proposed to remedy the problem of particle deficiency near or on boundaries of the original SPH.

Finally, we show the numerical results of the microscopic and macroscopic models and compare their qualitative behaviour and computation time. The advantages of using macroscopic models are pointed out.

Chapter 1

Exit Selection and Pedestrian Evacuation Models

1.1 Cellular Automata

In this section, first we describe details of our CA model. Then the exit selection models are proposed in presence and absence of smoke propagation. Afterwards the modeling of human behaviour in emergencies, i.e. the unadventurous effect, the inertial effect, the group effect, the smoke spreading effect and the flow with the stream effect, are explained in an extended model.

1.1.1 Model Description

The proposed CA model is used to simulate the evacuation process of pedestrians in a multiple exits room with and without fixed internal obstacles in two dimensions. The simulation domain is divided by a uniform rectangular grid of cells. Its size corresponds to $0.4m \times 0.4m$, which is the typical space occupied by a person in a dense crowd [95]. The time domain is discretized into a series of $t_1, t_2, ..., t_m, ...$, where m is an integer. Pedestrians can only move to an empty cell. The states of occupants are updated in parallel after each discrete time step. The update variables depend on the states of neighbouring cells and a set of update rules that are applied in the transition from time step t to $t + 1$. The moving range of an individual is limited to one cell per time step, i.e. $0.4m$ or $0.4\sqrt{2}m$ per time step. For convenience and consistency, the following assumptions of Yuan et al. [95] are slightly revised.

Definition 1.1.1. [95]

1. The Spatial Distance (SD) is the geometrical distance from a cell to an exit.

2. The exit line is defined as the line which is on the level of the door and has a gap of $0.2m$ to each end of the door.

3. Current Position (CP) and Possible Position (PP):

   - The Current Position (CP) is the cell that is occupied by a certain individual.
   - The Possible Position (PP) of an individual with respect to a certain target is a cell in the Moore neighbourhood which has a shorter or equal distance to this target than the CP of the individual. A target is a location in the environment that the individuals might desire to reach. Examples of targets could be platforms, exits, group centers, positions of guiders, etc.

4. Exit Area and Occupant Density (OD):

   - The Exit Area is defined as the semicircle area enclosing an exit.
   - Occupant Density (OD) is the number of individuals within the defined exit area.

5. Probability to be selected (PS):
   PS is the probability of an exit being selected as movement direction.

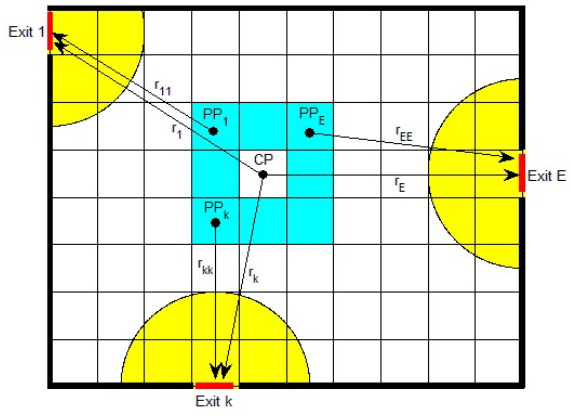

Figure 1.1: Multiple exits room without internal obstacle of the CA model. Exit area, exit line, CP, PP and Moore neighborhood.

Remark 1. The exit area can be specified in different ways. [81, 90] set rectangular exit areas. Nevertheless, there has been no general method to measure the size of exit area so far. The exit area can be adjusted to the size of the simulation area and the number of related pedestrians.

In Figure 1.1 the blue cells are the Moore neighborhood of the CP. The SDs from a CP to the nearest point on the exit line are labeled $r_1, ..., r_E$. Some selected cells in the Moore neighbourhood are named as $PP_1, ..., PP_k, ..., PP_E$, where subscripts $1, ..., E$ each refer to a particular exit. The SD from PP_k to exit k is marked as r_{kk}.

The main features of our proposed model can be represented by a 4-tuple $M =< A, Q_A, \delta_A, N_A >$ as introduced in [84] where

- A is a 2-dimensional array with closed boundary. Each cell is a square of space $0.4m \times 0.4m$.
- Q_A is a finite set of states of a cell. It is given by $Q_A = \{EC, PC, WC, OC, EA, LC, HC\}$, where

EC : Empty cell	EA : Exit area cell
PC : Cell with a person	LC : Low smoke concentration cell
WC : Wall cell	HC : High smoke concentration cell
OC : Obstacle cell	

- N_A is a specification of which cells are included in the neighborhood of a cell. The Moore neighborhood is used as neighborhood to the cell $c_{i,j}$ in our model. Thus we have $N_A = \{c_{i-1,j-1}, c_{i,j-1}, c_{i+1,j-1}, c_{i-1,j}, c_{i+1,j}, c_{i-1,j+1}, c_{i,j+1}, c_{i+1,j+1}\}$.
- $\delta_A : Q_A \times \sum \longrightarrow Q_A$ is the transition function for the states of the cells. $\sum \equiv Q_A^n$, where $n = |N^{-c_{i,j}}|$ is the number of adjacent cells to the cell $c_{i,j}$ and $N^{-c_{i,j}}$ are the adjacent cells to the cell $c_{i,j}$. The transition rules (δ_A) for the states of the cells from time t to $t+1$ is set up as follows in our model:

  1. Rule about the *building*: A cell in state WC, OC or EA (wall cell, obstacle cell or exit area cell) keeps its state unchange during simulation.
  2. Rules about the *smoke propagation*: A cell with low smoke concentration (LC) in time t becomes a HC in time $t+1$ if its smoke

concentration is higher or equal to μ_c (threshold density). A HC at time t changes to LC in time $t+1$ if its smoke concentration is less than μ_c. density).

3. Rules about the *pedestrian movements*:
   (a) An empty cell (EC), which is not a HC, changes its state at time t to PC at time $t+1$ if the following is satisfied:
      i. At least one adjacent cell is occupied by a person. This adjacent cell is noted as AE.
      ii. The EC is the PP of the AE.
   (b) An empty cell (EC), which is also HC, changes its state at time t to PC at time $t+1$ if the following is held:
      i. At least one adjacent cell is occupied by a person.
      ii. The EC is the AE's PP.
      iii. The EC has a minimum smoke density compared to all PPs of the AE.
   (c) A cell with a person (PC) changes its state at time t to EC at time $t+1$ if the following holds:
      i. Its selected cell is empty at time $t+1$ and a conflict does not arise (others do not want to move to this cell). If a conflict arises, the PC must be the winner.
      ii. Its adjacent cells do not move to PC at time $t+1$.

1.1.2 Exit Selection Model

The basic rule during an evacuation is, that pedestrians try to move out of the room as fast as possible. In the situation of multiple exits in the simulation domain, the route selection of a pedestrian has to be specified. Based on approach presented by Yuan et al. [95], we incorporate the degree of the pedestrian's impatience and smoke density into the route decision as well. In absence of smoke propagation, the exit selection in our model takes the spatial distance (SD), the occupant density (OD) and the degree of the pedestrian's impatience into account. Hence, the probability of pedestrian i selecting exit k as the evacuation route (PS) is defined as

$$P_k = (1 - n_i)P_{k-r} + n_i P_{k-d}, \tag{1.1}$$

where

- n_i is the impatience degree of pedestrian i, which is expressed in term of change in his actual speed. It is given by the following equation [3]

$$n_i = |\frac{v_i(t) - v_i(0)}{v_i^{max} - v_i(0)}|, \tag{1.2}$$

where $v_i(t)$ is the actual speed of pedestrian i at time t, $v_i(0)$ is the initial speed and v_i^{max} is the maximum speed desired by pedestrian i. Equation (1.2) indicates that when the actual speed of pedestrian i is close to the initial speed, n_i approaches 0 and pedestrian i is in a normal mood. When the actual speed of pedestrian i is close to the maximum speed, n_i approaches 1 and the pedestrian is in an extremely impatient mood and in a rush to get out from the system as fast as possible. The maximum desired speed v_i^{max}, that is reached by a pedestrian, is approximately $3.0m/s$. His initial speed $v_i(0)$ is about $1.0m/s$, as stated in [32, 39, 41].

- P_{k-r} is the distance-induced PS of exit k given by

$$P_{k-r} = 1 - \frac{(N_e - 1)r_k^{k_r}}{R_{(k_r)}}. \tag{1.3}$$

Here, r_k is the SD of the cell that pedestrian i occupies to exit k. In a room without obstacles, the SD is measured from the centre of that cell to the nearest point on the exit line using the Euclidean metric. In presence of obstacles in the room, $r_k = T(x_{c_i})$, where x_{c_i} is the centre of the cell that pedestrian i occupies and T is the solution of the Eikonal equation

$$\begin{aligned} |\nabla T(x)| &= \frac{1}{F(x)}, \quad x \in \Omega \\ T(x) &= 0, \quad x \in \Gamma_{0_k} \subset \Omega \\ \text{Front} = \Gamma_t &= \{x | T(x) = t\}, \end{aligned} \tag{1.4}$$

where Ω is a bounded domain and $T(x)$ is the arrival time of front crossing the point x. Γ_{0_k} is the initial front or initial positions on the exit line of exit k. If the speed of the front F is a constant, $T(x)$ is interpreted as the distance map with the desired units [53]. In our model $F = 1$ is set for walkable areas and $F = 0$ for areas obstructed by obstacles. Equation (1.4) is solved numerically using the fast marching method [79]. For simplification, grid points are placed at the centre of the CA cells where the Eikonal equation is solved. Therefore, each

cell of the CA model has information about the distance to the considered exit at its centre after the solution of the Eikonal equation is determined. To attain a more accurate distance value of each cell, one could use a finer grid to solve the Eikonal equation. The information about the distance in each cell can be achieved by interpolating using solutions on the Eikonal grids around the centre of the regarded cell. $R_{(k_r)} = \sum_{k=1}^{N_e} r_k^{k_r}$, k_r is a constant for adjusting the sensitivity of the distance effect and N_e is the total number of exits in the simulation domain. When r_k of pedestrian i is shorter than other exits, there is a high probability that pedestrian i chooses exit k for evacuation. By summing the distance-induced probabilities associated with every exit, we have

$$\begin{aligned}\sum_{k=1}^{N_e} P_{k-r} &= 1 - \frac{(N_e-1)r_1^{k_r}}{R_{(k_r)}} + 1 - \frac{(N_e-1)r_2^{k_r}}{R_{(k_r)}} + ... + 1 - \frac{(N_e-1)r_{N_e}^{k_r}}{R_{(k_r)}} \\ &= N_e - \frac{(N_e-1)[r_1^{k_r} + r_2^{k_r} + ... + r_{N_e}^{k_r}]}{\sum_{k=1}^{N_e} r_k^{k_r}} \\ &= 1.\end{aligned} \tag{1.5}$$

- P_{k-d} is the density-induced PS of exit k is given by

$$P_{k-d} = 1 - \frac{(N_e-1)d_k^{k_d}}{D_{(k_d)}}, \tag{1.6}$$

where d_k is the OD of exit k, $D_{(k_d)} = \sum_{k=1}^{N_e} d_k^{k_d}$, k_d is a constant to adjust the sensitivity of P_{k-d} due to the occupant density effect. Similar to the distance-induced probability is the fact that the more pedestrians flock around exit area k, the less probable is the selection of exit k. Proving in the same manner as in equation (1.5), we obtain that the sum of the respective probabilities equal 1, i.e. $\sum_{k=1}^{N_e} P_{k-d} = 1$.

Since $\sum_{k=1}^{N_e} P_{k-r} = 1$ and $\sum_{k=1}^{N_e} P_{k-d} = 1$, one obtains

$$\sum_{k=1}^{N_e} P_k = (1-n_i)\sum_{k=1}^{N_e} P_{k-r} + n_i \sum_{k=1}^{N_e} P_{k-d} = 1.$$

Equation (1.1) can be explained that when the actual velocity of a pedestrian is close to the initial one, n_i approximates 0 and the pedestrian i is in a normal mood. He then chooses the nearest exit to move out. When the actual velocity of pedestrian i is close to the maximum, n_i approximates 1

and pedestrian i is in an extremely impatient mood. He rushes to get out from the system as fast as possible. Consequently, he chooses an exit that has less congestion to move out.

Remark 2. One could define the PS of exit k by equation (1.1) through an exponential function as

$$P_k = N_m \exp((1-n_i)P_{k-r}) \exp(n_i P_{k-d}),$$

N_m is a normalization factor for ensuring $\sum_{k=1}^{E} P_k = 1$. In the case of an evacuation process under smoke spreading, the smoke density around the exit areas would affect the exit choice of pedestrians. They tend to avoid moving out through an exit that is covered by thick smoke. Regarding to the spatial distance (SD), the occupant density (OD), the degree of the pedestrian's impatience (n_i) and the smoke density around an exit, the probability of pedestrian i to choose exit k (PS) for evacuation under smoke propagation is illustrated as

$$P_k = N_m \frac{\exp(k_s(1-n_i)P_{k-r}) \exp(k_p n_i P_{k-d})}{\exp(k_m \alpha C_k)}. \tag{1.7}$$

k_s, k_p and k_m are three positive parameters. k_s is the parameter to adjust the distance and the degree of impatience, k_p regulates the congestion-degree of impatience and k_m adjusts the smoke density around k^{th} exit area. N_m is normalization factor given by

$$N_m = \frac{\sum_{k=1}^{N_e} \exp(k_m \alpha C_k)}{\sum_{k=1}^{N_e} \exp((1-n_i)P_{k-r}) \exp(n_i P_{k-d})}.$$

C_k is the average smoke density around a semicircle exit area of exit k reflecting the influence of the smoke density around an exit to a pedestrian's exit choice. When C_k is high, we attain a small probability of choosing exit k. α is valued as follows:

$$\alpha = \begin{cases} 0.5 & , \quad r_k \leq \sigma \\ 1 & , \quad r_k > \sigma. \end{cases}$$

Here, we set $\sigma = 6$ as in the references [98, 100]. When the distance from the cell that a pedestrian occupies to the k^{th} exit (r_k) is closer than σ, we set this value smaller. The reason for this setting is that when pedestrians are near to the exit, although there is thick smoke around them, the instinct of survival makes the effect of the smoke density smaller. Then, the probability that pedestrians will move out through this exit is larger.

Remark 3. The setting of equation (1.7) is similar to the fire floor fields of the pedestrians' transition probability in the references [98, 100].

Now let us consider the way to find cells in the exit area.

Find cells in an exit area

The cells that belong to an exit area have to be determined before starting a simulation. The number of pedestrians occupying these cells (OD) have to be updated in every time step which is used to calculate the exit choice of pedestrians. In order to find the exit area cells, we check, if a cell is in the semicircle exit area or not by the two following conditions:

1. $A \cdot P \geq 0$, where A, the vector perpendicular to the exit, points from the centre of the exit to a point on the semicircle of the exit area. P is the vector pointing from the centre of the exit to the centre of the calculated cell.

2. $|P| \leq r$, where r is the radius of an exit area.

In Figure 1.2 we see that cell B belongs to the exit area, since $|B| < |A|$ and $A \cdot B \geq 0$, while cell C is not in the exit area, because of $|C| > |A|$.

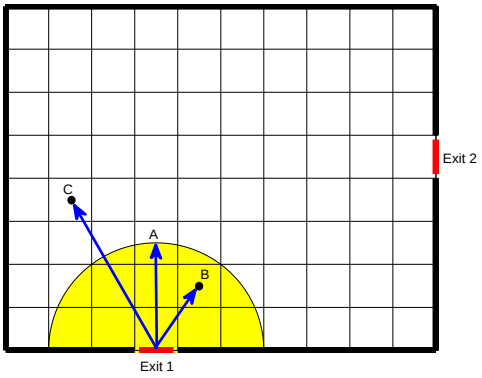

Figure 1.2: Exit Area.

Main Basic Update Rule Algorithm

The main algorithm for updating the pedestrians' current positions (CPs) can be summarized as follows:

Step 0 **(a)** Discretize the simulation domain into a rectangular grid with size $0.4m \times 0.4m$.

(b) Calculate the spatial distance (SD) corresponding to each exit.

- In absence of internal obstacle: The SD of each cell to an exit is measured from the centre of the cell to the nearest point on the exit line. The SDs of cells that belong to walls are set to 500.
- In presence of internal obstacles: The SD of each cell to an exit is attained by solving the Eikonal equation (1.4) numerically by the fast marching method with the same size of lattice spacing as in the CA model. $T(x) = 0$, where x is a grid point on the exit line of the considered exit. $F = 1$ is set for walkable cells and $F = 0$ for obstacle cells.

This field, initialized at the beginning of the model run, describes the shortest distance from the cell to each exit and keeps unchanged during the simulation.

(c) Find cells that are in the exit area of each exit.

(d) Randomly distribute pedestrians in the simulation domain. Each cell occupies only one occupant or none.

(e) The state of a cell, occupied by an individual, is assigned to 1. Empty cells receive the value 0.

Step 1 Each pedestrian stays within one CP cell at time t_s.

Step 2 Count the OD of each exit.

Step 3 Determine a target and calculate the distance from the CP and its neighborhood to the target.

- If the target is an exit, the pedestrian choose it according to the PS using equation (1.1) for a room without smoke source and equation (1.7) for a situation in a smoking source room. The distance from the CP and its neighborhood to the target is the SD of that cell to the chosen exit.
- If the target is the centre of a group of people, the position of a guider etc., calculate the distance from the CP and its neighborhood to the target.

Step 4 Find the PPs of the CP for each pedestrian.

Step 5 Each pedestrian selects randomly one cell among the PPs of the CP for the time step t_{s+1}.

Step 6 (Parallel update)
A conflict arises when two or more pedestrians attempt to move to the same cell. Pedestrians who have no conflict with others, move to their selected cell. For pedestrians with conflicts, the chosen cell is randomly assigned to one of them with equal probability. The selected pedestrian moves to the interrelated cell and the unselected pedestrians remain in their original CPs without moving until the next time step.

Step 7 All pedestrians update their CPs for the time step t_{s+1}.

Step 8 Update the state of each cell in the domain. The cell state is assigned to 1, if it is occupied by an occupant. Otherwise it is 0.

Step 9 Set t_s=t_{s+1} and return to Step 1 until $t_s = t_{end}$

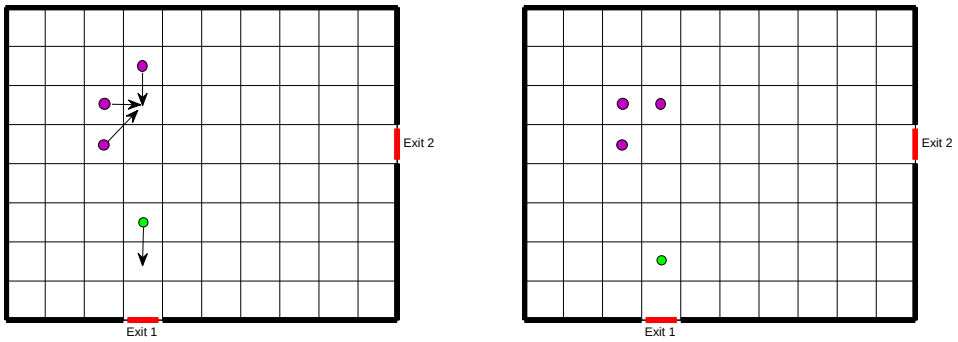

(a) t_s (b) t_{s+1}

Figure 1.3: Pedestrians' movements and conflicts: Arrows refer to intended movements: Three pedestrians, depicted by purple circles, try to move to the same cell (conflict arises). A random number decides who moves. The green circle pedestrian has no conflict with others and moves in time step t_{s+1} to his desired cell.

1.1.3 Extended Model

In an extended model, some human behaviours that are observed during emergency situations, such as in a room with fire or smoke-filled room, are modeled through simple mathematical formulations. In our study, we consider the unadventurous effect, the inertial effect and the group effect proposed in [95], the flow with the stream effect studied in [96] and the smoke spreading effect.

1. **Unadventurous Effect**
   It reflects the behaviour of pedestrians that try to evacuate the same route as they entered and reject to use an unexperienced exit. Pedestrians prefer familiar exit routes, such as the main entrance or exit, even if there are faster unfamiliar routes available, especially under time constraints [70].

   To model this effect, it is assumed that pedestrian i entered the origin fire room through exit k and the probability of choosing exit k for leaving equals P_k. The unadventurous effect of pedestrian i is modeled by enlarging P_k and reducing the probability of choosing other exits. A simple way to enhance P_k is by multiplying it with a factor α_{ke}, i.e.

$$P_{ke} = \alpha_{ke} P_k, \tag{1.8}$$

   where $\alpha_{ke} > 1$. Due to the increase of P_k to P_{ke}, all other exits except of exit k lose their probability of being chosen proportionally. The probability of choosing exit l is reduced to

$$P_{le} = P_l - (\frac{P_l}{1 - P_k})\Delta P_k,$$

   where $\Delta P_k = P_{ke} - P_k$. Hence, $P_{ke} > P_k$ and $P_{le} < P_l$, $\forall l \in N_e, l \neq k$.

By summing all the new PS of every exit, we obtain

$$\begin{aligned}
\sum_{k=1}^{N_e} P_{ke} &= P_{ke} + \sum_{le \neq ke}^{N_e} P_{le} \\
&= P_{ke} + \sum_{l \neq ke}^{N_e} (P_l - \frac{P_l}{1 - P_k}(\Delta P_k)) \\
&= P_{ke} + \sum_{l \neq ke}^{N_e} (P_l - \frac{P_l}{\sum_{l \neq ke}^{N_e} P_l}(P_{ke} - P_k)) \\
&= P_{ke} + \sum_{l \neq ke}^{N_e} P_l - P_{ke} + P_k \\
&= \sum_{l \neq ke}^{N_e} P_l + P_k \\
&= \sum_{k=1}^{N_e} P_k \\
&= 1.
\end{aligned}$$

There are a number of other algorithms that can be used to enlarge the PS of an exit. An alternative avenue to increase P_k is the use of a sine function

$$P_{ke} = P_k^{\omega_1} \sin(\frac{\pi}{2} P_k^{\omega_2}), \tag{1.9}$$

where ω_1 and ω_2 are two constants. P_k can be enhanced in a magnitude of ways through different settings of ω_1 and ω_2 in equation (1.9).

2. **Inertial Effect**
Once pedestrians choose a certain exit to leave, they usually continue to move towards that exit and do not like to stop or change the direction during the evacuation. They try to keep their preferred velocity and direction as long as possible. To model the inertial effect, it is supposed that a pedestrian moves towards exit k at time t_m. As a result of the inertial effect, he will not choose exit k again in the time step t_{m+1}, because he likes to keep his heading direction as mentioned above. Thus, the inertial effect is modeled by enlarging the PS of Exit k at time t_{m+1} by applying the same method as in the consideration of the unadventurous effect.

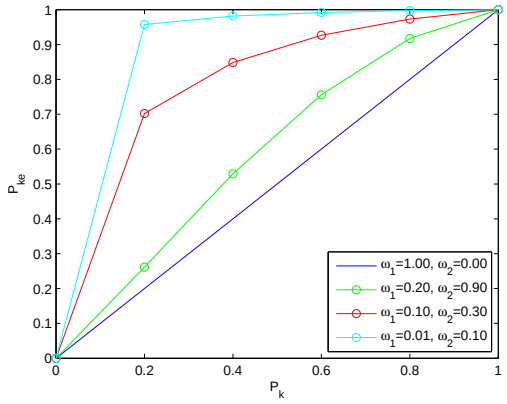

Figure 1.4: A plot of P_{ke} versus P_k with different values of ω_1 and ω_2.

3. **Group Effect**
   The difference in modeling the group effect from Yuan et al. [95] lies on the exit selection of a group. In their model they do not consider the impatient degree of group members for exit choice of a group. In our model, we take the impatience degree of group members into account and define it as the average of impatience degree of members in the group. Thus, the probability of group j selecting exit k as the evacuation route (PS) is stated as

$$P_k = (1 - n_{c-j})P_{k-r} + n_{c-j}P_{k-d}, \tag{1.10}$$

   where

$$n_{c-j} = \frac{1}{N_{g-j}} \sum_{i=1}^{N_{g-j}} n_{i-j}, \tag{1.11}$$

   where n_{c-j} is the average impatience degree of members in group j at time t_g. P_{k-r} is the distance-induced PS of exit k illustrated as in (1.3). It is noted that r_k in equation (1.3) for the group effect is measured from the centre of the group to the nearest point on the exit line. The group centre is defined as in equation (1.12) . P_{k-d} is the density-induced PS of exit k given by equation (1.6). N_{g-j} is the number of members of group j at time t_g. n_{i-j} is impatience degree of pedestrian i which is a member of group j. It is described as in equation (1.2).

   As clarified by [42, 71], group members, such as friends, families or people who travel together, tend to move with each other, orient their

actions and leave together. In an emergency incident, the members of a group would gather and attempt to move out together instead of instantly running to exits. Generally, the actions of a group are splitted into two stages:

(a) Gathering stage: The group members walk towards each other to combine the group. In this stage they try to move towards the centre of the group.

(b) Egress stage: The group members move together along the chosen exit route.

To simplify the study for the group effect, the following assumptions are made for the movement of each group member:

(a) At each time step, each group member is more likely to look for other group members and moves out of the room with them instead of moving out of the room first and looking for other members afterwards.

(b) Group members, who decide to move out together, approach other group members and move towards the targeted exit at the same time.

Therefore, the movement of each group member goes through three steps:

Step 1 A group member decides whether he moves out with his group or he abandons other group members. The probability that a group member looks for other members and they move out together is set to 0.9995 while the probability of a group member to abandon other group members is set very low to 0.0005.

Step 2 A group member who decides to abandon other group members (he will not consider other group members afterwards) selects one exit to move towards. A group member who does not abandon other group members, has two possibilities: He can move towards other group members (i) or move towards an exit (ii). The probability that he moves towards other group members is set to 0.95 while the probability that he moves towards an exit is 0.05. This step ensures, that group members approach other group members while at the same time they move altogether towards the targeted exit.

Step 3 A group member updates all information and then makes a new decision as in Step 1.

The point that the members of group j move towards is defined as the position that is in average closet to all members of group j given by

$$x_{c-j} = \frac{1}{N_{g-j}} \sum_{i=1}^{N_{g-j}} x_{i-j}, \tag{1.12}$$
$$y_{c-j} = \frac{1}{N_{g-j}} \sum_{i=1}^{N_{g-j}} y_{i-j},$$

where N_{g-j} is the number of members of group j at time t_g and $O_c = (x_{c-j}, y_{c-j})$ is the point that members of group j move towards. The group members are assumed to stop moving towards the point O_c when they are close enough to that point. Once all of the members are within a neighbouring region of O_c, they select one exit as the common direction to move out together given by equation (1.10). All members will immediately gather if some members are outside the neighbouring region. The neighbouring region of a group would be expected to be large when there is a huge number of members. In our model, the neighbouring region of a group at center O_c is specified as the area surrounded by a circle with radius $2m$.

4. **Smoke Spreading Effect**
The spreading of smoke is one of the most important factors impacting evacuees. Smoke contains some poisonous and unhealthy product, such as carbon monoxide (CO). Smoke soot can reduce a pedestrian's visibility range, which also leads to a decrease of his walking speed [12, 62, 72]. Therefore, the development of smoke and the interaction between smoke and people is very interesting and important to study.

Considering the smoke spreading effect, it is assumed that pedestrians attempt to move towards a targeted exit in an evacuation. At the same time they try to avoid high concentration of smoke to prevent heath damages and less visibility. Pedestrians also evade to move out through exits that are covered by lots of smoke. In our model, the probability for choosing an exit under smoke propagation is calculated with the help of equation (1.7), which takes the smoke density around the exit area into account. The smoke concentration is assumed to obey the linear advection-diffusion equation, which is used numerous applications in science and engineering to describe fluid motion, heat transfer, flow of gas, pollutant and chemical engineering problems [8, 26, 82]. It is

stated as

$$\frac{\partial C}{\partial t} + w \cdot \nabla C = \kappa_d \nabla^2 C + S(c_s, t) \in \Omega \times \mathbb{R}^+, \tag{1.13}$$

with Dirichlet boundary conditions $C = 0$ on $\partial\Omega$, diffusion constant $\kappa_d > 0$, velocity field $w = (w_1, w_2) \in \mathbb{R}^2$, source term $S(c_s, t)$ and simulation domain $\Omega \subset \mathbb{R}^2$. For simplification, we assume that smoke source emits at a constant rate $Q_c[g/s]$ from a single source point at $c_s = (x_s, y_s)$. Thus the source term can be written as

$$S(c_s) = Q_c \delta(x - x_s)\delta(y - y_s),$$

where δ is the Dirac delta function given by

$$\delta(x) = \begin{cases} 1, & x = 0 \\ 0, & x \neq 0. \end{cases}$$

The advection-diffusion equation (1.13) is coupled into the CA model and simulates the development of the smoke simultaneously with the movements of the pedestrians in the domain. We solve it numerically applying the operator splitting method. Details of this method is explained in section numerical method. To coincide well, the grid cells and the time steps, where the advection-diffusiont is solved, are set in the same way as in the CA model. Therefore, in every time step we obtain the information of the smoke concentration in every cell of the CA model. One could also use a finer mesh space to solve the advection-diffusion equation. The information of the smoke concentration in each cell of the CA model can be obtained by interpolation using information of the smoke density of the grid points around the considered cell of the CA model.

Now let us describe the way to couple this smoke concentration into our CA model. As already said in the basic rule of movements, a pedestrian who stays in the CP at time t_s chooses one cell among the PPs of the CP for time t_{s+1}. In the case of movements under smoke spreading, pedestrians do not choose a cell which has a high smoke concentration. The PPs of the CP are now both defined by their SDs from the same exit and by their smoke densities. The PPs that can be chosen for time t_{s+1}, are restricted by their smoke density with following procedure:

First we define μ_c, the threshold smoke concentration, that is assumed to be high enough to influence the movements of pedestrians. In this

model we set $\mu_c = 0.05$, because this value reduces the visibility range of a pedestrian to about $6m$ and his speed will be effected significantly [12, 62]. Then for each time step, we do the following

(a) Find cells in the Moore's neighborhood of the CP whose smoke concentrations are higher than μ_c. We denote these cells as HCs (high smoke concentration cells) of the CP.

(b) Check if the HCs of the CP are in the PPs of the CP.

i. In the case that there are no HC in the PPs of the CP, the pedestrian chooses one cell among the PPs randomly.

ii. In the case that some HCs of the CP are in the PPs and the number of the CP's HCs that are in the PPs of the CP is smaller than the number of the CP's PPs, the pedestrian chooses randomly one cell in the PPs that is not the HCs of the CP.

iii. In the case that the HCs of the CP are in the PPs and the number of the CP's HCs is larger or equal the number of the CP's PPs, the pedestrian chooses one cell in the PPs that has the minimum smoke concentration. If there are several cells that have a minimum concentration, one of them is chosen randomly.

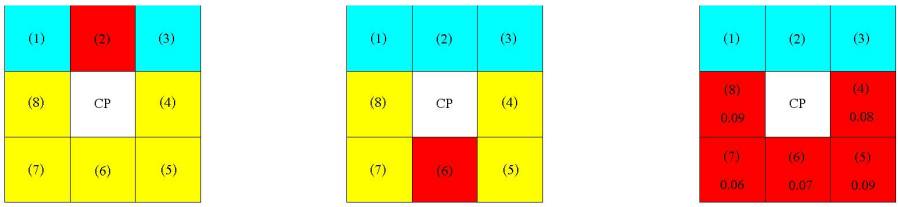

(a) HC is not in PPs (b) HC is in PPs (c) All PPs are HCs

Figure 1.5: PPs (yellow cells) and HCs (red cells) of the CP in the Moore neighborhood.

Figure 1.5 shows possible positions of HCs in the Moore neighborhood. The way how a pedestrian who stays at the CP in time step t_s chooses a cell in his PPs for time step t_{s+1} can be explained as following, considering smoke spreading effect. We suppose that pedestrian A stays at his CP in time step t_s and the yellow cells $\{(4), (5), (6), (7), (8)\}$ are the PPs of the CP. Pedestrian A chooses one of the PPs for time step t_{s+1} as follows: When the HC is not in the PPs of the CP, pedestrian

A chooses one of the PPs, i.e. $\{(4),(5),(6),(7),(8)\}$ randomly, see Figure 1.5(a). In Figure 1.5(b), cell (6) of the PPs is a HC and pedestrian A does not selected this cell. PPs of the CP, restricted to $\{(4),(5),(7),(8)\}$, however can be chosen. In the case that all PPs are HCs, see Figure 1.5(c), the cell with the minimum smoke concentration is chosen, i.e. cell (7).

5. **Flow with the Stream Effect**
   The flow with the stream effect in our model is considered in a room with multiple exits. Therefore, the exit selection of an individual who can see several exits and a guider, has to be specified. In our model, the exit selection of an individual is given by equation (1.1) which take his impatience degree into account which is different from the way proposed by [96].

   The psychology and behaviour that is considered in the flow with the stream effect is very common in daily life and also in an evacuation process. The characteristic feature of this effect is that a person gives up his own mind and takes the action of the mass around. People in an emergency case are likely affected by people around because of their nervousness and panic. They would like to close to the crowd and tend to follow the route of the mass rather than acting independently.

   The human behaviour termed as *flow with the stream effect* is proposed to simulate an emergency evacuation from a smoke-filled compartment. The effect of smoke to the visibility range of individuals is also considered in the model.

   The visibility of exit signs, doors and windows is very important to an occupant, who tries to survive from a fire in the building. Many factors affect the visibility, like the scattering and the absorption coefficient of the smoke. Mulholland [62] gives a formula to estimate the visibility range of an individual in a confined and well-mixed smoke room. The limited visibility of an individual due to smoke is calculated through the equation:

$$R_v = \frac{K_s V}{K_m M_s}, \tag{1.14}$$

   where R_v is the visibility range measured in meter. K_s is the constant which is 8 for light-emitting sign and 3 for light-reflecting sign. V

is the volume of space at the fire origin. K_m is a smoke extinction coefficient measured in m^2/g. Generally, $K_m = 7.6m^2/g$ is used for a soot produced during flaming combustion of wood and plastics, whereas $K_m = 4.42m^2/g$ is used for a soot produced during pyrolysis of these materials. M_s is the mass of smoke soot measured in gram and can be approximated by

$$M_s = \epsilon \cdot M, \tag{1.15}$$

where M is the burning material weight and ϵ is the smoke conversion factor. The visibility domain of a pedestrian at CP is specified as the circle area with radius R_v. It is noted that R_v can vary in the course of the time. It alters when the smoke concentration in the fire compartment changes.

To simulate the flow with the stream, we suppose that an individual at CP cannot see the exits since they are outside his visibility. Furthermore, it is also assumed that there are N individuals within his visible domain, including himself as well. According to CA model, each individual has eight movement directions numbered from d_1 to d_8 at each time step, see Figure 1.6. Among all N individuals, we assume that the j^{th} $(1 \leq j \leq N)$ individual is defined as a guider who is familiar with a fire compartment and knows where the exits are located. In spite of the fact that the visibility of the guider is also limited due to smoke, he is able to lead other pedestrians to an exit. In such a situation, the individual at CP determines his movement direction by the rule of the flow with the stream as explained in the following:

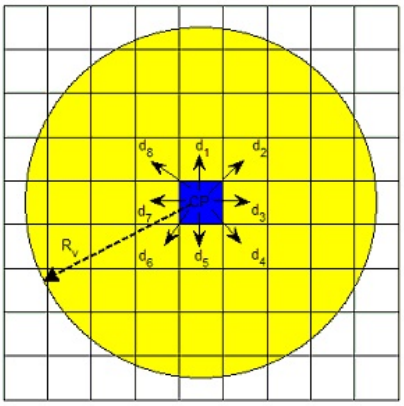

Figure 1.6: Visibility domain and movement directions

(a) At time t_s, check the status whether the pedestrian at his CP can see an exit. If he recognizes several exits, the pedestrian selects one exit to move towards by equation (1.1). Otherwise, the next step is performed.

(b) Check if there is a guider in the visibility of the pedestrian. If there is one, the pedestrian follows him with 0.9995 probability. Thus, with a probability of 0.0005 he gives up following the guider and moves in a randomly chosen direction. The pedestrian who decides to follow the guider has two choices: He can move towards the guider (i) or move along the movement direction of the guider (ii). The probability that he moves towards the guider is set to 0.1 while the probability that he moves along the movement direction of the guider is 0.9. In the case that there are two or more guiders within his visibility domain, one of them will be chosen randomly to follow. If there is no guider in his visibility, the pedestrian proceeds to the next step.

(c) Based on the state at time t_{s-1}, count the number of pedestrians who are within the visibility domain and divide them into groups according to their movement directions. The group which contains most pedestrians is defined as the leading group. The movement direction of the leading group is defined as the principal direction. With probability 0.9995 the pedestrian follows the leading group while he gives up following the leading group and moves in a randomly chosen direction with probability 0.0005. The pedestrian who decides to follow the leading group has two choices: He can move towards the centre of the leading group (i) or move along the movement direction of the leading group (ii). The probability that he moves towards the centre of the leading group is set to 0.1, while the probability that he moves along the principal direction of the leading group is 0.9. If there are two or more leading groups around the pedestrian at CP, one of them is chosen randomly to be followed.

Since it is assumed that the compartment is filled with well-mixed smoke, the smoke densities around the exits are approximately the same and do not effect the exit choice for guiders. Guiders choose their evacuation route through equation (1.1) and update their CPs following the main basic update rules mentioned in section 1.1.2.

It should be noted that once an individual is near a wall and his move-

ment direction would lead him to move into the wall in the next time step, he changes his direction randomly to avoid encountering the wall. In Figure 1.7 the green pedestrian is near wall 1 and it is supposed that his movement direction at time t_s is d_7. Therefore, he would change his movement direction to prevent walking into the wall in the next time step. He would choose one movement direction randomly from $\{d_1, d_2, d_3, d_4, d_5\}$ to move in time step t_{s+1}. Red arrows refer to movement directions which lead into the wall while blue arrows refer to possible movement directions leading away from this boarder.

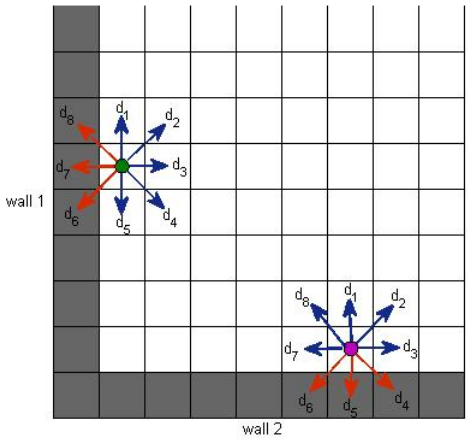

Figure 1.7: Possible movement directions (blue arrows) when individuals are near wall.

A pedestrian with visibility range R_v can see an exit from his CP if one of the following two conditions is satisfied.

(a) The SD of his CP is less than or equal to R_v.

(b) The intersection between the circle with his CP as centre and radius R_v and the complete straight line L_e of the exit has a solution, i.e. there are one or two points of intersection. The complete straight line L_e is the line that starts at point (e_x, e_y) and ends at point (l_x, l_y), see Figure 1.8.

Remark 4. (a) For simplification, we note the circle with center CP and radius R_v as Cir_{CP-R_v}.

(b) The complete straight line L_e of an exit is different from its exit line. The exit line which is the reference line used to compute each

cell's SD is a part of the complete straight line L_e, see Figure 1.8. In this figure the red line at the exit is the exit line.

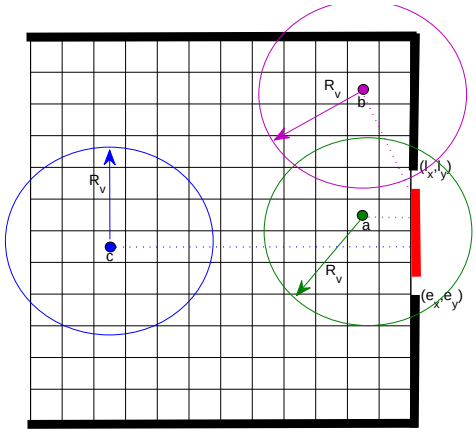

Figure 1.8: Intersection between Cir_{CP-R_v} and the straight line L_e of the exit.

In Figure 1.8 circles with radius R_v depict the visibility domain of the pedestrians a, b and c. A dotted line describes the spatial distance (SD) of an individual. Although the visibility circle Cir_{a-R_v} of pedestrian a does not intersect the complete straight line L_e of the right exit, his SD is less than R_v. Hence pedestrian a is able to see the exit. Pedestrian b can also see the exit as a result of the intersection of Cir_{b-R_v} with the straight line L_e, even though his SD is larger than R_v. Neither pedestrian c's SD is less than R_v, nor Cir_{c-R_v} intersects the straight line L_e of the exit. Therefore, Pedestrian c cannot see the exit.

The procedure for checking if Cir_{CP-R_v} intersects the complete straight line L_e of an exit is as follows:

(a) Write the parametric equation of the exit's straight line L_e. Suppose that the starting point of this line L_e is $e = (e_x, e_y)$ and its endpoint is $l = (l_x, l_y)$. Hence its parametric equation is given by

$$\begin{aligned} p &= e + t(l - e), \\ p &= (p_x, p_y), \quad d_x = (l_x - e_x), \quad d_y = (l_y - e_y), \\ p_x &= e_x + td_x, \quad p_y = e_y + td_y. \end{aligned}$$

(b) Write the circle equation of the circle with centre $CP = (h_x, h_y)$ and radius R_v and expand it:

$$\begin{aligned}(x - h_x)^2 + (y - h_y)^2 &= R_v^2, \\ x^2 - 2xh_x + h_x^2 + y^2 - 2yh_y + h_y^2 - R_v^2 &= 0. \qquad (1.16)\end{aligned}$$

(c) Plug $x = e_x + td_x$ and $y = e_y + td_y$ into equation (1.16). Then we obtain

$$\begin{aligned}(e_x + td_x)^2 - 2(e_x + td_x)h_x + h_x^2 + (e_y + td_y)^2 - \\ 2(e_y + td_y)h_y + h_y^2 - R_v^2 = 0, \qquad (1.17)\end{aligned}$$

or we can write equation (1.17) as

$$at^2 + 2bt + c = 0, \qquad (1.18)$$

where

$$\begin{aligned}a &= (d_x^2 + d_y^2), \\ b &= (e_x d_x + e_y d_y - d_x h_x - d_y h_y), \\ c &= (e_x^2 + e_y^2 - 2e_x h_x - 2e_y h_y + h_x^2 + h_y^2 - R_v^2).\end{aligned}$$

(d) Solve the quadratic equation (1.18) for t. Its solution is achieved by the formula

$$t = \frac{-b \pm \sqrt{b^2 - 4ac}}{2a}.$$

If $b^2 - 4ac \geq 0$, there is a solution, i.e. Cir_{CP-R_v} intersects the straight line L_e with one or two points. If $b^2 - 4ac < 0$, there is no solution, i.e. Cir_{CP-R_v} does not intersect the straight line L_e.

1.2 Social Force Model

This section focuses on the social force model. The same acpects as in section 1.1 with the cellular automata models are examined, but from another viewpoint. First we depict a detailed description of the components of the social force model. Then we demonstrate how to model elements which are not incorporated in the cellular automata models, concerning the exit selection and the extended models.

1.2.1 Model Description

The two-dimensional social force model with position $x_i \in \mathbb{R}^2$, $i = 1, ..., N$ and velocity $v_i \in \mathbb{R}^2$, describes the movements of pedestrians by following system of ordinary differential equations [34]:

$$\frac{dx_i}{dt} = v_i(t) \tag{1.19}$$

$$m_i \frac{dv_i}{dt} = f_i(t) + \xi_i(t), \tag{1.20}$$

where m_i is the mass of pedestrian i, $\xi_i(t)$ is an individual fluctuation term indicating chaotic behavioral changes. For simplifying, we set $m_i = 1$ and $\xi_i = 0$ for all $i = 1, ..., N$. $f_i(t)$ is the sum of all forces which influence pedestrian i given by

$$f_i(t) = f_i^d(t) + \sum_{j \neq i} (f_{ij}^{soc}(t) + f_{ij}^{ph}(t)) + \sum_w f_{iw}(t). \tag{1.21}$$

- $f_i^d(t)$ is the *desire force* that indicates the intention of pedestrian to reach his destination with a certain desired speed v^d in a given desired direction e^d. Its mathematical expression for pedestrian i is described by

$$f_i^d(t) = \frac{v_i^d(t) e_i^d(t) - v_i(t)}{\tau_i}, \tag{1.22}$$

  where $v_i^d(t)$ is the intended speed of pedestrian i and $e_i^d(t)$ is the unit vector pointing to the desired direction. $v_i(t)$ is the actual velocity and τ_i is the relaxation time in which the pedestrian adapts his actual velocity to the intended velocity $(v_i^d(t) e_i^d(t))$.

- $f_{ij}^{soc}(t)$ is the *repulsive social force*. It expresses the psychological tendency of pedestrians that prefer to have a personal space and keep a certain safety distance to other pedestrians. The repulsive social force is a monotonic force depending on the inter-pedestrian distance. It is modeled as an exponential decaying function:

$$f_{ij}^{soc}(t) = A_i \exp\left(\frac{r_{ij} - d_{ij}}{B_i}\right) n_{ij} \left(\lambda_i + (1 - \lambda_i) \frac{1 + \cos(\varphi_{ij})}{2}\right). \tag{1.23}$$

  Here, A_i is the interaction strength, B_i is the range of the repulsive interactions and $d_{ij} = |x_i - x_j|$ is the distance between the centres of mass

of the pedestrians i and j. $r_{ij} = r_i + r_j$ is the sum of the pedestrians' radii r_i and r_j and $n_{ij}(t) = (n_{ij}^{(1)}, n_{ij}^{(2)}) = \frac{x_i(t) - x_j(t)}{d_{ij}(t)}$ is the normalized vector pointing in the direction from pedestrian j to pedestrian i. λ_i is a value in the range $[0, 1]$ and $\lambda_i < 1$ reflects the behaviour of the pedestrian to react stronger to an event in front of him than to an event behind him. $\cos(\varphi_{ij}) = -n_{ij}(t) \cdot e_i(t)$, where $e_i(t) = \frac{v_i(t)}{|v_i(t)|}$ is the direction of motion of pedestrian i and $\varphi_{ij}(t)$ denotes the angle between the direction of motion of pedestrian i ($e_i(t)$) and the direction to the pedestrian j, which exerts the repulsive force on the pedestrian i, i.e. $-n_{ij}(t)$.

- $f_{ij}^{ph}(t)$ reflects the *physical interaction force*. It focuses on the aspect that pedestrians can get in physical contact with each other ($r_{ij} \geq d_{ij}$) in crowded environments. This force separates pedestrians when collisions occur. Motivated from the grannular force, the physical interaction force is expressed by

$$f_{ij}^{ph}(t) = k_n H(r_{ij} - d_{ij}) n_{ij} + k_t H(r_{ij} - d_{ij}) \Delta v_{ji}^t t_{ij}, \tag{1.24}$$

  where H is the Heaviside function, $t_{ij} = (-n_{ij}^{(2)}, n_{ij}^{(1)})$ is the unit tangential vector and orthogonal to n_{ij}, $\Delta v_{ji}^t = (v_j - v_i) \cdot t_{ij}$ is the tangential velocity difference, k_n and k_t are the normal and tangential constants respectively. The first term on the right hand side represents a *body force* for the body compression effect while the second term is a *sliding friction force* for relative tangential motion.

- $f_{iw}(t)$ is the *obstacle force* which is applied when a pedestrian opposes a boundary like walls or obstacles. The obstacle force has a similar effect as the pedestrian interaction force. The repulsive force from the obstacle w is stated as

$$f_{iw}(t) = [A_w \exp(\frac{r_i - d_{iw}}{B_w}) + k_w H(r_i - d_{iw})] n_{iw} - \kappa_w H(r_i - d_{iw})(v_i \cdot t_{iw}) t_{iw}, \tag{1.25}$$

  where d_{iw} denotes the distance from pedestrian i to obstacle w, n_{iw} is the direction perpendicular to the obstacle and t_{iw} is the direction tangential to this obstacle.

1.2.2 Exit Selection Model

The probability of an exit to be selected (PS) is defined in the same way as in the CA model by applying equation (1.1) in absence of smoke and equation (1.7) in presence of smoke. We note that, considering the social force model, r_k is the distance from a pedestrian's position to exit k in equation (1.3) . It is measured from the pedestrian's position to the nearest point on the exit line of exit k using the Euclidean metric for a room without obstacles. This distance has to be calculated every time step. Once a pedestrian chooses an exit to move out, the desired movement direction (e_i^d), which is used to navigate the movement direction of the individual towards the selected exit, is demonstrated as

$$e_i^d(t) = \frac{(x_k, y_k) - (x_i, y_i)}{|(x_k, y_k) - (x_i, y_i)|}, \tag{1.26}$$

where (x_i, y_i) is the position of pedestrian i and (x_k, y_k) is the nearest point on the exit line of the chosen exit. This desired direction points from the position of pedestrian i at (x_i, y_i) to the nearest point on the exit line of the chosen exit. Pedestrian i is made to move towards the point (x_k, y_k).

In a complex domain with scattered obstacles, e.g. pillars, walls, forbidden areas, furnishings, the distance acquired from the construction above is no longer applicable. Many points x in the domain are not connected to a target by a direct path due to the presence of obstacles. The method to obtain the distance map to an exit in a simulation domain with internal obstacles is based on the scalar potential $T : \Omega \to R$ which T satisfies the Eikonal equation (1.4) as in the CA model. We set $T(x) = 0$, where x is a grid point on the exit line of the considered exit. The speed F is assigned to 1 for a walkable area and to $F \to 0$ for an area obstructed by obstacles [53]. We solve the Eikonal equation numerically using the fast marching method with a lattice spacing of $0.10m \times 0.10m$.

Once the solution T has been calculated, the pedestrians are assumed to move in opposite to the gradient of the scalar potential T as suggested by Hughes [45, 46]. Notice that the gradient ∇T drives outwards from the initial front Γ_0 due to the growth of T. Hence, the desired direction e_i^d , describing the preferred direction of motion of a pedestrian towards his target, is achieved from the negative gradient $-\nabla T$ which points towards the initial front Γ_0. For illustration, we suppose that pedestrian i selects Exit 1 to move out. Then his desired direction is given by the negative gradient potential of T, with initial front on the exit line at Exit 1 measured

at point (x_i, y_i) and

$$e_i^d(t) = -\frac{\nabla T_1(x_i, y_i)}{|\nabla T_1(x_i, y_i)|}, \tag{1.27}$$

where $T_1(x_i, y_i)$ is the scalar potential corresponding to the initial front at Exit 1 determined at point (x_i, y_i). Once the position of pedestrian i is not on the lattice points, the value of $-\nabla T_1(x_i, y_i)$ is obtained by employing linear interpolation.

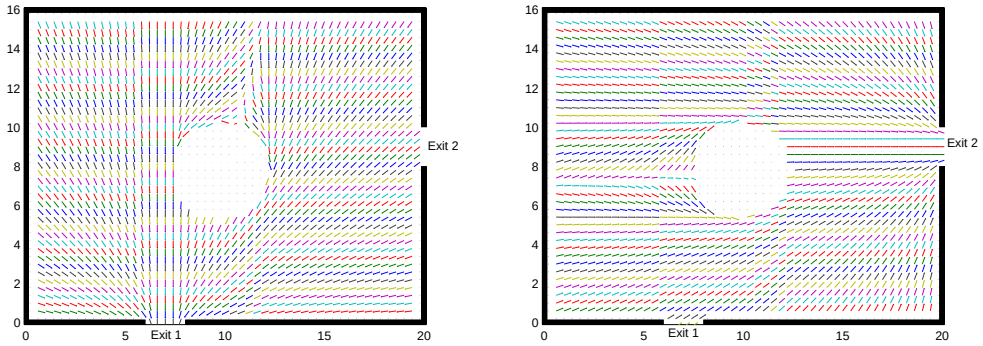

(a) Initial front at Exit 1 (b) Initial front at Exit 2

Figure 1.9: Negative gradient of the scalar potential plot corresponding to an exit in a room with circular obstacle.

Desired Speed

With the introduction of the degree of a pedestrian's impatience (1.2), the desired speed $v_i^d(t)$ can be varied according to his impatience level by the formula [34, 41]

$$v_i^d(t) = (1 - n_i(t))v_i(0) + n_i(t)v_i^{max}, \tag{1.28}$$

where $n_i(t)$ is the degree of a pedestrian's impatience, $v_i(0)$ is the initial speed and v_i^{max} is the maximum speed desired by pedestrian i. As a pedestrian is in a normal mood, $n_i(t)$ approximates 0 and the pedestrian's desired velocity approximates the initial speed. That means when an individual is in a normal mood, he prefers to walk with his initial speed. Once pedestrian is in an extremely impatient mood, $n_i(t)$ approximates 1 and the pedestrian's desired velocity increases to the maximum speed. That means he wishes to walk with maximum speed when he is greatly impatient.

Find Occupant Density (OD)

In the CA model, the cells in an exit area are marked at the beginning of the simulation. The occupant density of each exit is counted every time step by checking the state of the exit area cells, i.e. cell state=1 when a cell is occupied by a pedestrian and cell state=0 else. In the SF model, the occupant density (OD) of an exit in each time step is obtained by checking all pedestrians in the simulation if they are in the exit area, with two conditions as follows, see Figure 1.10.

1. $|B| <= r$, B is the vector pointing from the centre of the exit to position x_i of pedestrian i, r is the considered radius of an exit area,

2. $A \cdot B \geq 0$, vector A is perpendicular to the exit and points from the centre of the exit to a point on the semicircle of the exit area. This is used to ensure that the considering pedestrian i is in the room.

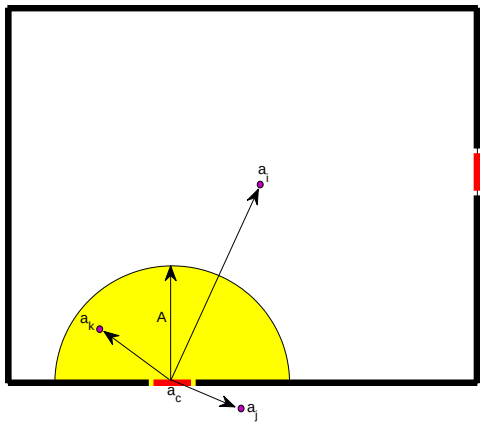

Figure 1.10: A room with 2 exits, the yellow half circle is the considered exit area

In Figure 1.10 a_c is the centre of the exit and A is an orthogonal vector to the exit which points from a_c to a point on the semicircle of the exit area. a_i, a_j and a_k are the positions of pedestrian i, j and k respectively. Pedestrian i is not in the defined exit area because of $|a_i - a_c| > |A|$. Since $A \cdot (a_j - a_c) < 0$, pedestrian j is not in the considered exit area. Pedestrian k on the other hand is in the exit area due to $|a_k - a_c| < |A|$ and $A \cdot (a_j - a_c) > 0$.

1.2.3 Extended Model

The unadventurous effect and the inertial effect in consideration of the social force model are modeled in the same way as they are considered in the cellular automata model. The differences and further details to model the group effect, the smoke spreading effect and the flow with the stream effect from the view point of the social force model, are expressed here.

1. **Group Effect**
   The movements of group members pass three steps as prescribed in the CA model. In the gathering stage, group members attempt to move towards the group centre. Hence, the desired moving direction e_i^d of the group member points towards the centre of the group and can be written as

$$e_i^d(t) = \frac{(x_{c-j}, y_{c-j}) - (x_i, y_i)}{|(x_{c-j}, y_{c-j}) - (x_i, y_i)|}, \tag{1.29}$$

   where (x_{c-j}, y_{c-j}) is the group center defined as in equation (1.12). The gathering continues until all of the members are in the neighbouring region. Once a group member is within the neighbouring region, he has to stop and wait until all group members are within this region. To make pedestrian i stop moving, his desired speed $(v_i^d(t))$ and his actual velocity $(v_i(t))$ in equation (1.22) are set to zero. When all members are within the neighbouring region, they select one exit to move out according to equation (1.10). Then they begin to egress along the direction of the selected exit and keep the group together. By random probability, as described in group effect of the CA model, some members move towards the group centre and some members move along the selected exit route. The desired direction of members who move towards the group centre is calculated in (1.29), while the desired direction of members who move along the selected exit route are represented by the equation (1.26).

   Remark 5. To stop the movement of pedestrian i, we need to set $v_i(t) = 0$. This would lead to a discontinuous $f_i^{soc}(t)$ since the denominator is zero. In order to avoid this situation, we can omit the anisotropic term in $f_i^{soc}(t)$, i.e. $(\lambda_i + (1-\lambda_i)\frac{1+\cos(\varphi_{ij})}{2})$ or set $\cos(\varphi_{ij}) = 0$.

2. **Smoke Spreading Effect**
Considering the smoke spreading effect, we simulate the individuals' temptation to move away from a high smoke density area and simultaneously move towards an exit to evacuate. The advection-diffusion equation (1.13), describing propagation of smoke, is coupled to the social force model. The route selection of a pedestrian is expressed by equation (1.7), which includes the distance, the occupant density, the degree of a pedestrian's impatience and the smoke density around the exit area.

To model the behaviour of a pedestrian that avoids moving to a high smoke density zone, the smoke force is added to the acceleration term of the social force model to push him away from the high smoke concentration cell (HC). The HC is defined in the same way as in the CA model, i.e. its smoke density is higher than the threshold smoke density μ_c. Therefore, considering the smoke spreading effect, we solve the following ODE system

$$\frac{dx_i}{dt} = v_i(t), \tag{1.30}$$

$$\frac{dv_i}{dt} = f_i^d(t) + \sum_{j \neq i}(f_{ij}^{soc}(t) + f_{ij}^{ph}(t)) + \sum_w f_{iw}(t) + \sum_s f_{is}, \tag{1.31}$$

where $f_i^d(t), f_{ij}^{soc}(t), f_{ij}^{ph}(t), f_{iw}(t)$ are defined as in equation (1.22), (1.23), (1.24) and (1.25) respectively. The smoke force f_{is} is given by

$$f_{is} = A_s \exp\left(((r_i + r_s) - d_{is})/B_s\right) n_{is}, \tag{1.32}$$

where A_s is the smoke interaction strength, B_s is the smoke range of repulsive interaction, r_i is the radius of a pedestrian and r_s is the radius of the high smoke concentration cell (HC). $d_{is} = |x_i - x_s|$ is the distance between pedestrian i's centre of mass and the centre x_s of the HC. $n_{is} = \frac{x_i - x_s}{d_{is}}$ is the normalized vector pointing from the HC's centre to pedestrian i.

The advection-diffusion equation (1.13) is solved numerically using the operator splitting method with a lattice spacing of size $0.4m \times 0.4m$. The size of time step to solve the advection-diffusion equation (1.13) is used the same as solving the ODE system (1.30-1.31). Thus, in each time step we obtain the information about the smoke density of every grid on the domain. This smoke density is used to determine the smoke

force (1.32) of each pedestrian. Positions and velocities of the pedestrians are updated every time step by solving equations (1.30 -1.31), considering smoke spreading effect.

The smoke force f_{is} decreases when the individual is far from the HC cell. It is the sum over all forces of the HCs that are near the pedestrian. The procedure to compute this force is as follows: For each time step,

(a) Find HC cells in the simulation domain.

(b) Check if pedestrian i is near any HCs, i.e. $|x_i - x_s| \leq d_\mu$, $d_\mu = 0.80m$ in our setting. If it is true, the smoke force is added to the acceleration term and summed over all HCs that are near him. Otherwise, $f_{is} = 0$.

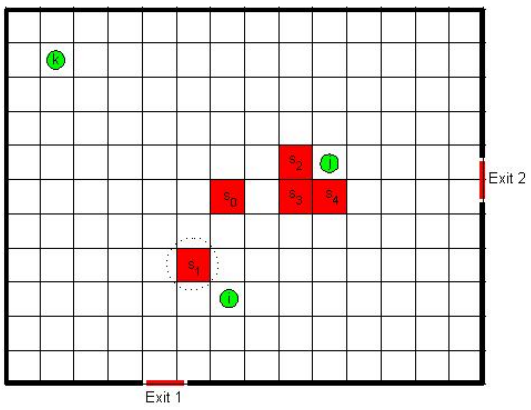

Figure 1.11: The red cells are high smoke concentration cells (HCs). The green circles are pedestrians.

In Figure 1.11 s_0, s_1, s_2, s_3 and s_4 are supposed to be high smoke concentration cells (HCs). The green circles are the pedestrians i, j and k. Pedestrian i receives the human-smoke repulsive force $f_{is} = f_{is_1}$ since he is near the cell s_1. This force pushes him away when he is close to the dotted circle around cell s_1. Pedestrian j is nearby the cells s_2, s_3 and s_4. Hence, the human-smoke repulsive force $f_{js} = f_{js_2} + f_{js_3} + f_{js_4}$ is applied to him. Pedestrian k is far from the high smoke concentration cells s_0, s_1, s_2, s_3, s_4. Therefore, he is not affected by the smoke and his smoke force is zero ($f_{ks} = 0$).

3. **Flow with the Stream Effect**
   To model the flow with the stream effect, the movement direction of a pedestrian in the social force model has to be specified. First, we write eight movement directions in Figure 1.6 as vectors: $d_1 = (0, 1)$, $d_2 = (1, 1)$, $d_3 = (1, 0)$, $d_4 = (1, -1)$, $d_5 = (0, -1)$, $d_6 = (-1, -1)$, $d_7 = (-1, 0)$, $d_8 = (-1, 1)$. $D = \{d_1, ..., d_8\}$. The movement direction of a pedestrian is the direction, $d_m \in D$, which yields the minimum regarding the angle between the movement direction ($d_m \in D$) and his desired direction $e_i^d(t)$. The angle between the two vectors is attained by the use of the dot product. Suppose that at time t pedestrian i is moving in direction $e_i^d(t)$, the movement direction of pedestrian i can be written as

$$md_i(t) = \min_{d_m \in D} \arccos\left(\frac{d_m \cdot e_i^d(t)}{|d_m|}\right), m = 1, ..., 8. \tag{1.33}$$

   If there is more than one movement direction that gives the minimum angle, one of them is chosen randomly. Once a pedestrian attains his movement direction, the procedure of considering the flow with the stream effect is the same as described in the CA model.

1.3 Numerical Method

This section is devoted to details and numerical methods to solve the Eikonal equation (1.4) and the advection-diffusion equation (1.13). We start with a brief introduction of the Eikonal equation and show a numerical scheme, which is applied to approximate its solutions. Then numerical solutions are compared with the exact solutions for different examples. Finally, details and numerical method to approximate the advection-diffusion equation are presented. The convergence of the proposed numerical method to solve the advection-diffusion equation is stated.

1.3.1 The Eikonal Equation

The Eikonal equation is a non linear first order hyperbolic partial differential equation of the form

$$\begin{aligned} |\nabla T(x)| &= \frac{1}{F(x)}, \quad x \in \Omega \\ T(x) &= 0, \quad x \in \Gamma_0 \subset \Omega \\ \text{Front} = \Gamma_t &= \{x | T(x) = t\}, \end{aligned} \tag{1.34}$$

where Ω is a bounded domain, $T(x)$ is the arrival time of front crossing the point x, Γ_0 is the initial front, Γ_t is the front at time t, $F(x) \geq 0$, which depends on the position of x, is a moving speed of the front and $|\cdot|$ is the Euclidean norm. The solution of this equation does not need to be differentiable, although smooth initial data is applied.

The Eikonal equation is applied in many fields of study, for example, in robot motion planing [54], in the shape from shading [52, 74], in path planning [52, 53, 60] and in segmentation [19].

Numerical Scheme

There exists several methods are applied to solve the Eikonal equation, for instance, the fast marching method [2, 31, 61, 79, 80], the fast marching level set method [77, 78], the fast sweeping method [31] and the fast iterative method [47]. The fast marching method (FMM) is a well-established and efficient numerical scheme to approximate the solution of the Eikonal equation, introduced by J.A. Sethian. The method is based on an entropy-satisfying upwind scheme.

The solution, which is obtained from the fast marching method, is constructed outwards from the boundary data, ordered from the smallest to the largest arrival time and used the upwind scheme to discretize equation (1.34). The procedure to solve the Eikonal equation is as follows:

1. Approximation Scheme
   The exact numerical result of the Eikonal equation (1.34) is due to a proper scheme used to approximate its gradient. One prominent choice, slightly different from the upwind scheme but more conductive, is the Godunov upwind [74, 79]. According to the Godunov upwind, the gradient is discretized in two dimensions as

   $$|\nabla T| \approx (\max(D^{-x}T_{i,j}, -D^{+x}T_{i,j}, 0)^2 + \max(D^{-y}T_{i,j}, -D^{+y}T_{i,j}, 0)^2)^{\frac{1}{2}},$$

   where the first order difference operators are

   $$D^{-x}T_{i,j} = \frac{T_{i,j} - T_{i-1,j}}{\Delta x}, \quad D^{+x}T_{i,j} = \frac{T_{i+1,j} - T_{i,j}}{\Delta x},$$
   $$D^{-y}T_{i,j} = \frac{T_{i,j} - T_{i,j-1}}{\Delta y}, \quad D^{+y}T_{i,j} = \frac{T_{i,j+1} - T_{i,j}}{\Delta y}.$$

   Hence, the Godunov upwind scheme approximation of the Eikonal

equation (1.34) is given by

$$\max(D^{-x}T_{i,j}, -D^{+x}T_{i,j}, 0)^2 + \max(D^{-y}T_{i,j}, -D^{+y}T_{i,j}, 0)^2 = (\frac{1}{F_{i,j}})^2, \tag{1.35}$$

2. Fast Marching Algorithm
   The FMM builds the solution outwards from boundary condition in downwind direction, i.e. from the smallest value of T to the largest one. It corresponds to the upwind difference structure of equation (1.35). The information propagates in one way from smaller to larger values. In the FMM, each grid point $T_{i,j}$ is in one of three categories:

   - *Accepted*: Set of all grid points which are known and will not be changed.
   - *Close*: Set of accepted grid points' neighbors.
   - *Far*: Set of grid points which are not in the Accepted or in the Close set.

   The algorithm of the fast marching method is demonstrated as following:

   (a) Initialize
   In first stage, we classify grid points in the domain as follows: Points at the initial front are in *Accepted*, their neighbors are in *Close* and other grid points are in *Far*. Then, value T of each grid point is:

   (a) $T_{i,j} = 0$, $\forall (i,j) \in$ *Accepted*

   (b) $T_{i,j}$ is obtained by solving equation (1.35), $\forall (i,j) \in$ *Close*.

   (c) $T_{i,j} = \infty$, $\forall (i,j) \in$ *Far*

   (b) Marching Forwards

   (a) Find the smallest arrival time grid point (i_{min}, j_{min}) in *Close*.

   (b) Add (i_{min}, j_{min}) to *Accepted* and remove it from *Close*.

   (c) Compute the arrival time of all neighbors of (i_{min}, j_{min}) that are not in *Accepted* by solving the quadratic equation (1.35). If a neighbor is in *Far*, remove it from that set and place it in *Close*.

   (d) If all nodes are not in *Accepted* set, return to (a).

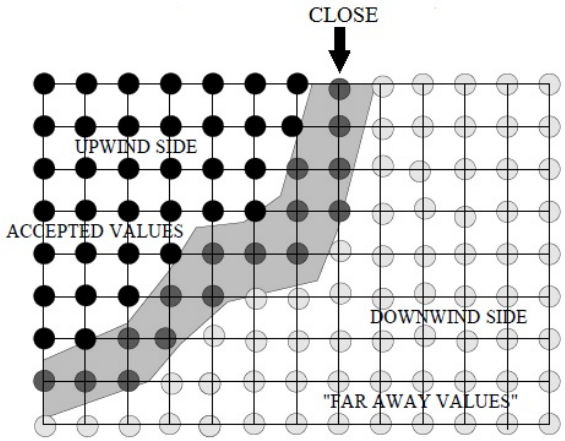

Figure 1.12: Upwind construction of accepted values [79]

Numerical Examples

In this section, we show the efficiency and accuracy of the fast marching method. To measure the accuracy, the following error functions are adopted as in the references [18, 24]

$$\text{Root mean square error:} \quad RMS = \frac{1}{L}\sqrt{\sum_{j=1}^{L}(\frac{T(j) - T_{exact}(j)}{T_{exact}(j)})^2}, \tag{1.36}$$

$$\text{Average absolute error:} \quad aerr = \sqrt{\frac{1}{L}\sum_{j=1}^{L}(T(j) - T_{exact}(j))^2}, \tag{1.37}$$

$$\text{Relative error:} \quad rerr = \sqrt{\frac{\sum_{j=1}^{L}(T(j) - T_{exact}(j))^2}{\sum_{j=1}^{L}(T_{exact}(j))^2}}, \tag{1.38}$$

where L is the number of nodes of the simulation domain, T_{exact} is analytical solution and T is the numerical solution computed from the fast marching method. In our numerical examples, we computed the numerical solution in a cartesian grid with different step size Δx, where Δx is the step size in x and y directions. The numerical solution is compared with the analytical solution. We also present error values which are measured by the error functions (1.36-1.38).

Example 1. In the first example, we consider the Eikonal equation (1.34) with $\Omega = [-1, 1] \times [-1, 1]$, $F(x, y) = 1$ and $\Gamma_0 = (0, 0)$. The exact solution is

$$T(x, y) = \sqrt{x^2 + y^2}.$$

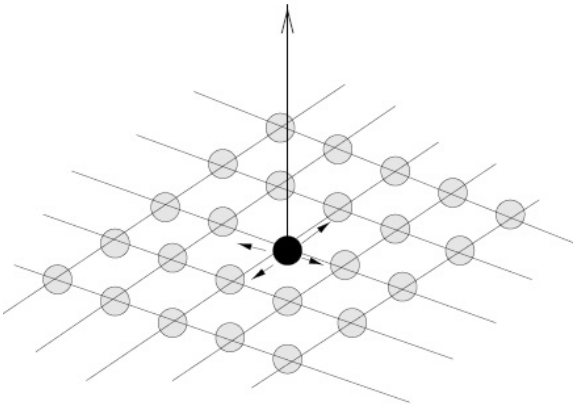

(a) Update 'Close'

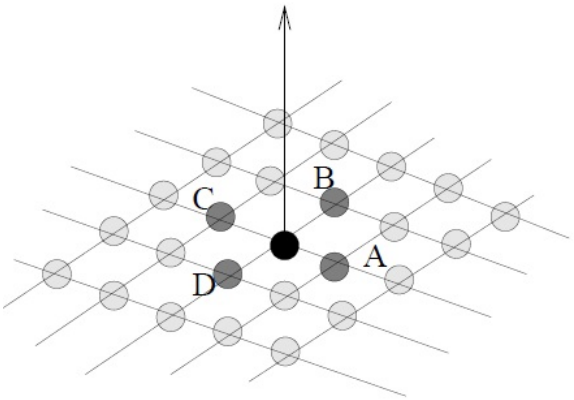

(b) Compute new possible values

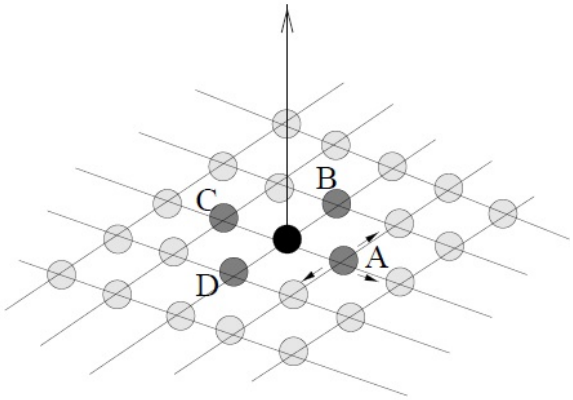

(c) Choose the smallest element in 'Close'(e.g. 'A')

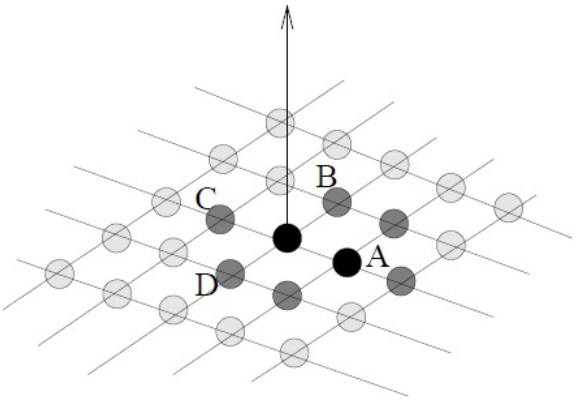

(d) Freeze the value at A and update neighbouring downwind points

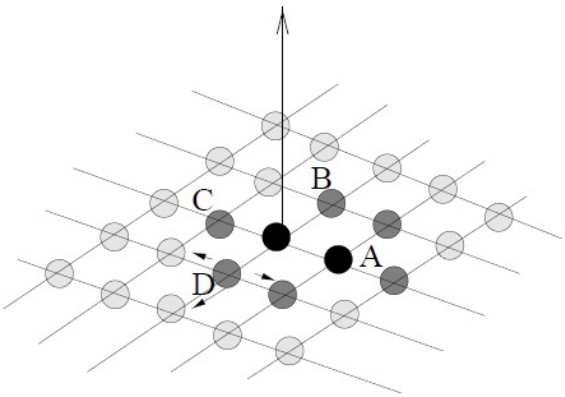

(e) Choose the smallest element in 'Close'(e.g. 'D')

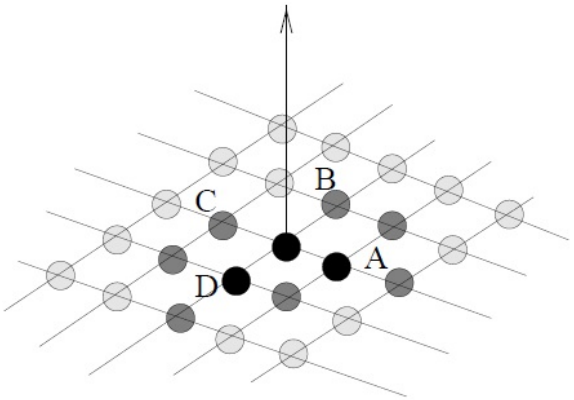

(f) Freeze the value at D and update neighbouring downwind points

Figure 1.13: Update procedure of the fast marching method [79].

The computation time, the root mean square errors, the average absolute errors and the relative errors for cartesian grids with different grid sizes are shown in Table 1.1. The plot of the exact solution and numerical solution is demonstrated in Figure 1.14. RMS and computation time versus number of nodes (L) plots are shown in Figure 1.15, 1.16 successively

Δx	L	Computation time (s)	RMS	$aerr$	$rerr$
0.1	441	0.193786	$3.30E$-03	$5.10E$-02	$5.96E$-02
0.05	1681	0.585955	$1.10E$-03	$3.21E$-02	$3.83E$-02
0.025	6561	2.712741	$3.79E$-04	$1.97E$-02	$2.38E$-02
0.0125	25921	16.879889	$1.20E$-04	$1.12E$-02	$1.43E$-02

Table 1.1: Computation time and error values for Example 1.

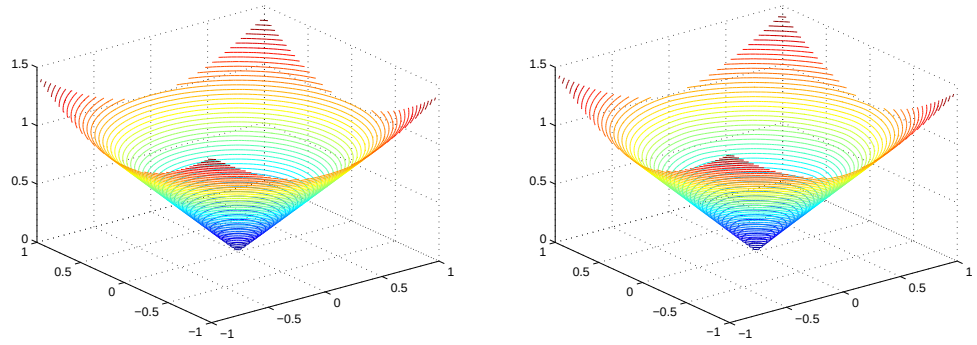

(a) Exact Solution (b) Numerical Solution

Figure 1.14: Solution description of Example 1.

Example 2. We consider the Eikonal equation (1.34) with $\Omega = [-1, 1] \times [-1, 1]$, $F(x, y) = 1$ and Γ_0 is a circle with centre at $(0, 0)$ and radius $R = 0.5$. The exact solution is

$$T(x, y) = |\sqrt{x^2 + y^2} - R|.$$

The computation time, the root mean square errors, the average absolute errors and the relative errors for cartesian grids with different grid space are shown in Table 1.2. The plot of the exact solution and the numerical solution is demonstrated in Figure 1.17.

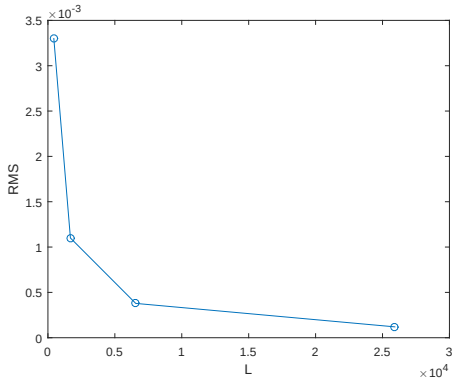

Figure 1.15: Root mean square error (RMS) plot for the Example 1.

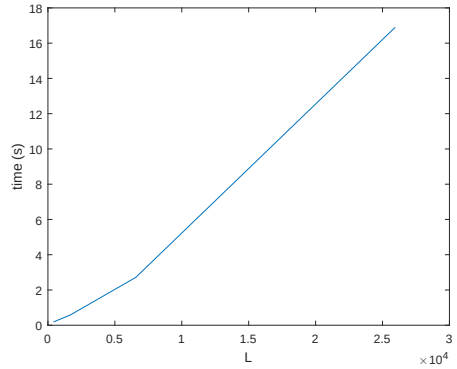

Figure 1.16: Computation time versus number of nodes plot for the Example 1.

Δx	L	Computation time (s)	RMS	$aerr$	$rerr$
0.1	441	0.202377	$4.59E$-02	$9.31E$-02	$2.19E$-01
0.05	1681	0.741481	$2.58E$-02	$9.01E$-02	$2.21E$-01
0.025	6561	3.611357	$1.38E$-03	$8.99E$-02	$2.26E$-01
0.0125	25921	20.749651	$7.70E$-03	$9.00E$-02	$2.29E$-01

Table 1.2: Computation time and error values for Example 2.

Example 3. The Eikonal equation (1.34) is considered with $\Omega = [-1,1]\times[-1,1]$, $F(x,y) = \frac{1}{\sqrt{x^2(1-y^2)+y^2(1-x^2)}}$ and $\Gamma_0 = \partial\Omega$. The exact solution is

$$T(x,y) = (1-x^2)(1-y^2).$$

The computation time, the root mean square errors, the average absolute

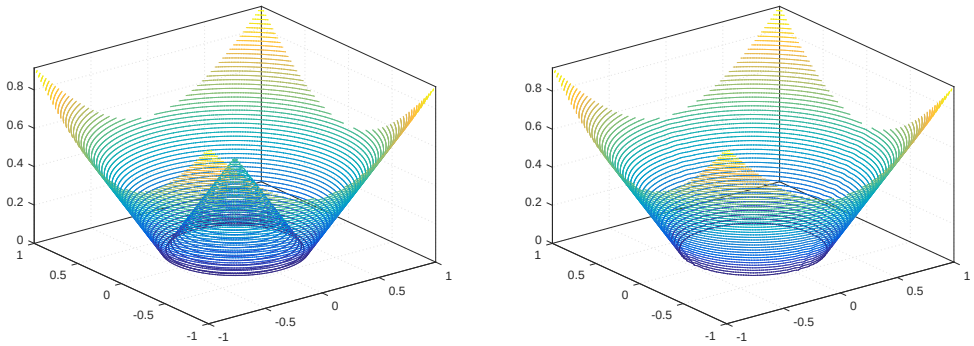

(a) Exact Solution (b) Numerical Solution

Figure 1.17: Solution description of Example 2.

errors and the relative errors for cartesian grids with different grid space are shown in Table 1.3. The plot of the exact solution and numerical solution is demonstrated in Figure 1.18.

Δx	L	Computation time (s)	RMS	$aerr$	$rerr$
0.1	441	0.135094	$2.46E$-02	$2.57E$-01	$5.07E$-01
0.05	1681	0.566002	$1.15E$-02	$2.54E$-01	$4.88E$-01
0.025	6561	2.773940	$5.60E$-03	$2.53E$-01	$4.80E$-01
0.0125	25921	17.783165	$2.80E$-03	$2.52E$-01	$4.76E$-01

Table 1.3: Computation time and error values for Example 3.

1.3.2 The Advection-Diffusion Equation

The advection-diffusion equation, which is a second-order partial differential equation of parabolic type, is expressed by [8]

$$\frac{\partial C}{\partial t} + w \cdot \nabla C = \kappa_d \nabla^2 C + S(c_s, t) \in \Omega \times \mathbb{R}^+, \tag{1.39}$$

with Dirichlet boundary conditions $C = 0$ on $\partial\Omega$, diffusion constant $\kappa_d > 0$, velocity field $w = (w_1, w_2) \in \mathbb{R}^2$, source term $S(c_s, t)$, $c_s = (x_s, y_s)$ is position of source and simulation domain $\Omega \subset \mathbb{R}^2$. The term $w \cdot \nabla C$ is the advection term and it is subject to the smoke concentration distribution being convected with velocity field w. $\kappa_d \Delta C$ is referred to the diffusion term, which

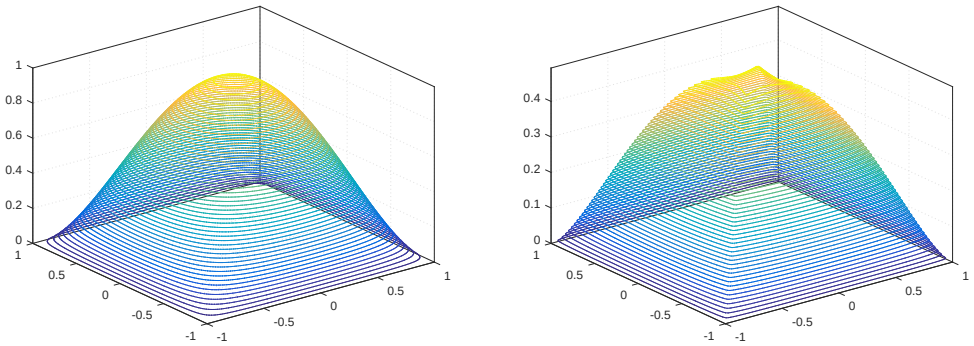

(a) Exact Solution (b) Numerical Solution

Figure 1.18: Solution description of Example 3.

is responsible for the spreading of the smoke concentration. The spread is a little dispersion when the diffusion coefficient is small.

Numerical Scheme

Various numerical techniques exist in literature to solve problems of the advection-diffusion equation for example, the finite difference method, the finite element method, the finite volume method, sprectral method and the method of lines. For our purpose, we apply the finite difference method to solve the advection-diffusion equation. Employing the explicit Euler algorithm for time-advancement scheme to the two dimensional advection-diffusion equation leads to severe stability restriction. If FTCS (Forward Time Central Space) discretization is used [26], following restriction has to be satisfied according to Hindmarsh et al. [26] to obtain a stable solution

$$s_x + s_y \leq \frac{1}{2}, \qquad \frac{[(w_1^t \Delta t)/\Delta x]^2}{s_x} + \frac{[(w_2^t \Delta t)/\Delta y]^2}{s_y} < 2,$$

where $s_x = (\kappa_d^t \Delta t)/\Delta x^2$ and $s_y = (\kappa_d^t \Delta t)/\Delta y^2$. Hence, the maximum allowable time step is

$$\Delta t \leq \min\left(\frac{1}{2\kappa_d^t} \frac{\Delta x^2 \Delta y^2}{\Delta x^2 + \Delta y^2}, \frac{2\kappa_d^t}{(w_1^t)^2 + (w_2^t)^2}\right).$$

To avoid this strictly limitation, we treated it implicitly by backward Euler for all terms. This leads to

$$C_{i,j}^{t+1} = C_{i,j}^{t} - \Delta t(w_1^{t+1}\frac{\partial C^{t+1}}{\partial x} + w_2^{t+1}\frac{\partial C^{t+1}}{\partial y} - \kappa_d^{t+1}\frac{\partial^2 C^{t+1}}{\partial x^2} - \kappa_d^{t+1}\frac{\partial^2 C^{t+1}}{\partial y^2}) + \Delta t S_{i,j}^{t}.$$

The disadvantage of this scheme is that it is expensive to solve numerically. We need to store a pentadiagonal matrix and require its inverse to obtain the solution. To reduce this difficulty, we apply the operator splitting method, which usually solves multidimensional problems efficiently. In two dimensions it is split into two parts. The x-direction and the y-direction are handled separately over two time steps. Accordingly, three implicit terms form a tridiagonal matrix and its inverse is required to obtain the solution for each direction. This is less computationally intense and easier to program compared to a pentadiagonal matrix. Thus we perform the operator splitting on the two-dimensional equation by writing them as

$$C_{i,j}^{*} = C_{i,j}^{t} - \Delta t(w_1^{*}\frac{\partial C^{*}}{\partial x} - \kappa_d\frac{\partial^2 C^{*}}{\partial x^2}), \tag{1.40}$$

$$C_{i,j}^{t+1} = C_{i,j}^{*} - \Delta t(w_2^{t+1}\frac{\partial C^{t+1}}{\partial y} - \kappa_d\frac{\partial^2 C^{t+1}}{\partial y^2}) + \Delta t S_{i,j}^{t}, \tag{1.41}$$

where

$$\frac{\partial C^{*}}{\partial x} = \frac{C_{i,j}^{*} - C_{i-1,j}^{*}}{\Delta x}, \quad \frac{\partial^2 C^{*}}{\partial x^2} = \frac{C_{i+1,j}^{*} - 2C_{i,j}^{*} + C_{i-1,j}^{*}}{\Delta x^2},$$
$$\frac{\partial C^{t+1}}{\partial y} = \frac{C_{i,j}^{t+1} - C_{i,j-1}^{t+1}}{\Delta y}, \quad \frac{\partial^2 C^{t+1}}{\partial y^2} = \frac{C_{i,j+1}^{t+1} - 2C_{i,j}^{t+1} + C_{i,j-1}^{t+1}}{\Delta y^2},$$

with Dirichlet boundary conditions:

$$C(0,y,t) = 0, \quad C(N_x,y,t) = 0, \quad C(x,0,t) = 0, \quad C(x,N_y,t) = 0,$$

and initial conditions given by

$$C(x,y,0) = Q_c\delta(x-x_s)\delta(y-y_s).$$

During the first stage, we solve equation (1.40) with a discretization of the advection by backward difference and the diffusion term by second order difference in space. In this stage C is known at all grid points (i,j) at time-level t but it is unknown at time-level *. Nonetheless, the unknown nodal values C^{*} are associated with the x-direction only, i.e. the value for j is

constant. After the rearrangement of C^* in equation (1.40), we obtain a system of equations

$$l_x C^*_{i-1,j} + d_x C^*_{i,j} + r_x C^*_{i+1,j} = C^t_{i,j},$$

where

$$l_x = -\frac{w_1^* \Delta t}{\Delta x} - \frac{\kappa_d \Delta t}{\Delta x^2}, \quad d_x = 1 + \frac{w_1^* \Delta t}{\Delta x} + 2\frac{\kappa_d \Delta t}{\Delta x^2}, \quad r_x = -\frac{\kappa_d \Delta t}{\Delta x^2}. \quad (1.42)$$

We write the equations out for $i = 1, ..., N_x - 1$:

$$\begin{aligned} l_x C^*_{0,j} + d_x C^*_{1,j} + r_x C^*_{2,j} &= C^t_{1,j} \\ l_x C^*_{1,j} + d_x C^*_{2,j} + r_x C^*_{3,j} &= C^t_{2,j} \\ &\vdots \\ l_x C^*_{N_x-2,j} + d_x C^*_{N_x-1,j} + r_x C^*_{N_x,j} &= C^t_{N_x-1,j}. \end{aligned} \quad (1.43)$$

The Dirichlet boundary conditions $C(0, y, t) = 0$ and $C(N_x, y, t) = 0$ are employed. Thus, we obtain the matrix of equations written for the unknown value $C^*_{i,j}$ as

$$\underbrace{\begin{pmatrix} 1 & & & & & & & \\ l_x & d_x & r_x & & & & & \\ & l_x & d_x & r_x & & & & \\ & & \cdot & & & & & \\ & & & \cdot & & & & \\ & & & & \cdot & & & \\ & & & & & l_x & d_x & r_x \\ & & & & & & & 1 \end{pmatrix}}_{L_x} \begin{pmatrix} C^*_{0,j} \\ C^*_{1,j} \\ C^*_{2,j} \\ C^*_{3,j} \\ \cdot \\ \cdot \\ \cdot \\ C^*_{N_x-1,j} \\ C^*_{N_x,j} \end{pmatrix} = \begin{pmatrix} 0 \\ C^t_{1,j} \\ C^t_{2,j} \\ C^t_{3,j} \\ \cdot \\ \cdot \\ \cdot \\ C^t_{N_x-1,j} \\ 0 \end{pmatrix}.$$

It is seen that the matrix L_x is strictly diagonally dominant and its inverse exists as proof in [22].Therefore, we can inverse the matrix L_x and obtain the intermediate solution $C^*_{i,j}$. The solution of the system (1.43) gives the solution $C^*_{i,j}$, $i = 1, ..., N_x - 1$ for only one value of j. Therefore, we solve the system of equations (1.43) for $C^*_{i,j}$, $i = 1, ..., N_x - 1$, for each row $j = 1, ..., N_y - 1$.

In the second stage we perform the similar procedure as in the first stage, but in y-direction. We solve equation (1.41) with discretization of the advection by backward difference and the diffusion term by second order difference in space. In this stage C is known at all grid points (i, j) at time-level $*$ but

it is unknown at the time-level $t+1$. However, the unknown nodal C^{t+1} are associated with the y-direction only, i.e. the value of i is constant. After rearrangement of C^{t+1} in equation (1.41), we obtain a system of equations:

$$l_y C_{i,j-1}^{t+1} + d_y C_{i,j}^{t+1} + r_y C_{i,j+1}^{t+1} = C_{i,j}^{*} + \Delta t S_{i,j}^{t},$$

where

$$l_y = -\frac{w_2^{t+1}\Delta t}{\Delta y} - \frac{\kappa_d \Delta t}{\Delta y^2}, \quad d_y = 1 + \frac{w_2^{t+1}\Delta t}{\Delta y} + 2\frac{\kappa_d \Delta t}{\Delta y^2}, \quad r_y = -\frac{\kappa_d \Delta t}{\Delta y^2}. \tag{1.44}$$

We write the equations out for $j = 1, ..., N_y - 1$

$$\begin{aligned} l_y C_{i,0}^{t+1} + d_y C_{i,1}^{t+1} + r_y C_{i,2}^{t+1} &= C_{i,1}^{*} + \Delta t S_{i,1}^{t} \\ l_y C_{i,1}^{t+1} + d_y C_{i,2}^{t+1} + r_y C_{i,3}^{t+1} &= C_{i,2}^{*} + \Delta t S_{i,2}^{t} \\ &\vdots \\ l_y C_{i,N_y-2}^{*} + d_y C_{i,N_y-1}^{*} + r_y C_{i,N_y}^{*} &= C_{i,N_y-1}^{*} + \Delta t S_{i,N_y-1}^{t}. \end{aligned} \tag{1.45}$$

The Dirichlet boundary conditions $C(x,0,t) = 0$ and $C(x,N_y,t) = 0$ are assumed. Then, we obtain the matrix of equations written for the unknown $C_{i,j}^{t+1}$ as

$$\underbrace{\begin{pmatrix} 1 & & & & & & & \\ l_y & d_y & r_y & & & & & \\ & l_y & d_y & r_y & & & & \\ & & \cdot & & & & & \\ & & & \cdot & & & & \\ & & & & \cdot & & & \\ & & & & & l_y & d_y & r_y \\ & & & & & & & 1 \end{pmatrix}}_{L_y} \begin{pmatrix} C_{i,0}^{t+1} \\ C_{i,1}^{t+1} \\ C_{i,2}^{t+1} \\ C_{i,3}^{t+1} \\ \cdot \\ \cdot \\ \cdot \\ C_{i,N_y-1}^{t+1} \\ C_{i,N_y}^{t+1} \end{pmatrix} = \begin{pmatrix} 0 + \Delta t S_{i,0}^{t} \\ C_{i,1}^{*} + \Delta t S_{i,1}^{t} \\ C_{i,2}^{*} + \Delta t S_{i,2}^{t} \\ C_{i,3}^{*} + \Delta t S_{i,3}^{t} \\ \cdot \\ \cdot \\ \cdot \\ C_{i,N_y-1}^{*} + \Delta t S_{i,N_y-1}^{t} \\ 0 + \Delta t S_{i,N_y}^{t} \end{pmatrix}.$$

Since matrix L_y is strictly diagonal dominant, we can inverse the matrix L_y and obtain the solution $C_{i,j}^{t+1}$. The solution of the system (1.45) gives the solution $C_{i,j}^{t+1}$, $j = 1, ..., N_y - 1$ for only one value of i. To obtain the solution for all grid points in the simulation domain, we solve the system of equations (1.45) for $C_{i,j}^{t+1}$, $j = 1, ..., N_y - 1$, for each column $i = 1, ..., N_x - 1$.

The convergence of the proposed method to solve the advection-diffusion equation (1.39) can be assured by the Lax-Richtmyer equivalence theorem [83].

It is the fundamental theorem of finite difference methods. Below we give a definition of consistency and stability of a numerical method. Then we state the Lax-Richtmyer equivalence theorem. After that we prove that the operator splitting method (1.40-1.41) which is used to approximate the advection-diffusion equation (1.39) is convergent.

Definition 1.3.1 (Consistency)**.** [27] A finite difference scheme $L_h\phi(x_i) = f(x_i)$ is said to be *consistent* with the partial differential equation $L\phi(x) = f(x)$, if for any sufficiently smooth solution ϕ of this equation the truncation error of the scheme, corresponding to the vector $\epsilon_h \in \mathbb{R}$ whose components are defined as

$$(\epsilon_h)_i = L_h\phi(x_i) - L\phi(x_i), \quad \forall i \in \{1, ..., N_x\}$$

tends uniformly towards zero when h tends to zero, i.e. if

$$\lim_{h\to 0} |\epsilon_h|_\infty = 0.$$

Moreover, if there exists a constant $c > 0$, independent of ϕ and of its derivatives, such that, for all $h \in [0, h_0], h_0 > 0$ we have

$$|\epsilon_h| \leq ch^p,$$

then the scheme is said to be accurate at the order p for the norm $|\cdot|$.

Definition 1.3.2 (Von Neumann Stability)**.** [14] A numerical method is said to be stable in the sense of von Neumann Stability if the amplification factor G does not grow in time, i.e.

$$|G| = \frac{|Z_m^{t+1}|}{|Z_m^t|} \leq 1, \quad \forall \theta_m,$$

where Z_m^t is the amplitude of the mth harmonic of the numerical error in a Fourier series

$$a(x_i, t) = \sum_{m=-M_x}^{M_x} Z_m^t e^{I\theta_m i},$$

where $x_i = i\Delta x$, i is the mesh index ranging from 0 to M_x, $I = \sqrt{-1}$, $\theta_m = m\frac{\pi}{M_x}$ is represented as a phase angle.

Theorem 1 (Lax Equivalence Theorem)**.** *[55] For a consistent finite difference scheme approximation to a well posed linear initial value problem, stability is equivalent to convergence.*

Lemma 2. *The operator splitting method given by equation (1.40-1.41) , approximating the advection-diffusion equation (1.39), is convergent.*

Proof. To apply the Lax equivalence theorem, we show that the operator splitting method (1.40-1.41) is consistent and stable:

1. Consistency: Let L be the advection-diffusion operator and L_h be the operator splitting to approximate the advection-diffusion equation. First, pluging C^* in equation (1.40) to (1.41), we have the operator splitting method written as

$$\begin{aligned}\frac{C_{i,j}^{t+1}-C_{i,j}^{t}}{\Delta t} = -[w_1^*(\frac{C_{i,j}^{*}-C_{i-1,j}^{*}}{\Delta x}) - \kappa_d(\frac{C_{i+1,j}^{*}-2C_{i,j}^{*}+C_{i-1,j}^{*}}{\Delta x^2}) \\ +w_2^{t+1}(\frac{C_{i,j}^{t+1}-C_{i,j-1}^{t+1}}{\Delta x}) - \kappa_d(\frac{C_{i,j+1}^{t+1}-2C_{i,j}^{t+1}+C_{i,j-1}^{t+1}}{\Delta y^2})+ \\ S_{i,j}^{t}].\end{aligned} \tag{1.46}$$

Then we write the advection-diffusion equation as

$$LC = C_t + w\cdot\nabla C - \kappa_d\nabla^2 C - S. \tag{1.47}$$

The operator splitting method approximating the advection-diffusion equation is written as

$$\begin{aligned}L_hC = \frac{C_{i,j}^{t+1}-C_{i,j}^{t}}{\Delta t} + w_1^*(\frac{C_{i,j}^{*}-C_{i-1,j}^{*}}{\Delta x}) - \kappa_d(\frac{C_{i+1,j}^{*}-2C_{i,j}^{*}+C_{i-1,j}^{*}}{\Delta x^2}) \\ +w_2^{t+1}(\frac{C_{i,j}^{t+1}-C_{i,j-1}^{t+1}}{\Delta x}) - \kappa_d(\frac{C_{i,j+1}^{t+1}-2C_{i,j}^{t+1}+C_{i,j-1}^{t+1}}{\Delta y^2}) - S_{i,j}^{t},\end{aligned}$$

where $C_{i,j}^{t} = C(t\Delta t, i\Delta x, j\Delta y)$. We begin by taking the Taylor expansion of the function C in t, x and y about (t_t, x_i, y_j). We have

$$\begin{aligned}C_{i,j}^{t+1} &= C_{i,j}^{t} + \Delta t C_t + \frac{1}{2}\Delta t^2 C_{tt} + \mathcal{O}(\Delta t^3),\\ C_{i-1,j}^{*} &= C_{i,j}^{*} - \Delta x C_x + \frac{1}{2}\Delta x^2 C_{xx} - \frac{1}{6}\Delta x^3 C_{xxx} + \mathcal{O}(\Delta x^4),\\ C_{i+1,j}^{*} &= C_{i,j}^{*} + \Delta x C_x + \frac{1}{2}\Delta x^2 C_{xx} + \frac{1}{6}\Delta x^3 C_{xxx} + \mathcal{O}(\Delta x^4),\\ C_{i,j-1}^{t+1} &= C_{i,j}^{t+1} - \Delta y C_y - \frac{1}{2}\Delta y^2 C_{yy} - \frac{1}{6}\Delta x^3 C_{yyy} + \mathcal{O}(\Delta y^4),\\ C_{i,j+1}^{t+1} &= C_{i,j}^{t+1} + \Delta y C_y + \frac{1}{2}\Delta y^2 C_{yy} + \frac{1}{6}\Delta x^3 C_{yyy} + \mathcal{O}(\Delta y^4).\end{aligned}$$

This gives us

$$\begin{aligned}
L_hC &= C_t + \frac{1}{2}\Delta t C_{tt} + \mathcal{O}(\Delta t^2) + w_1^*(C_x - \frac{1}{2}\Delta x C_{xx} + \mathcal{O}(\Delta x^2)) - \\
&\quad \kappa_d(C_{xx} + \mathcal{O}(\Delta x^2)) + w_2^{t+1}(C_y - \frac{1}{2}\Delta y C_{yy} + \mathcal{O}(\Delta y^2)) - \\
&\quad \kappa_d(C_{yy} + \mathcal{O}(\Delta y^2)) - S_{i,j}^t \\
&= C_t + w \cdot \nabla C - \kappa_d \nabla^2 C - S_{i,j}^t + \frac{1}{2}\Delta t C_{tt} + \mathcal{O}(\Delta t^2) - \\
&\quad w_1^*(\frac{1}{2}\Delta x C_{xx} - \mathcal{O}(\Delta x^2)) - w_2^{t+1}(\frac{1}{2}\Delta y C_{yy} - \mathcal{O}(\Delta y^2)) - \\
&\quad \kappa_d \mathcal{O}(\Delta x^2) - \kappa_d \mathcal{O}(\Delta y^2),
\end{aligned}$$

where $w = (w_1^*, w_2^{t+1})$. Hence

$$\begin{aligned}
\epsilon_h(t_t, x_i, y_j) &= L_hC(t_t, x_i, y_j) - LC(t_t, x_i, y_j) \\
&= \frac{1}{2}\Delta t C_{tt} + \mathcal{O}(\Delta t^2) - w_1^*(\frac{1}{2}\Delta x C_{xx} - \mathcal{O}(\Delta x^2)) - \\
&\quad w_2^{t+1}(\frac{1}{2}\Delta y C_{yy} - \mathcal{O}(\Delta y^2)) - \kappa_d \mathcal{O}(\Delta x^2) - \kappa_d \mathcal{O}(\Delta y^2).
\end{aligned}$$

for $(\Delta t, \Delta x, \Delta y) \to 0$ we have $|\epsilon_h|_\infty \to 0$. Thus, the operator splitting scheme (1.40-1.41) which approximates the advection-diffusion equation (1.39) is consistent.

2. Stability:
Let $\overline{C_{i,j}^t}$ be the exact solution of the difference equation and $C_{i,j}^t$ be the actual computed solution of the difference equation which may have errors due to round-off or from initial data. Hence, we have

$$C_{i,j}^t = \overline{C_{i,j}^t} + a_{i,j}^t, \tag{1.48}$$

where $a_{i,j}^t$ is the error at time level t in mesh point (i, j). We insert equation (1.48) into (1.40) and (1.41). Then we have

$$\begin{aligned}
\frac{\overline{C_{i,j}^*} - \overline{C_{i,j}^t}}{\Delta t} + \frac{a_{i,j}^* - a_{i,j}^t}{\Delta t} &= -[w_1^*(\frac{\overline{C_{i,j}^*} - \overline{C_{i-1,j}^*}}{\Delta x} + \frac{a_{i,j}^* - a_{i-1,j}^*}{\Delta x}) \\
&\quad -\kappa_d(\frac{\overline{C_{i+1,j}^*} - 2\overline{C_{i,j}^*} + \overline{C_{i-1,j}^*}}{\Delta x^2} + \frac{a_{i+1,j}^* - 2a_{i,j}^* + a_{i-1,j}^*}{\Delta x^2})],
\end{aligned} \tag{1.49}$$

$$\begin{aligned}
\frac{\overline{C_{i,j}^{t+1}} - \overline{C_{i,j}^*}}{\Delta t} + \frac{a_{i,j}^{t+1} - a_{i,j}^*}{\Delta t} &= -[w_2^{t+1}(\frac{\overline{C_{i,j}^{t+1}} - \overline{C_{i,j-1}^{t+1}}}{\Delta x} + \frac{a_{i,j}^{t+1} - a_{i,j-1}^{t+1}}{\Delta x}) \\
&\quad -\kappa_d(\frac{\overline{C_{i,j+1}^{t+1}} - 2\overline{C_{i,j}^{t+1}} + \overline{C_{i,j-1}^{t+1}}}{\Delta y^2} + \frac{a_{i,j+1}^{t+1} - 2a_{i,j}^{t+1} + a_{i,j-1}^{t+1}}{\Delta y^2}) + S_{i,j}^t].
\end{aligned} \tag{1.50}$$

$\overline{C^t_{i,j}}$, and $\overline{C^*_{i,j}}$ in equation (1.49) satisfy exactly equation (1.40) and $\overline{C^*_{i,j}}$, and $\overline{C^{t+1}_{i,j}}$ in equation (1.50) fulfill exactly equation (1.41). Therefore, we obtain the equations for errors $a^t_{i,j}, a^*_{i,j}$ and $a^{t+1}_{i,j}$ as

$$\frac{a^*_{i,j} - a^t_{i,j}}{\Delta t} = -[w^*_1(\frac{a^*_{i,j} - a^*_{i-1,j}}{\Delta x}) - \kappa_d(\frac{a^*_{i+1,j} - 2a^*_{i,j} + a^*_{i-1,j}}{\Delta x^2})], \quad (1.51)$$

$$\frac{a^{t+1}_{i,j} - a^*_{i,j}}{\Delta t} = -[w^{t+1}_2(\frac{a^{t+1}_{i,j} - a^{t+1}_{i,j-1}}{\Delta y}) - \kappa_d(\frac{a^{t+1}_{i,j+1} - 2a^{t+1}_{i,j} + a^{t+1}_{i,j-1}}{\Delta y^2})]. \quad (1.52)$$

We decompose the errors into a Fourier series. Since the difference equation for an error is linear, it is adequate to consider the growth of the error of a single harmonic, i.e.

$$a^t_{i,j} = Z^t e^{I\theta_x i} e^{I\theta_y j}. \quad (1.53)$$

Substituting (1.53) into (1.51) and (1.52), we attain

$$\frac{Z^* e^{I\theta_x i} e^{I\theta_y j} - Z^t e^{I\theta_x i} e^{I\theta_y j}}{\Delta t} = -[w^*_1(\frac{Z^* e^{I\theta_x i} e^{I\theta_y j} - Z^* e^{I\theta_x (i-1)} e^{I\theta_y j}}{\Delta x}) - \kappa_d(\frac{Z^* e^{I\theta_x (i+1)} e^{I\theta_y j} - 2Z^* e^{I\theta_x i} e^{I\theta_y j} + Z^* e^{I\theta_x (i-1)} e^{I\theta_y j}}{\Delta x^2})], \quad (1.54)$$

$$\frac{Z^{t+1} e^{I\theta_x i} e^{I\theta_y j} - Z^* e^{I\theta_x i} e^{I\theta_y j}}{\Delta t} = -[w^{t+1}_2(\frac{Z^{t+1} e^{I\theta_x i} e^{I\theta_y j} - Z^{t+1} e^{I\theta_x i} e^{I\theta_y (j-1)}}{\Delta y}) - \kappa_d(\frac{Z^{t+1} e^{I\theta_x i} e^{I\theta_y (j+1)} - 2Z^{t+1} e^{I\theta_x i} e^{I\theta_y j} + Z^{t+1} e^{I\theta_x i} e^{I\theta_y (j-1)}}{\Delta y^2})]. \quad (1.55)$$

Divided equations (1.54) and (1.55) by $e^{I\theta_x i} e^{I\theta_y j}$ we have

$$\frac{Z^* - Z^t}{\Delta t} = -[w^*_1(\frac{Z^* - Z^* e^{-I\theta_x}}{\Delta x}) - \kappa_d(\frac{Z^* e^{I\theta_x} - 2Z^* + Z^* e^{-I\theta_x}}{\Delta x^2})], \quad (1.56)$$

$$\frac{Z^{t+1} - Z^*}{\Delta t} = -[w^{t+1}_2(\frac{Z^{t+1} - Z^{t+1} e^{-I\theta_y}}{\Delta y}) - \kappa_d(\frac{Z^{t+1} e^{I\theta_y} - 2Z^{t+1} + Z^{t+1} e^{-I\theta_y}}{\Delta y^2})]. \quad (1.57)$$

Rearranging equations (1.56) and (1.57) we attain

$$\frac{Z^*}{Z^t} = \frac{1}{l_x e^{-I\theta_x} + d_x + r_x e^{I\theta_x}}, \tag{1.58}$$

$$\frac{Z^{t+1}}{Z^*} = \frac{1}{l_y e^{-I\theta_y} + d_y + r_y e^{I\theta_y}}, \tag{1.59}$$

where l_x, d_x, r_x are given as in (1.42) and l_y, d_y, r_y are defined as in (1.44). Multiplying equations (1.58) and (1.59) gives us

$$\frac{Z^{t+1}}{Z^t} = (\frac{1}{l_x e^{-I\theta_x} + d_x + r_x e^{I\theta_x}})(\frac{1}{l_y e^{-I\theta_y} + d_y + r_y e^{I\theta_y}}). \tag{1.60}$$

The stability condition of the operator splitting method (1.40-1.41) will be satisfied if the amplitude factor

$$\begin{aligned} |G| &= |\frac{Z^{t+1}}{Z^t}| \\ &= |(\frac{1}{l_x e^{-I\theta_x} + d_x + r_x e^{I\theta_x}})(\frac{1}{l_y e^{-I\theta_x} + d_y + r_y e^{I\theta_x}})| \\ &= |(\frac{1}{l_x e^{-I\theta_y} + d_x + r_x e^{I\theta_y}})||(\frac{1}{l_y e^{-I\theta_y} + d_y + r_y e^{I\theta_y}})| \leq 1, \end{aligned}$$

i.e. we have to show that $|l_x e^{-I\theta_x} + d_x + r_x e^{I\theta_x}| \geq 1$ and $|l_y e^{-I\theta_y} + d_y + r_y e^{I\theta_y}| \geq 1$. First we consider the term $|l_x e^{-I\theta_x} + d_x + r_x e^{I\theta_x}|$ and let $b_1 = \frac{w_1^* \Delta t}{\Delta x}$, $b_2 = \frac{\kappa_d \Delta t}{\Delta x^2}$. Note that $l_x = -b_1 - b_2, r_x = -b_2$, and $d_x = 1 + b_1 + 2b_2,$. Then we write

$$\begin{aligned} |l_x e^{-I\theta_x} + d_x + r_x e^{I\theta_x}| &= |l_x(\cos\theta_x - I\sin\theta_x) + d_x + \\ &\quad r_x(\cos\theta_x + I\sin\theta_x)| \\ &= |(-b_1 - b_2)(\cos\theta_x - I\sin\theta_x) + d_x - \\ &\quad b_2(\cos\theta_x + I\sin\theta_x)| \\ &= |d_x - (b_1 + 2b_2)\cos\theta_x + b_1 I\sin\theta_x| \\ &= \sqrt{\underbrace{[d_x - (b_1 + 2b_2)\cos\theta_x]^2 + (b_1\sin\theta_x)^2}_{A_x}}, \end{aligned}$$

$$A_x = d_x^2 \underbrace{-2d_x(b_1 + 2b_2)\cos\theta_x}_{a} \underbrace{+(b_1 + 2b_2)^2\cos^2\theta_x + b_1^2\sin^2\theta_x}_{c}.$$

Now let us consider d_x^2, a and c.

$$\begin{aligned}
d_x^2 &= (1 + b_1 + 2b_2)^2 \\
&= 1 + 2(b_1 + 2b_2) + (b_1 + 2b_2)^2 \\
&= 1 + 2(b_1 + 2b_2) + b_1^2 + 4b_1b_2 + 4b_2^2. \\
a &= -2(1 + b_1 + 2b_2)(b_1 + 2b_2)\cos\theta_x \\
&= -2(b_1 + 2b_2)\cos\theta_x - 2(b_1^2 + 4b_1b_2 + 4b_2^2)\cos\theta_x \\
&= \underbrace{-2(b_1 + 2b_2)\cos\theta_x}_{a_1}\underbrace{-2b_1^2\cos\theta_x}_{a_2}\underbrace{-2(4b_1b_2 + 4b_2^2)\cos\theta_x}_{a_3}. \\
c &= (b_1^2 + 4b_1b_2 + 4b_2^2)\cos^2\theta_x + b_1^2\sin^2\theta_x \\
&= b_1^2 + (4b_1b_2 + 4b_2^2)\cos^2\theta_x.
\end{aligned}$$

Summing between d_x^2 and c, we have

$$d_x^2 + c = 1 + \underbrace{2(b_1 + 2b_2)}_{d_1} + \underbrace{2b_1^2}_{d_2} + \underbrace{(4b_1b_2 + 4b_2^2)(1 + \cos^2\theta_x)}_{d_3}.$$

Comparing each term of a and each term of $d_x^2 + c$, we receive $d_1 \geq a_1$ and $d_2 \geq a_2$ because of $-1 \leq \cos\theta_x \leq 1$. It remains to show that $1 + \cos^2\theta_x \geq 2\cos\theta_x$. Since

$$\begin{aligned}
(1 - \cos\theta_x)^2 &\geq 0 \\
1 - 2\cos\theta_x + \cos^2\theta_x &\geq 0 \\
1 + \cos^2\theta_x &\geq 2\cos\theta_x.
\end{aligned}$$

So we have $A_x = d_x^2 + c + a \geq 1$ and therefore $|l_x e^{-I\theta_x} + d_x + r_x e^{I\theta_x}| \geq 1$. Proof in the same way we also have $|l_y e^{-I\theta_y} + d_y + r_y e^{I\theta_y}| \geq 1$. Hence the operator splitting method (1.40-1.41) approximating the advection-diffusion equation (1.39) is unconditionally stable.

Applying the Lax equivalence theorem 1, we attain that the operator splitting method (1.40-1.41) that approximates the advection-diffusion equation (1.39) is convergent. ■

Table 1.4 shows the computation times and the errors in L^1 norm for the numerical solutions of the advection-diffusion equation on the domain $\Omega = [-1, 1] \times [-1, 1]$. The advection-diffusion equation is solved by the operator splitting method in a cartesian grid with different step size Δx, where Δx is the step size in x and y directions. L is the number of nodes of the simulation domain. The total time is set to $10s$ and time step is $\Delta t = 0.02$. The smoke source emits with a constant rate $Q_c = 0.1[g/s]$ at

the centre of the domain. The velocity field is $(w_1, w_2) = (0.2, 0)$ and the diffusion coefficient has value 0.05. We compute the L^1-error as the difference between the solution with two different grid spacings:

$$\int_0^t \int_{-1}^1 \int_{-1}^1 |C_{\Delta x}(s,x,y) - C_{\frac{\Delta x}{2}}(s,x,y)| dx dy ds \approx$$
$$\sum_k \sum_i \sum_j |C_{\Delta x}(s_k, x_i, y_j) - C_{\frac{\Delta x}{2}}(s_k, x_i, y_j)| (\Delta x)^2 \Delta t.$$

Δx	L	Computation time (s)	L^1-error
0.1	441	1.4062	$2.84E$-02
0.05	1681	4.2755	$7.20E$-03
0.025	6561	17.9067	$1.80E$-03
0.0125	25921	63.2908	$4.48E$-04

Table 1.4: Computation time and error values with different space grid sizes for the numerical solutions of the advection-diffusion equation.

Figure 1.19 shows the smoke concentration which is obtained from solving the advection-diffusion equation applied with the operator splitting method at time $0.29s$ and $22.62s$. It can be observed that the smoke spreads out as time increases. The evolution of the smoke propagation with different settings of the velocity field is displayed in Figure 1.20. The spreading direction of the smoke is controlled by the velocity field. The smoke expands to the right when the velocity field is set to $w_1 = 0.5, w_2 = 0$, to the north when the velocity field is $w_1 = 0, w_2 = 0.5$ and in all direction when the velocity field is chosen randomly in the interval $[-0.5, 0.5]$.

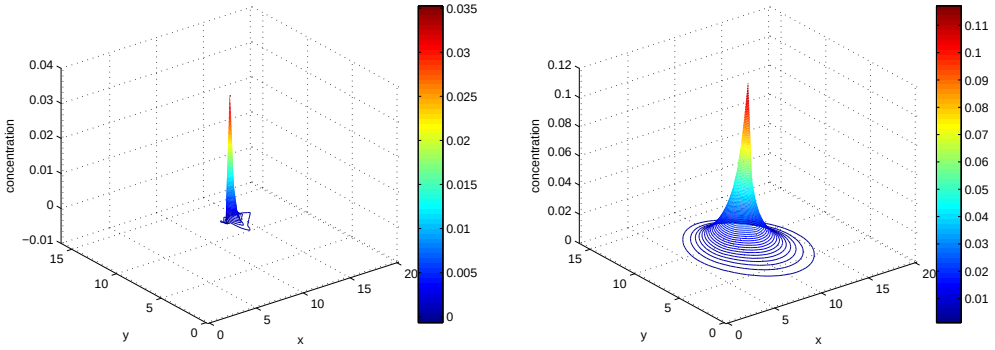

(a) t=0.29s (b) t=22.62s

Figure 1.19: Smoke concentration from a single source point which emits smoke with a constant rate $Q = 0.1[g/s]$. The velocity field (w_1, w_2) is chosen randomly in the interval [-0.5,0.5]

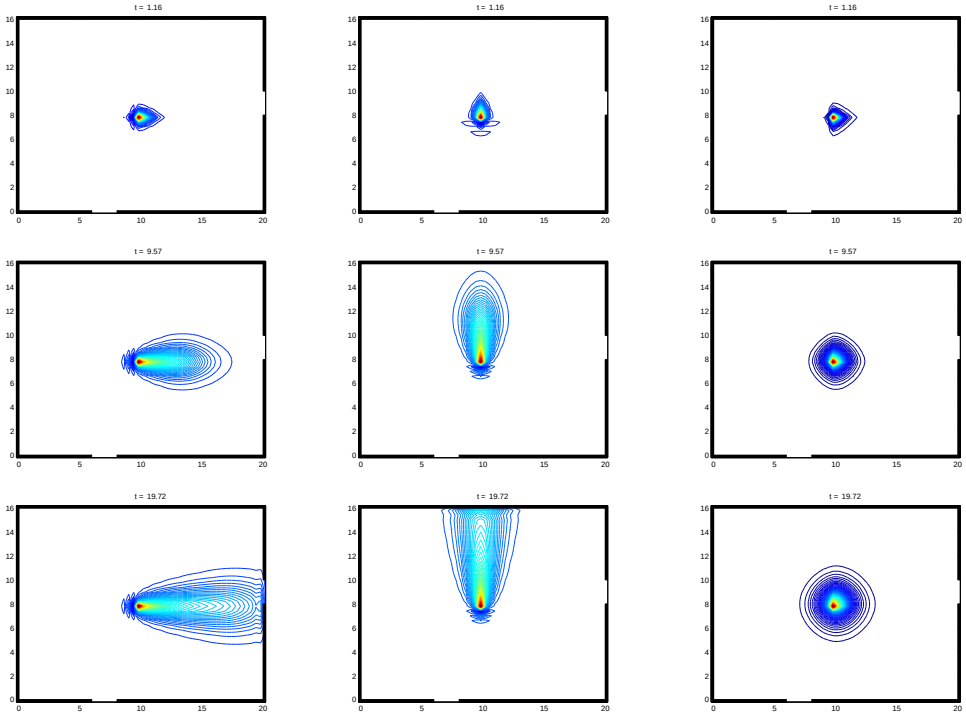

(a) $w_1 = 0.5, w_2 = 0$ (b) $w_1 = 0, w_2 = 0.5$ (c) $(w_1, w_2) \in [-0.5, 0.5]$

Figure 1.20: Smoke propagation for different settings of the velocity field with constant emitting rate $Q = 0.1[g/s]$

1.4 Numerical Results

In this section we present the computational comparisons between the cellular automata model and the social force model in two dimensions. Exclusively, it comprises of following features:

- Unadventurous and Group Effect.
- Inertial Effect.
- Smoke Spreading Effect.
- Flow with the Stream Effect.
- Obstacle Effect.
- No Effect.

The numerical experiments on the unadventurous and the group effect, the inertial effect, the smoke spreading effect and the flow with the stream effect are performed with 300 pedestrians randomly distributed in the room at the initial time of the simulation. The modeling area is a rectangular ($16m \times 20m$) with two exits which are located at the bottom and on the right of the room. The exits are labeled Exit 1 and Exit 2 respectively. The width of each exit is set to $2m$, see Figure 1.21. To model the obstacle effect, 300 pedestrians are randomly allocated on top of the room at the initial time. The modeling area is a square of size $20m \times 20m$. Two exits are located at the bottom of the room and their widths are $2m$. Different obstacle placements in the room are shown in Figure 1.37 and Figure 1.42.

The simulation domain of the cellular automata model is meshed into grid cells. Each cell has a size of $0.4m \times 0.4m$ which is the typical space occupied by a person in a dense area [67, 92, 95]. Thus, the average movement of an individual in each time step is $0.48m$ (pararell movement $0.4m$ or diagonal movement $0.4\sqrt{2}$). As the average velocity of pedestrians in a nervous state is about $1.65m/s$ [41, 93], one time step in the CA model is $0.29s$.The explicit Euler method is applied to solve the social force model with fixed time step of size 0.02. The initial velocities of the pedestrians are randomly chosen and the initial desired speed $v_i^d(0)$ is set to $1.65m/s$.

Since our models are non-deterministic approaches, different trial runs will present different results. Therefore, to obtain more general results, ten trial runs are performed for the same example and their average is used. The

model parameters, used in evacuation simulations, are given as in Table 1.5. All simulations programs are implemented in MATLAB.

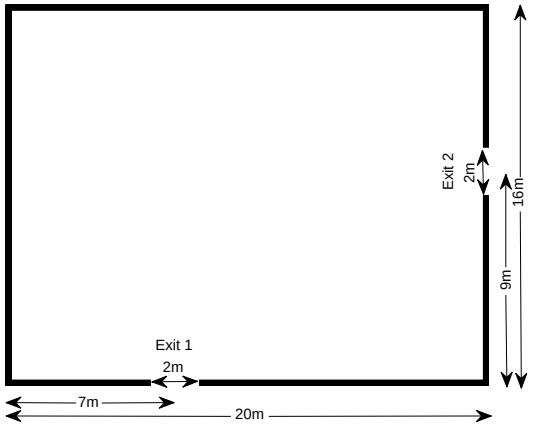

Figure 1.21: The modeling area for numerical experiments about the unadventurous and the group effect, the inertial effect, the smoke spreading effect, the flow with the stream effect and no effect.

1.4.1 Unadventurous and Group Effects

To demonstrate the scenario of pedestrians' evacuation considering both the unadventurous and the group effect, we assume that there are two groups with ten members among 300 pedestrians. These groups members are assumed to be familiar with the room. The two groups are distinguished by using the colour pink and green while the red colour is used for unadventurous pedestrians. The colour blue refers to non-group members and non-unadventurous pedestrians. All pedestrians are randomly distributed in the room at the beginning of the evacuation. To model the unadventurous effect, we assume that 60% of the pedestrians who are not familiar with the room enter the modelling area through Exit 1, P_1 is enlarged through (1.8) for scenario (i) and P_1 is enlarged through (1.9) for scenario (ii).

Table 1.6 shows the average evacuation time and the percentage of pedestrians moving out through Exit 1 in the cellular automata model and the social force model considering the unadventurous effect and the two groups effect. The computation time of ten trial runs in the CA model and the SF model is shown in Table 1.7. The evaluation of the pedestrians' evacuation

Parameter	Symbol	Value	Equation
The initial speed	$v_i(0)$	1	(1.2)
The maximum desired speed	v_i^{max}	3	(1.2)
Constant for adjusting the *SD* effect	k_r	1	(1.3)
Total number of exits	N_e	2	(1.3)
Constant for adjusting the *OD* effect	k_d	1	(1.6)
Parameters for adjusting the *SD* and n_i	k_s	0.1	(1.7)
Parameters for adjusting the *OD* and n_i	k_p	0.05	(1.7)
Parameters for adjusting the smoke density effect	k_m	0.37	(1.7)
Multiplying factor	α_{ke}	1.2	(1.8)
Constant for enhancing P_k	ω_1	0.01	(1.9)
Constant for enhancing P_k	ω_2	0.10	(1.9)
Velocity field in x-direction	w_1	[-0.5,0.5]	(1.13)
Velocity field in y-direction	w_2	[-0.5,0.5]	(1.13)
Diffusion constant	κ_d	0.05	(1.13)
The initial desired speed	$v_i^d(0)$	1.65	(1.22)
Relaxation time	τ_i	0.5	(1.22)
Human-human interaction strength	A_i	2	(1.23)
Human-human range of repulsive interaction	B_i	0.1	(1.23)
Contact distance	r_{ij}	0.5	(1.23)
Anisotropic parameter	λ_i	0.61	(1.23)
Body force coefficient	k_n	2	(1.24)
Friction force coefficient	k_t	2	(1.24)
Body radius	r_i	0.25	(1.25)
Human-wall interaction strength	A_w	0.2	(1.25)
Human-wall range of repulsive interaction	B_w	0.2	(1.25)
Body force coefficient of the wall	k_w	100	(1.25)
Friction force coefficient of the wall	κ_w	100	(1.25)
Smoke interaction strength	A_s	1	(1.32)
Human-smoke range of repulsive interaction	B_s	0.2	(1.32)
Radius of the high smoke concentration cell	r_s	$0.4\sqrt{2}$	(1.32)

Table 1.5: Parameters for evacuation simulations.

considering the unadventurous and the two groups effect is demonstrated in Figure 1.22.

When the evacuation starts, all pedestrians move towards exits. Then

Model	Evacuation time (s)		Exit 1 (%)	
	scenario (i)	scenario (ii)	scenario (i)	scenario (ii)
CA model	27.8690	31.7840	65.43	75.47
SF model	30.7180	35.4840	66.50	82.53

Table 1.6: Average evacuation times and percentage of pedestrians moving out through exit 1 considering *the two group effect and the unadventurous effect* in the CA and SF model. P_1 is enlarged through (1.8) for scenario (i) and P_1 is enlarged through (1.9) for scenario (ii).

Model	Run time (10 rounds)	
	scenario (i)	scenario (ii)
CA model	$28.5064s$	$41.0378s$
SF model	$1.7914h$	$1.7157h$

Table 1.7: Computation time of ten trial runs considering *the two group effect and the unadventurous effect* in the CA and SF model. P_1 is enlarged through (1.8) for scenario (i) and P_1 is enlarged through (1.9) for scenario (ii).

two crowds are formed around the two exit areas. A jamming phenomena is observed as many pedestrians try to leave the room at the same time. This clogging effect is a bottleneck situation, where the flow is limited by a door or narrowing. A few walkers can go out through the exits, but most of them have to wait around the exit area.

Apparently, the number of pedestrians who leave the room through Exit 1 is higher than the number of pedestrians who move out of the room through Exit 2. This behaviour reflects the unadventurous effect, because most of the pedestrians leave through the same exit where they entered (60% entered through Exit 1). This produces an inefficient use of exits which is agreeable in the actual evacuation process under the emergency condition that people sometimes lack intellect to select the proper exit. Large crowds move through Exit 1 while Exit 2 is rarely used.

Group members move towards exits when the evacuation starts, but at the same time they also walk towards other group members. Different group members may choose different exits as their initial movement directions. Once group members congregate together inside the room, they select one

exit as a common direction to egress. Figure 1.22 shows that after green and pink group members have assembled together, both groups choose Exit 2 as their evacuation route as a result of the relatively high occupant density (OD) of Exit 1.

The unadventurous effect is studied through equation (1.8) and (1.9) using the same evacuation process. We set $\alpha_{ke} = 1.2$ in equation (1.8) and $\omega_1 = 0.01$, $\omega_2 = 0.1$ in equation (1.9). Modeling the unadventurous effect through equation (1.8) yields about 66% of all pedestrians moving out through Exit 1 while applying equation (1.9) results approximately 78% of all pedestrians evacuating through Exit 1 which leads to longer evacuation in scenario (ii). More than 60% of all pedestrians move out of the room through Exit 1 in both scenarios. That means besides the unadventurous pedestrians, some other pedestrians also move out through Exit 1 at the initial stage where the OD of Exit 1 is rather small.

Figure 1.24 depicts the comparisons of the average number of outside pedestrians and the usage of each exit versus time between the CA model and the SF model in scenario (i) and scenario (ii). Both models show the similar result that larger crowds evacuate through Exit 1 and the difference usage of the exits is higher in scenario (ii) compared to scenario (i).

The average occupant density (OD) of each exit versus time considering the two groups effect and the unadventurous effect is shown in Figure 1.25. For both scenarios in the CA and SF model, the average OD of Exit 1 is remarkably higher than Exit 2 due to the unadventurous effect. The average OD of Exit 1 in scenario (i) and (ii) rises up at the beginning and reaches the peak at about $10s$. Afterwards, the average OD remains at this value since the clogging effect leads few pedestrians to leave and others to stand around the exit area. Later the OD of Exit 1 decreases continuously and becomes zero at the end of the simulation. In contrast, the average OD of Exit 2 increases at the beginning, reaches the peak, then decreases immediately and rises again little later. Noticeably, using the SF model, the average OD of Exit 1 is greatly higher in both scenarios than in connection with the CA model.

We also perform the simulation experiments considering the group effect exclusively, without including the unadventurous effect. One group, three groups and five groups, with 15 members for each group, are evaluated in our study. The number of groups influences the evacuation considerably as shown in Table 1.8. An increasing number of group leads to a smaller outflow

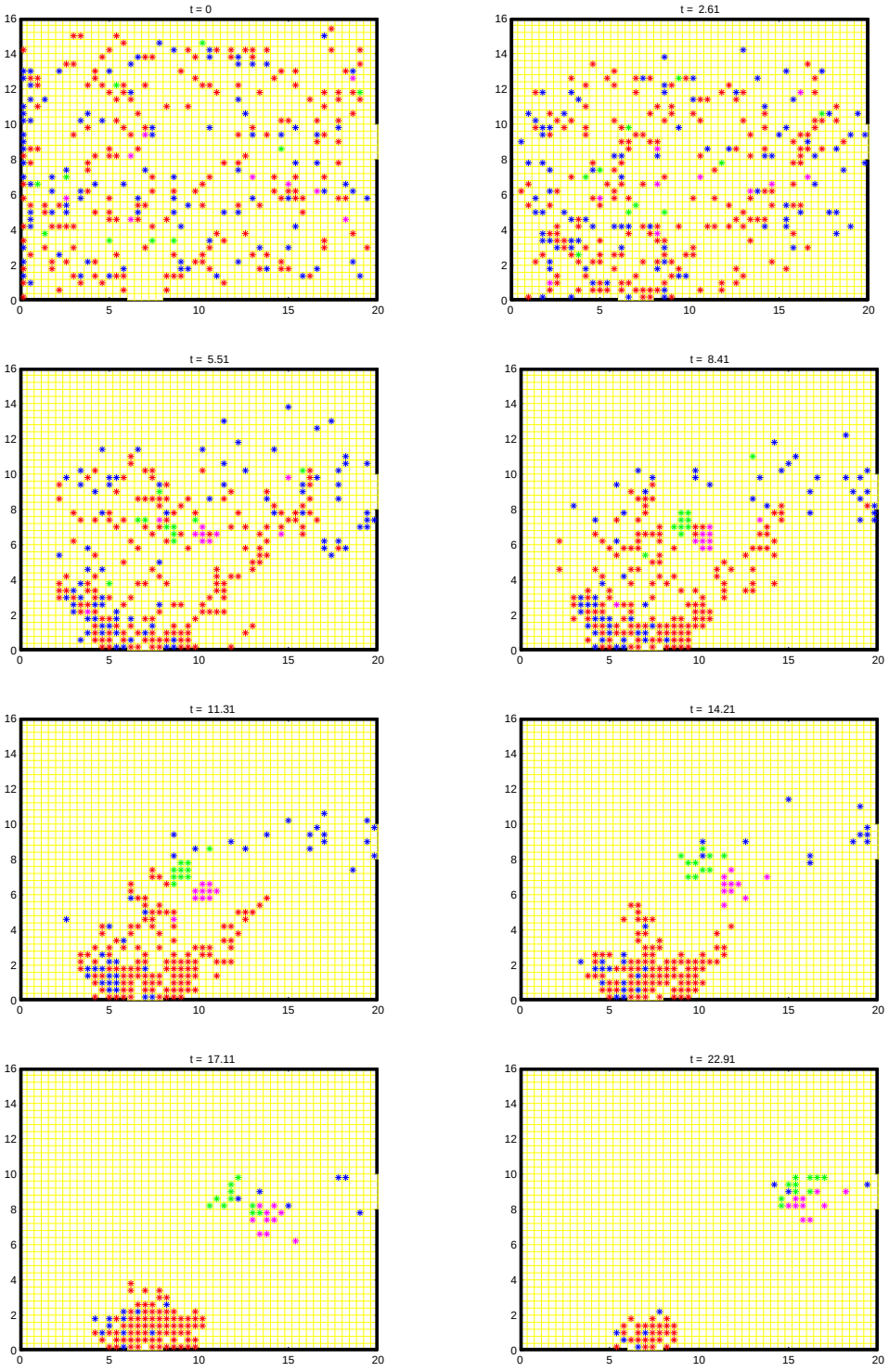

Figure 1.22: Movements of pedestrians in *the unadventurous effect and the two groups effect* using the CA model.

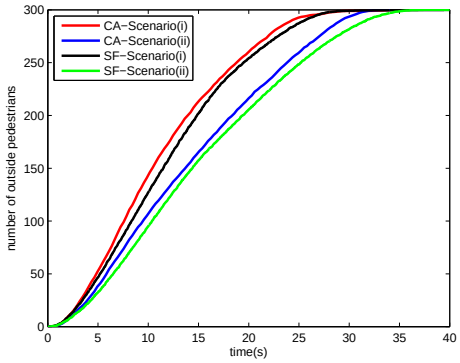

Figure 1.23: Comparisons of average number of outside pedestrians versus time of *the unadventurous and the group effects* in scenario (i) and scenario (ii).

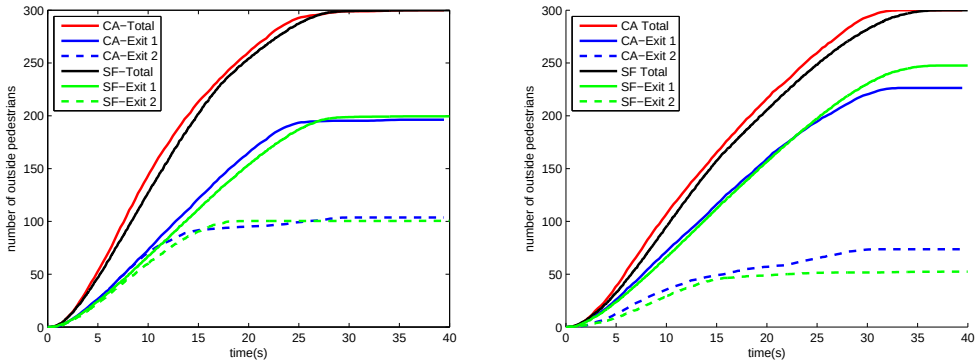

(a) P_1 is enlarged through (1.8) (b) P_1 is enlarged through (1.9)

Figure 1.24: Average number of outside pedestrians versus time considering *the two groups effect and the unadventurous effect.*

rate and to a longer evacuation time. This result is realistic since the group members waste time to congregate inside the room and to exit together.

Model	Evacuation time (s)		
	1 group	3 groups	5 groups
CA model	24.1570	28.1300	36.3370
SF model	25.5140	27.2120	32.4840

Table 1.8: Average evacuation times considering *the group effect* in the CA and SF model. Each group contains 15 members.

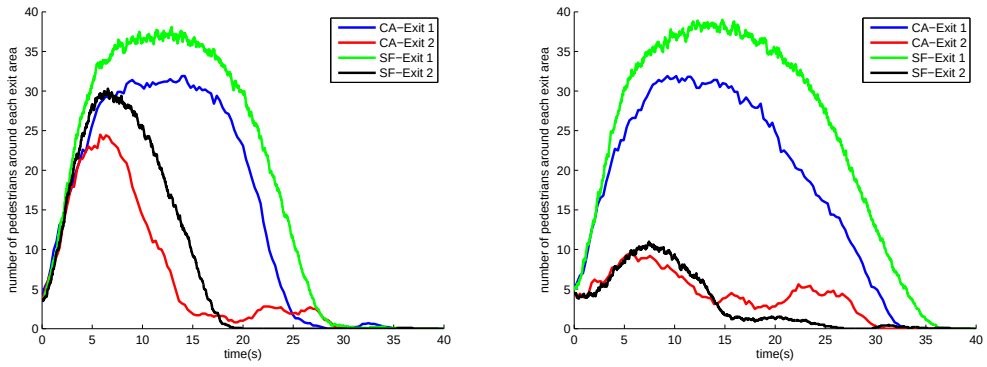

(a) P_1 is enlarged through (1.8) (b) P_1 is enlarged through (1.9)

Figure 1.25: Average number of pedestrians around each exit area versus time considering *the two groups effect and the unadventurous effect*.

Model	Run time (10 rounds)		
	1 group	3 groups	5 groups
CA model	$23.0801s$	$54.2976s$	$105.9035s$
SF model	$1.6741h$	$1.7684h$	$1.8738h$

Table 1.9: Computation time of ten trial runs considering *the group effect* in the CA and SF model. Each group contains 15 members.

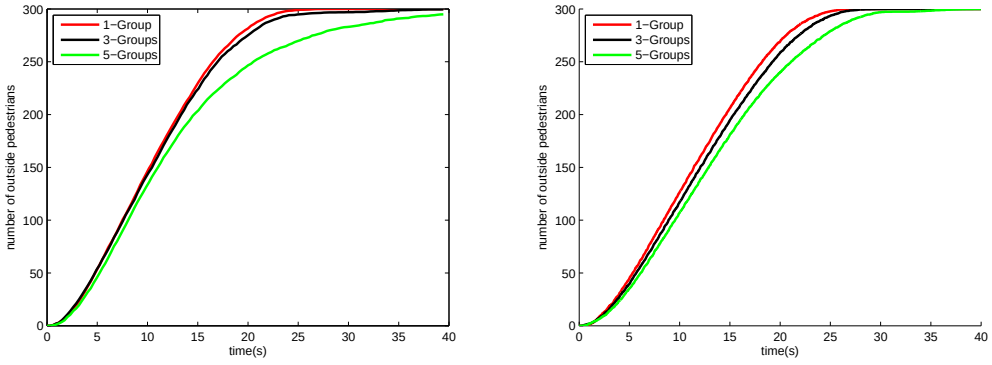

(a) CA model (b) SF model

Figure 1.26: Average number of outside pedestrians versus time considering *the group effect*. Each group contains 15 members.

1.4.2 Inertial Effect

Inertial pedestrians try to continue heading in the selected movement direction during the evacuation. This is modeled by increasing the probability of the chosen exit. The inertial effect is studied with the assumption that there are 60% inertial pedestrians in the simulation domain. Once these inertial pedestrians select an exit to move out, the probability of choosing that exit in next time step is increased through equation (1.8) for scenario (i) and equation (1.9) for scenario (ii). The probabilities of choosing other exits become smaller proportionally. The simulation results considering the inertial effect are shown in Table 1.10.

It is obvious that the total evacuation time is slightly smaller in scenario (i) both in the CA model and with the SF model compared to scenario (ii). This can be explained by the fact that (1.9) strongly increases the probability of choosing a certain exit. Inertial pedestrians therefore become less flexible and try to keep their own way to the exit route.

Model	Evacuation time (s)	
	scenario (i)	scenario (ii)
CA model	22.3880	24.1860
SF model	25.3500	25.6500

Table 1.10: Average evacuation times considering *the inertial effect* in the CA and SF model. The PS is enlarged through (1.8) for scenario (i) and through (1.9) for scenario (ii).

Model	Run time (10 rounds)	
	scenario (i)	scenario (ii)
CA model	$48.5458s$	$55.3993s$
SF model	$1.7752h$	$1.7397h$

Table 1.11: Computation time in ten trial runs considering *the inertial effect* in the CA and SF model. The PS is enlarged through (1.8) for scenario (i) and through (1.9) for scenario (ii).

1.4.3 Smoke Spreading Effect

In order to see the fast effect of smoke spreading on the people's movements in an evacuation, we assume that the smoke density at the source point is rather high at the initial time. Furthermore, the source emits a constant smoke density of $0.01g/s$ afterwards, i.e.

$$Q_c = \begin{cases} 10g/s & , \quad t = 0 \\ 0.01g/s & , \quad t > 0. \end{cases}$$

The velocity field (w_1, w_2) in equation (1.13) is chosen randomly out of the interval $[-0.5, 0.5]$ at each time step. All pedestrians in the simulation are assumed to be familiar with the environment and the exits. They choose one exit to move out through equation (1.7) which takes also smoke density around each exit into account. To examine the influence of the smoke density on the exit choice of pedestrians, the smoke source location is considered in two cases: In the middle of the room for scenario (i) and in front of Exit 1 for scenario (ii).

Model	Evacuation time (s)		Exit 1 (%)	
	scenario (i)	scenario (ii)	scenario (i)	scenario (ii)
CA model	22.1850	33.6980	56.90	6.23
SF model	24.8860	32.5140	56.47	17.30

Table 1.12: Average evacuation time and percentage of pedestrians moving out through Exit 1 considering *the smoke spreading effect* in the CA and the SF model. The source is in the middle of the room in scenario (i) and in front of Exit 1 in scenario (ii).

Model	Run time (10 rounds)	
	scenario (i)	scenario (ii)
CA model	$39.5834s$	$54.3758s$
SF model	$1.9677h$	$1.8073h$

Table 1.13: Computation time in ten trial runs considering *the smoke spreading effect* in the CA and the SF model. The source is in the middle of the room in scenario (i) and in front of Exit 1 in scenario (ii).

Table 1.12 displays average evacuation time and percentage of pedestrians moving out through Exit 1 considering the smoke spreading effect in the CA and the SF model in scenario (i) where source is in the middle of the room and in scenario (ii) where source is in front of Exit 1. The location of the smoke source has a great impact on the evacuation time. When the smoke source is near the exit, it takes more time to evacuate all people compared to the situation of a source in the middle of room. This can be interpreted as the fact that pedestrians reject to move out through the smoking exit since it refers to danger or insecure for them to move out. Most of the pedestrians then use Exit 2 to escape. Therefore the usage of Exit 2 is absolutely high and a large jamming is observed around this exit in scenario (ii) which leads to a longer evacuation. When the smoke source is in the centre of room, the usage of both exits is slightly different.

Comparison of the average number of outside pedestrians versus time between the CA model and SF model is demonstrated in Figure 1.28. Both models yield the similar results that more pedestrians evacuate through Exit 2 in scenario (ii) and that there is a balanced usage of the exits in scenario (i).

Figure 1.29 shows comparison of the average number of pedestrians around each exit area (OD) considering the smoke spreading effect. When the smoke source is in the centre of the room, average OD of Exit 1 is lightly higher than Exit 2 in both the CA and SF model. In the case that smoke source is in front of Exit 1, average OD of Exit 2 is significantly higher than Exit 1 in connection with CA and SF model. This is because of formation of huge crowd around Exit 2.

Comparison of pedestrians' movements in the smoke spreading effect where the source is in the middle of the room and in front of Exit 1 using the SF model is illustrated in Figure 1.30.

It is interesting to point out the explanation for the results of scenario (ii), see Figure 1.31. At the beginning of the simulation pedestrians who are near Exit 1 move out through this exit due to their short spatial distance and the little smoke density effect. As time progresses the smoke density around Exit 1 becomes higher, the pedestrians move away from it and large crowds are formed around Exit 2.

Figure 1.32 shows pedestrians' movements using the CA model in the smoke spreading effect with different settings of velocity field (w) in the advection-diffusion equation.

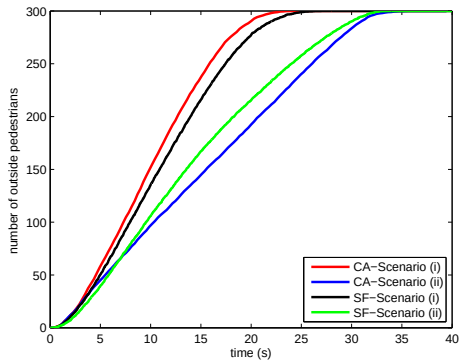

Figure 1.27: Comparisons of average number of outside pedestrians versus time considering *the smoke spreading effect* in scenarios(i) and scenarios(ii).

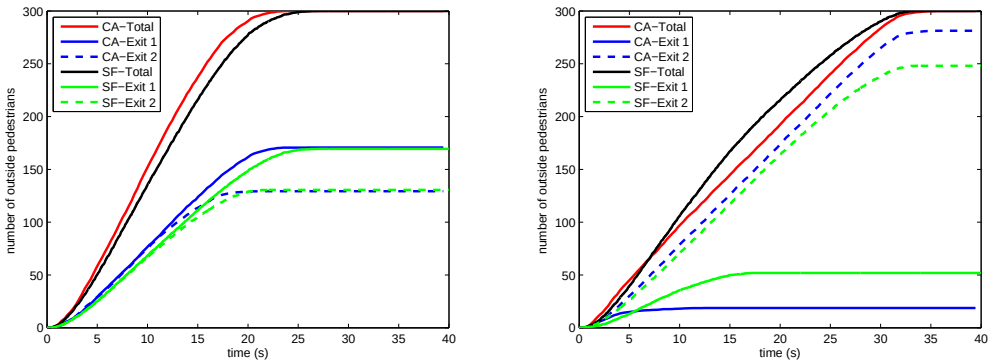

(a) Smoke source is in the centre of room (b) Smoke source is near Exit 1

Figure 1.28: Average number of outside pedestrians versus time considering *the smoke spreading effect*.

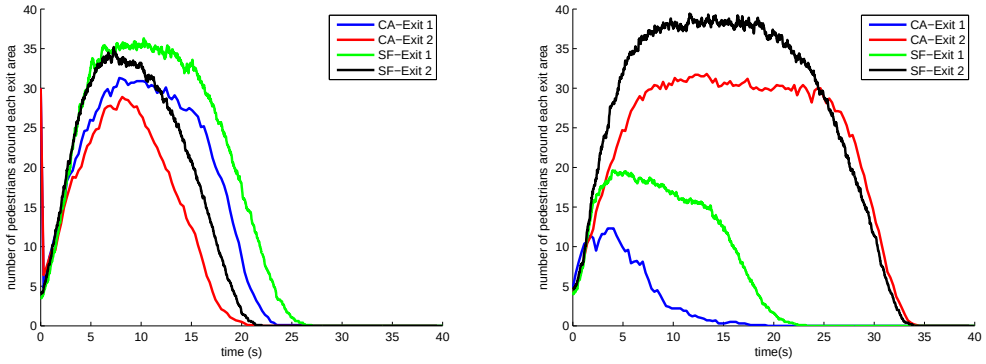

(a) Source is in the middle (b) Source is near Exit 1

Figure 1.29: Average number of pedestrians around each exit area versus time considering *the smoke spreading effect*.

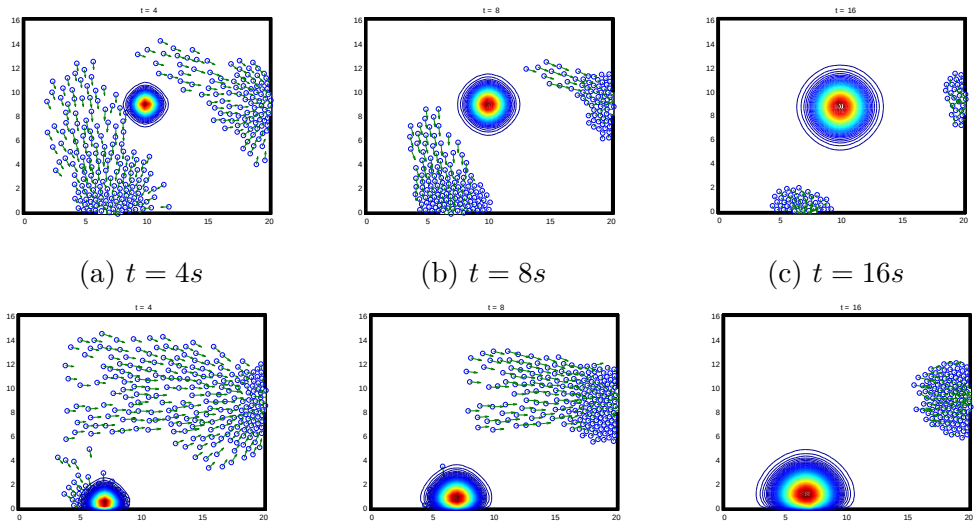

(a) $t = 4s$ (b) $t = 8s$ (c) $t = 16s$

(d) $t = 4s$ (e) $t = 8s$ (f) $t = 16s$

Figure 1.30: Comparison of pedestrians' movements in *the smoke spreading effect* in scenarios (i) ((a)-(c)) and scenarios (ii) ((d)-(f)) at time $t = 4s$, $t = 8s$ and $t = 16s$ using the SF model.

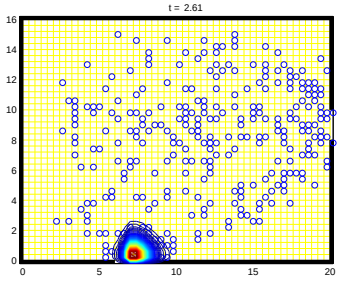

(a) CA, $t = 2.61s$

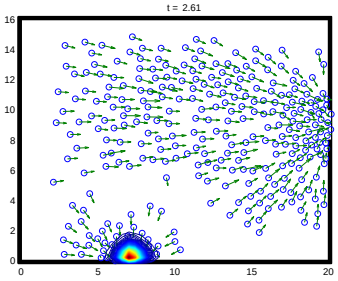

(e) SF, $t = 2.61s$

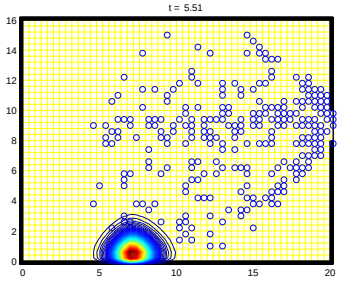

(b) CA, $t = 5.51s$

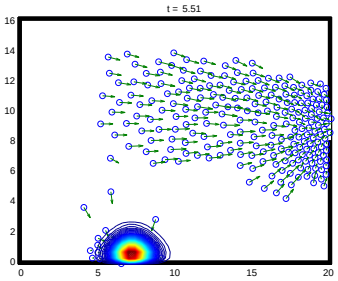

(f) SF, $t = 5.51s$

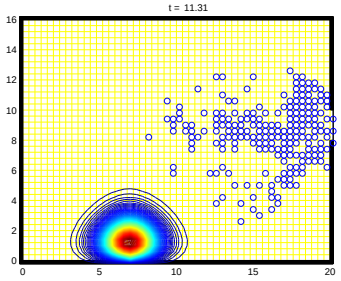

(c) CA, $t = 11.31s$

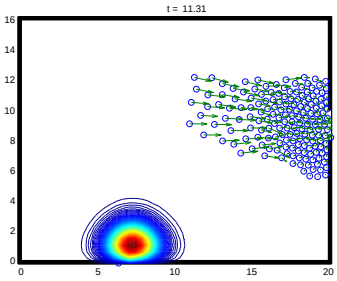

(g) SF, $t = 11.31s$

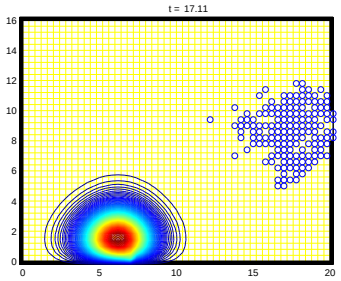

(d) CA, $t = 17.11s$

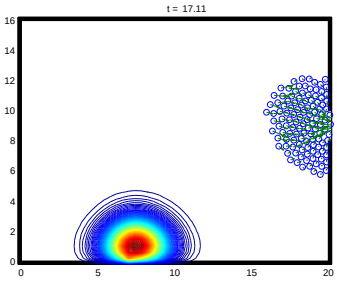

(h) SF, $t = 17.11s$

Figure 1.31: Movements of pedestrians in *the smoke spreading effect* where the source is at Exit 1 of the CA model and SF model.

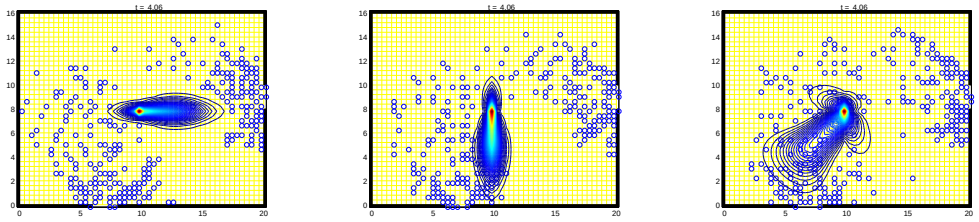

(a) $t = 4.08s$ (e) $t = 4.08s$ (i) $t = 4.08s$

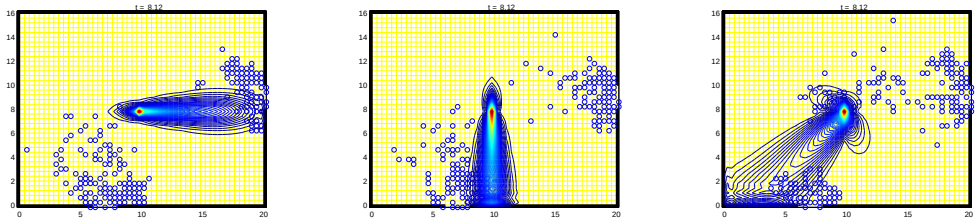

(b) $t = 8.12s$ (f) $t = 8.12s$ (j) $t = 8.12s$

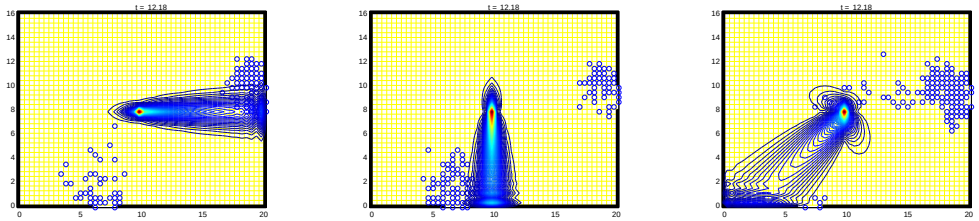

(c) $t = 12.18s$ (g) $t = 12.18s$ (k) $t = 12.18s$

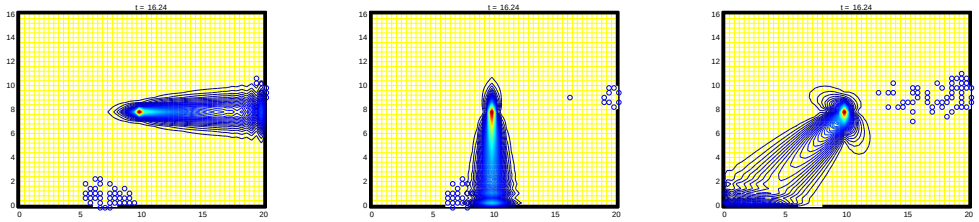

(d) $t = 16.24s$ (h) $t = 16.24s$ (l) $t = 16.24s$

Figure 1.32: Pedestrians' movements in *the smoke spreading effect* with different settings of velocity field (w) in the advection-diffusion equation. The CA model is used for the simulations. $w = (1, 0)$ for (a)-(d), $w = (0, -1)$ for (e)-(h) and $w = (-1, -1)$ for (i)-(l).

1.4.4 Flow with the Stream Effect

To simulate the flow with the stream effect, the fire compartment forms $20m \times 16m \times 4m$ and $1kg$ of polystyrene is assumed to burn in the flame inside the compartment. The smoke conversion factor of polystyrene is 0.15 as reported in [62]. The visibility range can be estimated by equation (1.14).

$$R_v = \frac{K_s V}{K_m M_s} = \frac{3 \times 20 \times 16 \times 4}{7.6 \times 0.15 \times 1000} = 3.37m.$$

In reality the visibility range is not constant and varies all the time dependent on the burning rate of the material. Hence, we assume that the visibility range of the pedestrians is changed linearly from $3.37m$ to $2m$ within $100s$. Two scenarios are demonstrated for experiments, without guider (i) and with 5 guiders (ii) in the smoke filled compartment. The entire period of a simulation is set to $150s$.

Model	Evacuation time (s)		Evacuated pedestrians(%) in $150s$	
	scenario (i)	scenario (ii)	scenario (i)	scenario (ii)
CA model	> 150	> 150	59.63	80.40
SF model	44.9940	33.2300	100	100

Table 1.14: Average evacuation time and percentage of evacuated pedestrians considering *the flow with the stream effect* in the CA and SF model without guider in scenario (i) and with 5 guiders in scenario (ii).

Table 1.14 shows average evacuation time and percentage of evacuated pedestrians considering the flow with the stream effect in the CA and SF model without guider in scenario (i) and with 5 guiders in scenario (ii). It is seen that average percentage of evacuated pedestrians is higher in presence of guiders than without guider both in the CA model and the SF model. This is because guiders can lead some of people around them to the exit. In case that there is no guider, pedestrians have to move with the flow in a selected direction or move randomly until they can see an exit by chance and leave it.

The difference between the CA model and the SF model considering the flow with the stream effect is that all pedestrians in the SF model can evacuate within $150s$ while in the CA model about 90% of all pedestrians are able to leave the room. This can be explained by two reasons:

(i) The time step to update the pedestrians' positions in the CA model (0.29) is larger than in the SF model (0.02). The pedestrians' positions

are updated more frequently in the SF model than in the CA model. Therefore, the chance for a pedestrian to see, move with others and leave the room is higher when using the SF model than when using the CA model.

(ii) For each time step, a move of a pedestrian in the CA model is limited to 9 cells (Moore's neighborhood+his own cell) around him while movement of a pedestrian in the SF model is not limited to cells. In the situation that a pedestrian of the CA model is far from others and not close to an exit, his movement is randomly chosen from the Moore's neighborhood (8 cells) in each time step. Therefore, there is a high possibility that he traces his old paths and cannot find the exit.

In Figure 1.33 we can see the evolution of the pedestrians' movements without a guider considering the flow with the stream effect in the SF model. Pedestrians who are near the exit move out of the room. In the mean time, individuals who cannot see the exit move in the direction determined by the flow with the stream. Several groups are observed in this stage. The crowds search for an exit randomly until they see one and move out.

The footprints of five randomly chosen pedestrians considering the flow with the stream effect without a guider in the CA and SF model are plotted in Figure 1.34. It can be seen that the footprints provide rather smooth traces in the SF model compared to the CA model. Using the CA model, Figure 1.34(a) shows that the black colour pedestrian who is close to Exit 2 can evacuate through this exit without difficulty. On account of the limited visibility, the blue, deep blue and red pedestrians cannot find the exit directly. They follow others by the flow with the stream and move around the room until they see an exit and move out. The pink individual is unfortunate, traces an overlap path and fails to evacuate in a given period of time.

Figure 1.36 shows the flow with the stream effect in presence of 5 guiders in the CA model. Five guiders are randomly distributed in the room at initial stage. As the simulation starts, the guiders (red stars) move towards a selected exit since they are familiar with the environment and know well where the exits are located. They lead other people around them to the exit even if they cannot see it. The presence of guiders is significant for the evacuation simulation since the number of evacuated pedestrians per time step is much higher in presence of guiders compared to the case of without guiders, see Figure 1.35.

1.4.5 Obstacle Effect

To study the effect of obstacles on the pedestrians' motions, we consider a square room of $20m \times 20m$ which contains two exits with $2m$ width and are placed at the bottom of the room. 300 individuals are initially distributed randomly on top of the room, see Figure 1.37 and Figure 1.42. Obstacles with smooth boundaries, e.g., circular and rectangular obstacle, are exploited for experiments. An individual chooses one exit to move out by considering the distance, the occupant density (OD) and his degree of impatience. It is given by equation (1.1). The distance map of the simulation room in presence of obstacles is obtained by solving the Eikonal equation (1.4) numerically applied the fast marching method mentioned in section 1.3.1

1. **Comparison of circlular and rectangular obstacles**
   We consider two types of obstructions with the same area, circular and rectangular obstacles, which are placed about in the middle of the room, see Figure 1.37.

Model	Evacuation time (s)	
	Circular obstacle	Rectangular obstacle
CA model	33.0600	34.6550
SF model	32.7080	32.9420

Table 1.15: Average evacuation times in the presence of circular and rectangular obstacles in the simulation room using the CA and SF model.

Model	Run time (10 rounds)	
	Circular obstacle	Rectangular obstacle
CA model	$22.4735s$	$23.0570s$
SF model	$2.9949h$	$3.1282h$

Table 1.16: Computation time of ten trial runs in the presence of circular and rectangular obstacles in the simulation room using the CA and SF model.

Table 1.15 shows the average evacuation times in the presence of circular and rectangular obstacles in the simulation room using the CA and SF models. The computation time of ten trial runs is presented in Table 1.15. The average number of outside pedestrians versus time of Exit 1, Exit 2 and their sum are demonstrated in Figure 1.39, again on the one hand with the SF model and on the other hand with the CA

model. The room with a rectangular obstacle provides a little longer evacuation time and a little less outflow compared to the room with a circular obstacle. The usage of each exit is slightly different in both scenarios.

Figure 1.40 illustrates the comparison of the average number of pedestrians around each exit (OD) in a room with a circular obstacle and in a room with a rectangular obstacle. Again both the SF and the CA models are considered in this context separately. The average OD is approximately the same for the room with circular and the room with rectangular obstacle. In the SF model, green and black curves (average OD of Exit 1 and Exit 2 respectively) rise up at the beginning and reach the peak of about 38 pedestrians around exit area. Consequently they directly decrease to zero at about $32s$. In the CA model, blue and black curves (average OD of Exit 1 and Exit 2 respectively) first grow up and reach the peak at about 23 occupants in the exit area. Then they remain at this level in the interval from 15 to 30 and drop slowly to zero subsequently. As a result the SF model produces a higher OD at the beginning and drops faster to zero after reaching the peak compared to the CA model.

Comparison of the individuals' movements in a room with a circular and a rectangular obstruction using the CA model at different time is displayed in Figure 1.41.

2. **Comparison of the placement of rectangular obstacles**
We now investigate the effect of the obstacles' positions on the total evacuation time. Figure 1.42 shows rooms with rectangular obstacles arranged in different ways, i.e. parallel and vertical to exits. The total area of the obstacles is the same in both rooms. The maximum distance in room (a) obtained from solving the Eikonal equation with initial front at Exit 1 and with initial front at Exit 2 is the same. It equals to $23.6927m$. The maximum distance in room (b) is $23.9272m$ if it is calculated from the initial front at Exit 1 and $23.8080m$ if it is calculated from the initial front at Exit 2. That means by placing rectangular obstacles as in room (b) a longer distance is provided than in room (a), see Figure 1.43.

Table 1.17 illustrates the average total evacuation times when the rectangular obstructions are placed in parallel and vertical to exits. Using

Model	Evacuation time (s)	
	Parallel to Exits	Vertical to Exits
CA model	39.7010	33.6690
SF model	40.0840	33.4760

Table 1.17: Average evacuation times considering *the obstacle effect* using the CA and SF model. Obstacles are arranged parallel (a) and vertical (b) to exits as in Figure 1.42.

Model	Run time (10 rounds)	
	Parallel to Exits	Vertical to Exits
CA model	$52.3077s$	$24.1022s$
SF model	$4.3367h$	$4.6903h$

Table 1.18: Average evacuation times considering *the obstacle effect* using the CA and SF model. Obstacles are arranged parallel (a) and vertical (b) to exits as in Figure 1.42.

the CA and SF models, we receive the same result: Arranging rectangular obstacles vertically to exits yields a lower evacuation time compared to placing them parallel to exits. Hence, the arrangement of obstacles in a room affects the evacuation significantly although the total area of the obstacles is the same.

By putting rectangular obstacles vertically to exits, the crowd is separated into three flows. Individuals have more ways to move compared to the situation of rectangular obstructions which are placed parallel to exits. Therefore, less congestion and pressure at the top corners are observed. The time evolution of the pedestrians' movements in a room, where two pillars are placed parallel and vertical to exits, are exhibited in Figure 1.44.

The average number of outside pedestrians per time step of a room with rectangular obstacles arranged in parallel to exits and vertical to exits of the CA and SF models is compared in Figure 1.45 and with respect to each exit is shown in Figure 1.46. Placing rectangular obstacles vertical to exits results in higher number of outside pedestrians compared to laying rectangular obstacles parallel to exits. The number

of pedestrians move out through Exit 1 and Exit 2 is lightly different both with parallel and vertical obstacles.

The average number of pedestrians around each exit per time step of the rooms with parallel obstacles and vertical obstacles is expressed in Figure 1.47 and corresponding to each exit is demonstrated in Figure 1.48.

Regarding the SF model, the occupant density is approximately the same for exit 1 and exit 2 both with parallel and vertical obstacles. The same can be said when we consider the CA model and focus again on the OD of exit 1 and exit 2 (Figure 1.47). Comparison of pedestrians' movements in the room with parallel obstacles of the CA model and the SF model is presented in Figure 1.49.

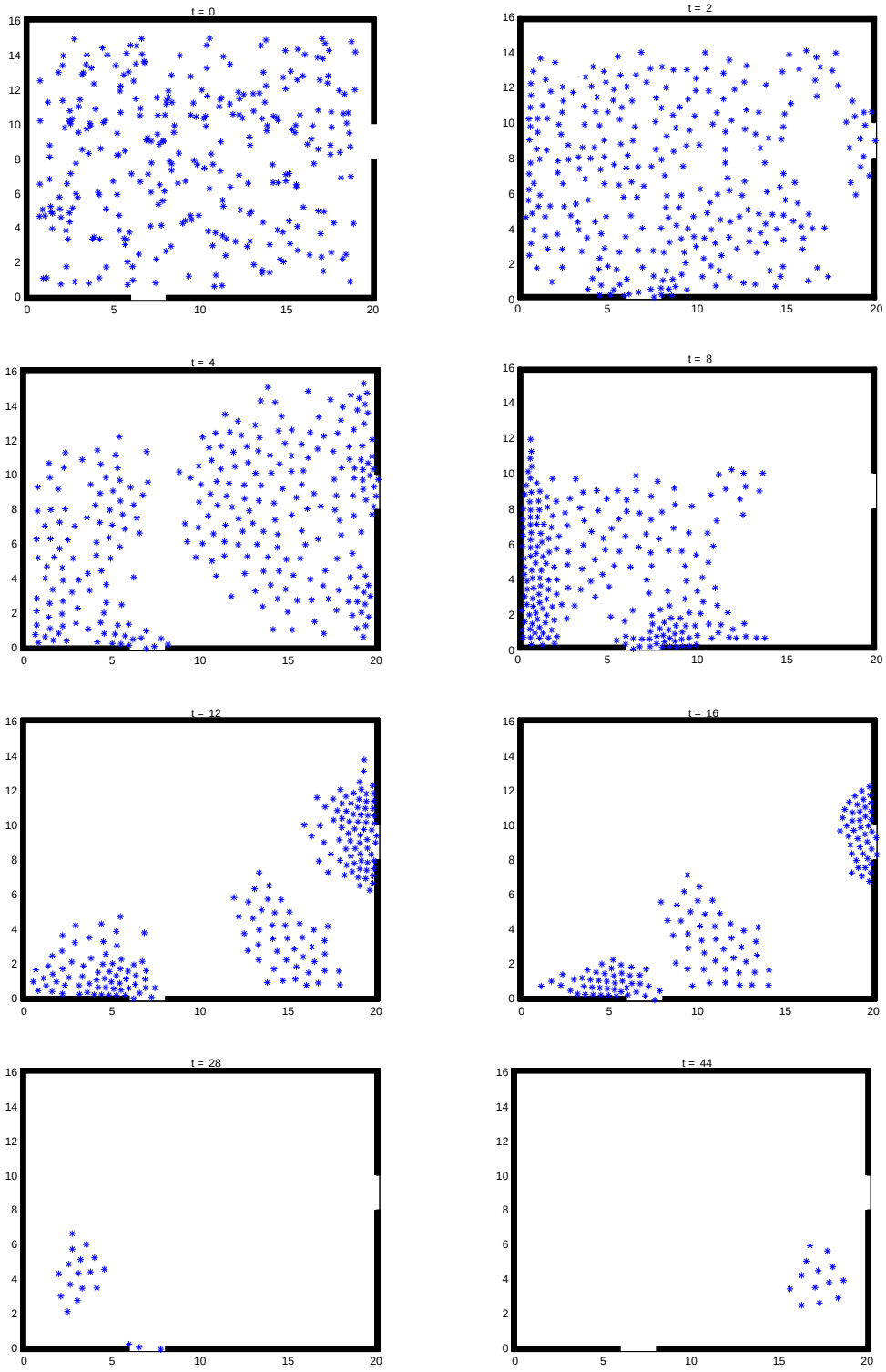

Figure 1.33: The evacuation considering *the flow with the stream effect* using the SF model.

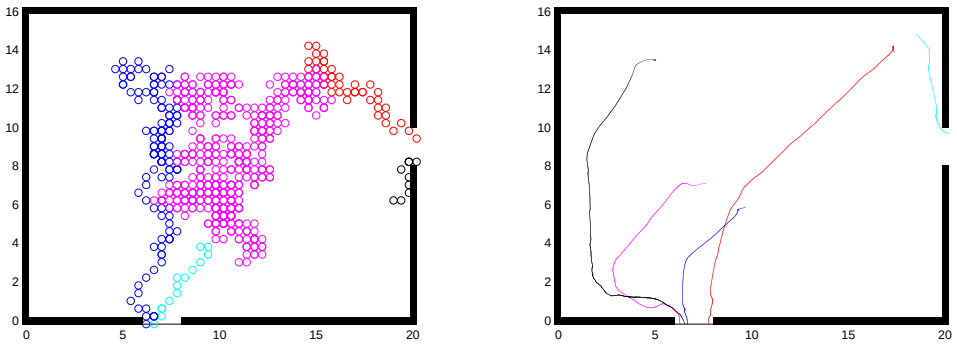

(a) CA model (b) SF model

Figure 1.34: Footprints of five randomly chosen pedestrians considering *the flow with the stream effect* without guider using the CA and SF model.

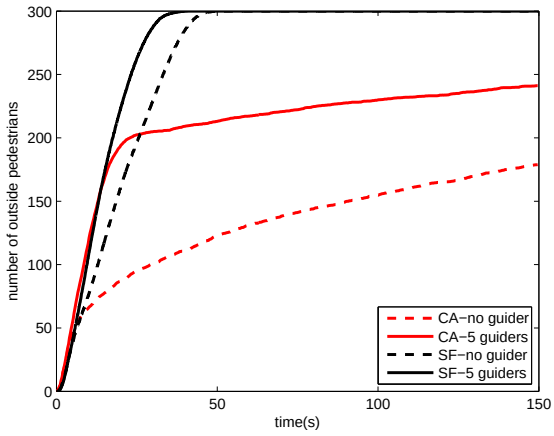

Figure 1.35: Average number of evacuated pedestrians considering *the flow with the stream effect*.

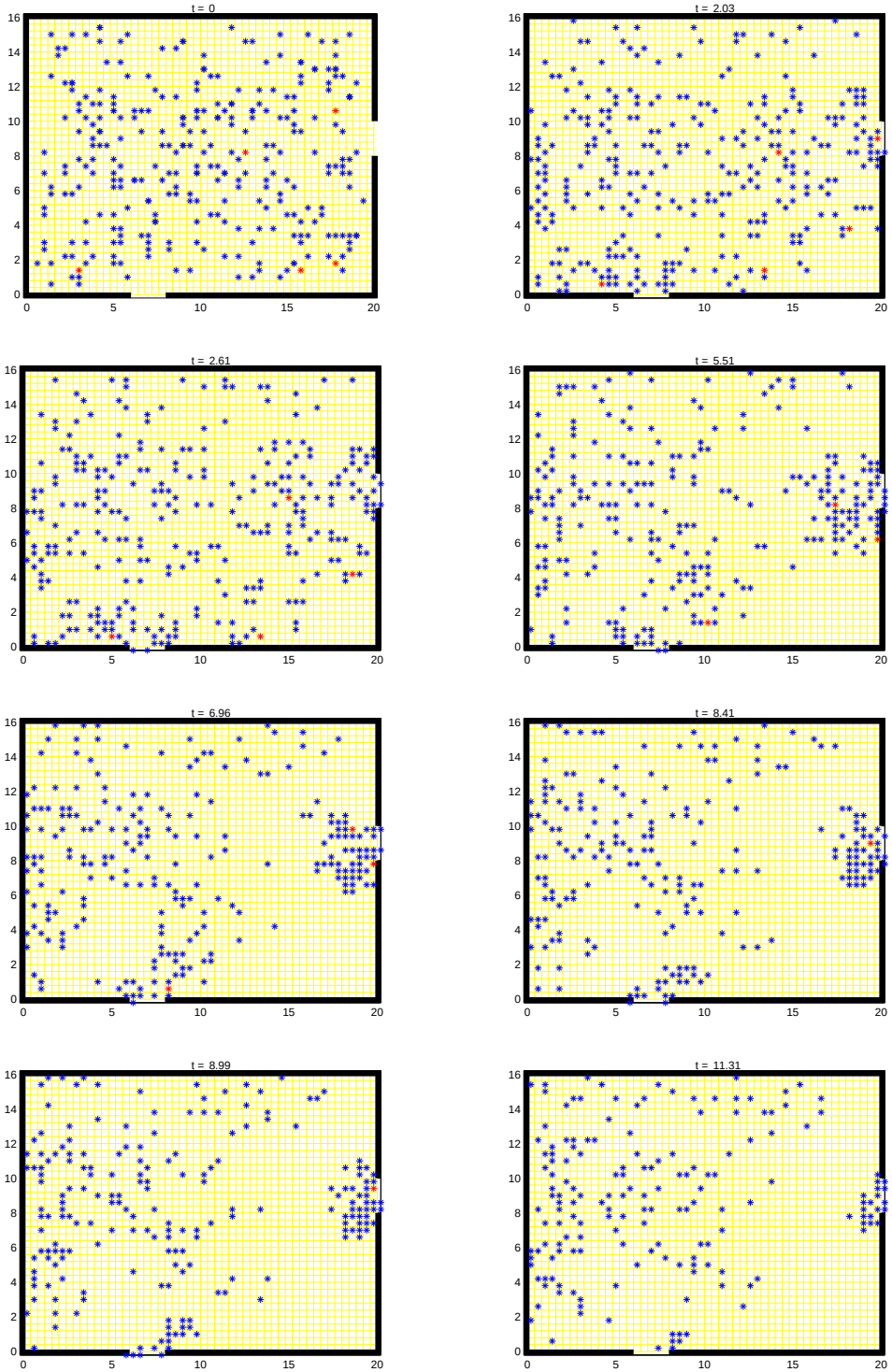

Figure 1.36: The time evolution of *the flow with the stream effect* with 5 guiders using the CA model. Red stars refer to guiders.

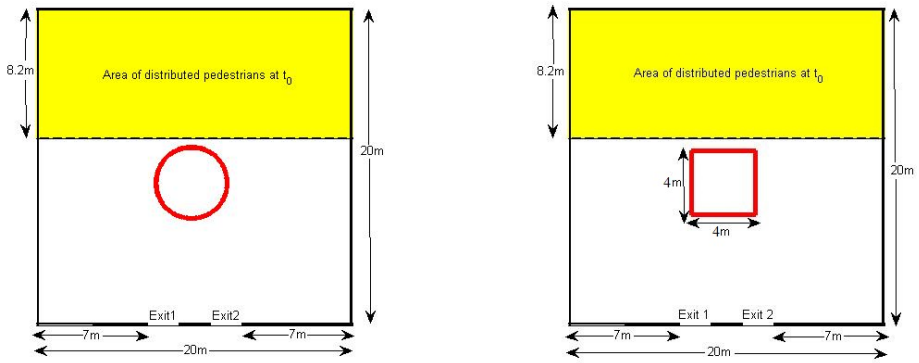

(a) Circular obstacle (b) Rectangular obstacle

Figure 1.37: Setting rooms with the same area of obstacles: A circular obstacle in (a) and a rectangular obstacle in (b).

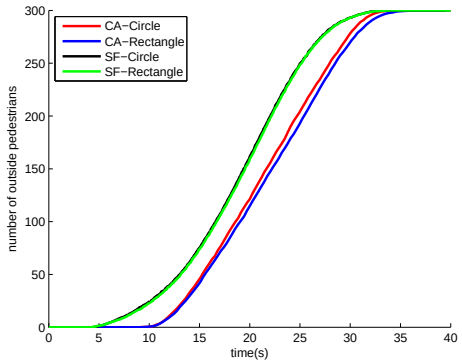

Figure 1.38: Comparison of the average number of outside pedestrians per time step simulating in a room with a circular obstacle and a room with a rectangular obstacle using the CA and SF models.

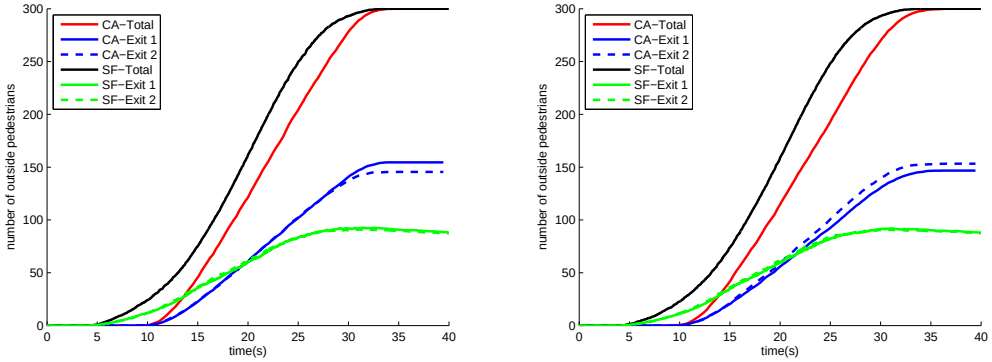

(a) Circular obstacle (b) Rectangular obstacle

Figure 1.39: Average number of outside pedestrians per time step simulating in a room with a circular and a room with a rectangular obstacle.

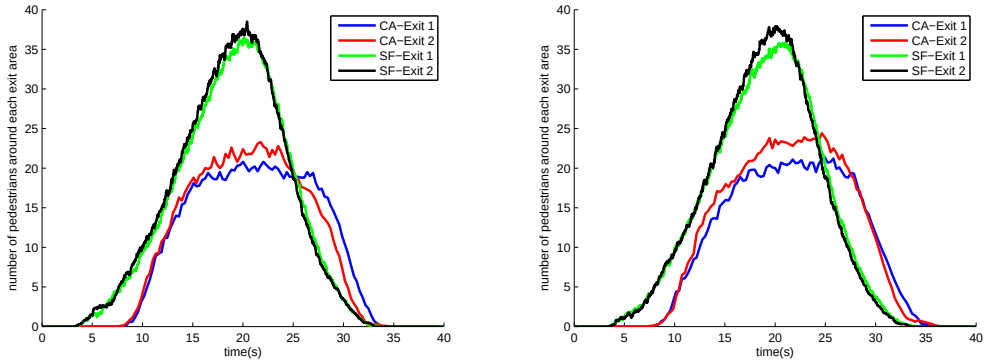

(a) Circular obstacle (b) Rectangular obstacle

Figure 1.40: Average number of pedestrians around each exit per time step simulating in a room with a circular and a room with a rectangle obstacle.

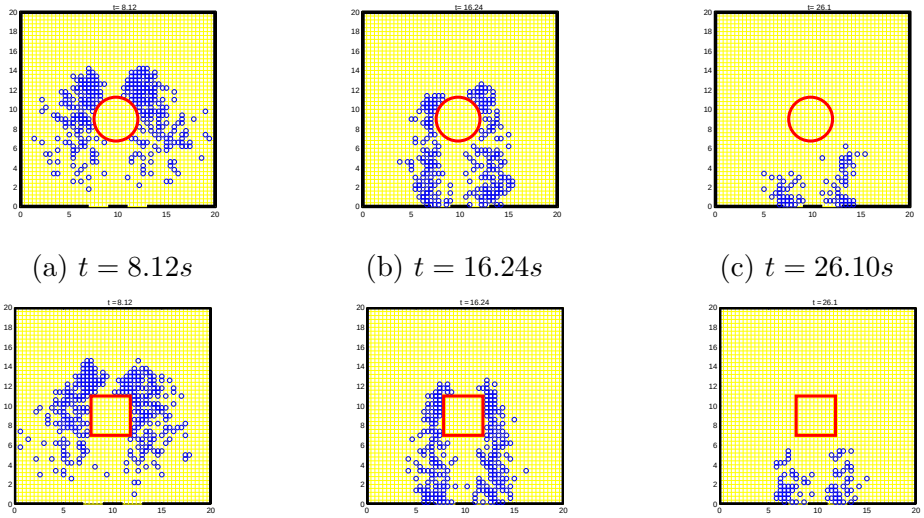

(a) $t = 8.12s$ (b) $t = 16.24s$ (c) $t = 26.10s$

(d) $t = 8.12s$ (e) $t = 16.24s$ (f) $t = 26.10s$

Figure 1.41: Comparison of pedestrians' movements in rooms with circular and rectangular obstacles at time $t = 8.12s$, $t = 16.24s$ and $t = 26.10s$ using the CA model.

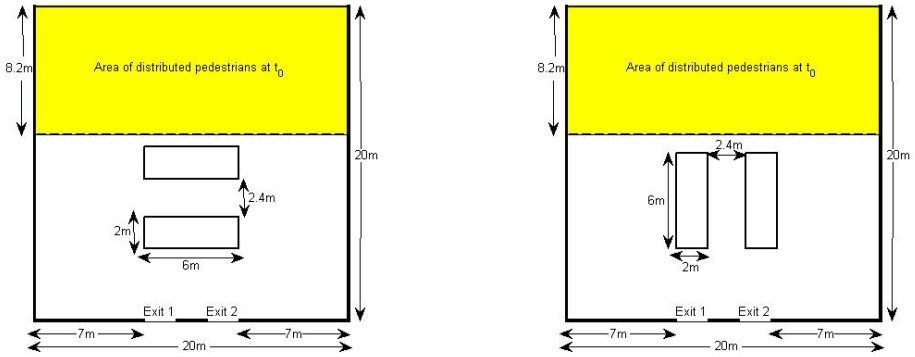

(a) Parallel to Exits (b) Vertical to Exits

Figure 1.42: Rooms with obstacles that require the same area and are arranged in a different way.

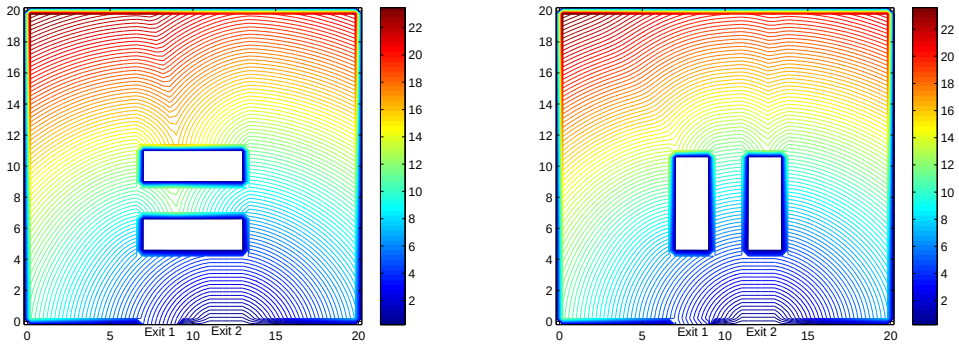

(a) Parallel to Exits (b) Vertical to Exits

Figure 1.43: Distance map with initial front at Exit 2 of the rooms with rectangular obstacles that require the same area and are arranged in a different way.

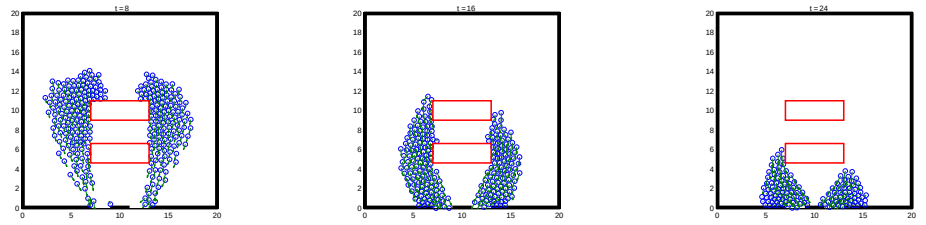

(a) $t = 8s$ (b) $t = 16s$ (c) $t = 24s$

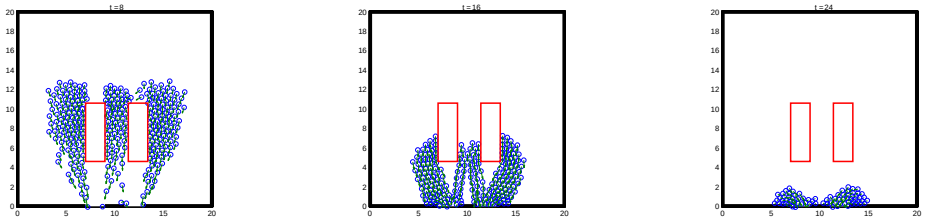

(d) $t = 8s$ (e) $t = 16s$ (f) $t = 24s$

Figure 1.44: Comparison of pedestrians' movements in a room with rectangular obstacles placing in parallel and vertical to Exits at time $t = 8s$, $t = 16s$ and $t = 24s$ using the SF model.

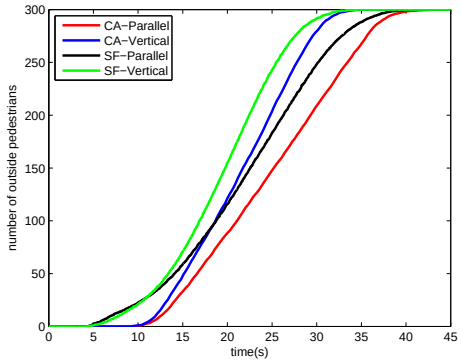

Figure 1.45: Comparison of average number of outside pedestrians per time step of the rooms with rectangular obstacles arranged in parallel to exits and vertical to exits of the CA and SF models.

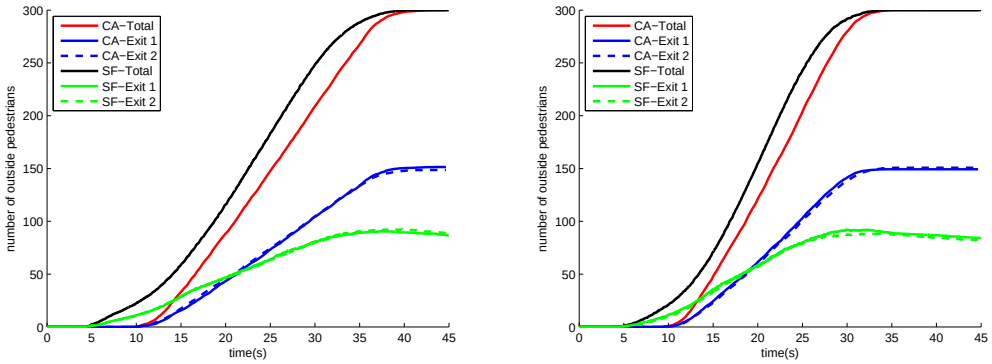

(a) Parallel to Exits (b) Vertical to Exits

Figure 1.46: Average number of outside pedestrians per time step of the rooms with rectangular obstacles arranged in parallel to exits and vertical to exits.

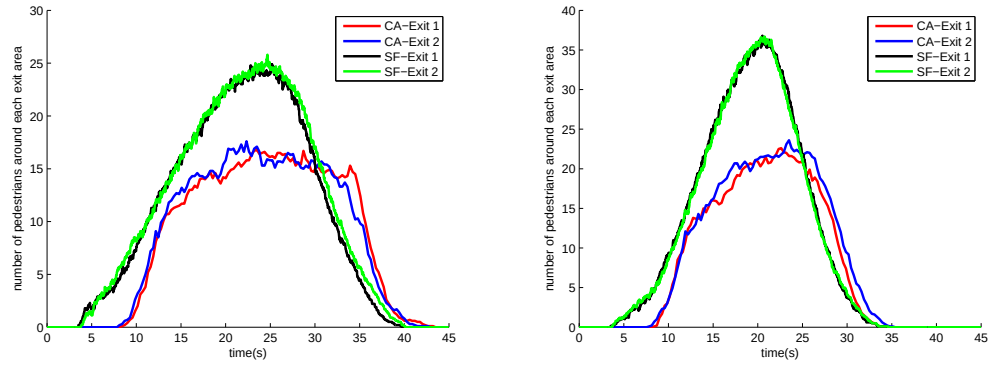

(a) Parallel to Exits (b) Vertical to Exits

Figure 1.47: Average occupant density (OD) per time step of the rooms with rectangular obstacles arranged in parallel to exits and vertical to exits.

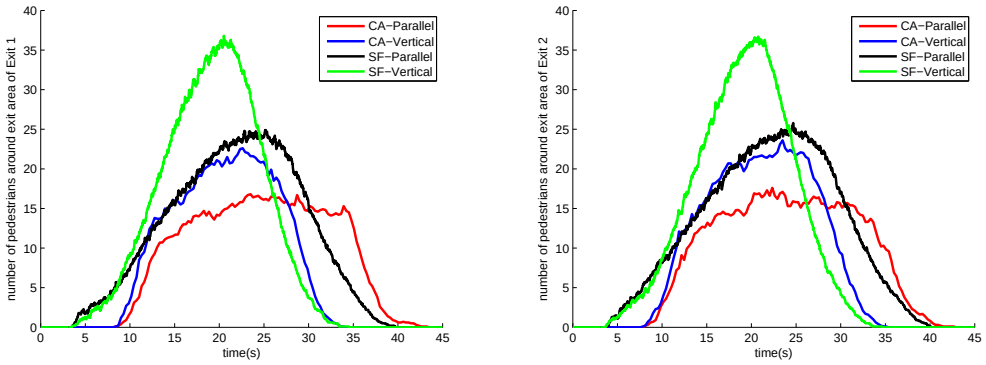

(a) Exit 1 (b) Exit 2

Figure 1.48: Average occupant density (OD) per time step with respect to each exit of the rooms with rectangular obstacles arranged in parallel to exits and vertical to exits.

1.4.6 No Effect

In this abstract, we simulate movements of pedestrians in the simulation domain setting as in Figure 1.21. An individual chooses one exit to move out using equation (1.1). Two aspects are considered here. First we study how pedestrian's impatience degree (panic level) influence the evacuation time. Different panic levels are set and the average evacuation time corresponding to each panic level is recorded and analyzed. Second, we consider different numbers of pedestrians in the simulation, compare the evacuation time and the run time of the CA model on one hand and of the SF model on the other hand.

1. Panic level vs Evacuation time

We study different panic levels (degrees of the pedestrian's impatience) versus the evacuation time of 300 pedestrians. For a certain setting of the panic level in the simulation, all individuals are assumed to have this panic level. The panic level is described as the change of a pedestrian's actual velocity as given by equation (1.2) in our model. Hence, for a certain panic level of pedestrians in the simulation, one needs to set actual velocities of the pedestrians according to this panic level using equation (1.2). In the CA model all pedestrians are assumed to move with the same velocity. The computed actual velocity will be applied to all pedestrians and is also used to compute the time step in the simulation. For illustration, suppose we set the panic level of the pedestrians in the simulation equal 0. Using equation (1.2), we attain the actual velocity of a pedestrian equal to his initial speed ($v_i(0)$) which is set to 1 in our model. Since the average movement of an individual in the CA model for each time step is $0.48m$, one time step in the CA model with panic level 0 is $0.48s$.

In the SF model, once we set a panic level of pedestrians in the simulation, the desired speed v_i^d would change according to this setting given by equation (1.28). Therefore, the actual velocities of pedestrians would lead to this desired speed as the time progress. We do not need to set up the actual speed of an individual in the SF model.

Table 1.19 shows average of the evacuation times and the run times for different panic levels. In the SF model, the average evacuation time is less than in the CA model for all settings of the panic level but the computation times are longer in all cases. Nevertheless, both models can represent the *faster is slower effect*. It means that if the pedestrians tend to move faster

when their panic levels are small or under a certain panic level, the evacuation time decreases. However, if the pedestrians try to move faster above a certain panic level, this leads to a longer evacuation.

Figure 1.50 shows that when we increase the panic level from 0 to 0.4, the evacuation time tends to decrease both in the CA model and in the SF model. Once we increase the panic level from 0.6 to 0.9, the evacuation time tends to increase significantly in the CA model. In the SF model, the evacuation time increases from panic level 0.7 to 0.9.

Panic level	Evacuation time		Run time (10 rounds)	
	CA model	SF model	CA model	SF model
0	$40.2720s$	$40.2520s$	$31.1297s$	$2.0335h$
0.1	$35.0400s$	$32.1760s$	$25.5353s$	$1.6178h$
0.2	$29.0436s$	$27.2060s$	$24.9755s$	$1.4946h$
0.3	$25.5000s$	$23.5320s$	$24.7128s$	$1.5174h$
0.4	$24.9098s$	$20.4560s$	$23.9352s$	$1.2170h$
0.5	$26.5920s$	$18.9280s$	$27.4730s$	$1.1655h$
0.6	$24.5911s$	$20.2320s$	$29.7647s$	$1.1725h$
0.7	$32.5000s$	$18.5340s$	$37.3569s$	$1.3620h$
0.8	$46.2238s$	$19.4500s$	$49.4243s$	$1.3452h$
0.9	$64.4978s$	$52.0260s$	$60.7825s$	$2.8876h$

Table 1.19: Comparisons of the average evacuation time and the computation time for different settings of the panic levels using the CA model and the SF model.

2. #Pedestrians vs Evacuation & Computation times

We set $100, 200, ..., 1000$ pedestrians in the simulations and compare the evacuation times and computation times between the SF model and the CA model. Table 1.20 illustrates the evacuation times and computation times for different numbers of pedestrians in the simulation. The evacuation time and the run time are increased when the number of pedestrians in the simulation is increased. The computation time is in all simulations relatively larger in the SF model than in the CA model. Now let us consider the time complexities of the CA model and the SF model in no effect. The algorithms of the CA and SF model in no effect are shown in Algorithm 1 and in Algorithm 2 respectively.

#Pedestrians	Evacuation time		Run time (1 round)	
	CA model	SF model	CA model	SF model
100	19.1400s	17.6000s	0.7670s	66.7452s
200	19.4300s	24.2200s	1.1114s	193.8752s
300	23.4900s	27.2200s	2.0116s	369.5026s
400	26.3900s	32.0000s	2.4726s	594.8443s
500	37.7000s	35.8800s	4.1497s	915.8316s
600	38.5700s	42.0800s	5.6163s	1384.9900s
700	48.7200s	47.6800s	7.2155s	1836.5371s
800	50.7500s	53.9200s	8.4307s	2532.8070s
900	57.1300s	54.9400s	10.7262s	3423.5167s
1000	61.7700s	59.9000s	12.9477s	3856.4215s

Table 1.20: Comparisons of the evacuation and the computation time for different numbers of pedestrians in the simulations using the CA model and the SF model.

Time Complexity

1. CA model
   Let N be the number of individuals in the simulation, N_{tc} is the number of time step in the CA iteration, N_c is the number of cells on the domain, N_e is the number of exits and N_{cf} is the number of cells which have conflicts.

   (a) Line codes 1-8: In these steps the distances of each cell to the exits are calculated and the exit area cells are determined. To find the exit area cells and the distance of each cell to the exits, it takes $\mathcal{O}(N_c N_e)$.

   (b) Line codes 13-16: These lines are used to count the occupant density of each exit (OD). This computation requires $\mathcal{O}(N_{tc} N_e)$

   (c) Line codes 18-25: In this process each individual determines the probability of each exit to be selected (PS), selects one exit to move out and selects one cell in his PPs for the next move. This process takes $\mathcal{O}(N_{tc} N N_e)$.

   (d) Line codes 27-33: It is used for parallel update. This process takes $\mathcal{O}(N_{tc} N_{tf})$, where N_{tf} is the total number of conflicts. N_{tf} is normally less than N.

   (e) Line codes 34-40: The position of each pedestrian and the state

of each cell are updated. The number of outside pedestrians is counted. This iteration takes $\mathcal{O}(N_{tc}N)$.

Since the process (c) takes most of the time compared to other processes, the total computational cost of the CA algorithm is bounded by $\mathcal{O}(N_{tc}NN_e)$.

2. SF model
Let N be the number of individuals in the simulation, N_{ts} is the number of time step in the SF iteration, N_e is the number of exits and N_w is the number of walls and obstacles.

   (a) Line codes 4-11: In these steps we count the OD corresponding to each exit. It takes $\mathcal{O}(N_{ts}N_eN)$.

   (b) Line codes 13-16: We measure the distance from each individual to each exit and compute the PS of each exit. This process requires $\mathcal{O}(N_{ts}NN_e)$.

   (c) Line codes 20-26: The repulsive social force (f^{soc}) and the physical interaction force (f^{phy}) of each individual is calculated. It takes $\mathcal{O}(N_{ts}N(N-1))$.

   (d) Line codes 27-31: We compute the obstacle force. It requires $\mathcal{O}(N_{ts}NN_w)$.

   (e) Line codes 32-35: The position and velocity of each pedestrian is updated. Number of outside pedestrians is counted. This iteration takes $\mathcal{O}(N_{ts}N)$.

   In the SF algorithm the process (c) takes most of the time compared to others. Thus, the time complexity of the SF model in no effect is bounded by $\mathcal{O}(N_{ts}N^2)$, which increases quadratically with the number of individuals in the simulation. The time complexity of the SF algorithm can be reduced by taking the repulsive social force (f^{soc}) in process (c) into account, when an individual has contact with others, i.e. $r_{ij} \geq d_{ij}$. This reduces the computational cost of the SF algorithm to $\mathcal{O}(N_{ts}NN_{it})$, where N_{it} is the total number of interaction individuals.

It is obvious that the time complexity of the SF algorithm is relatively larger than the complexity of the CA algorithm. It increases quadratically with the number of individuals in the SF algorithm and linearly with the number of individuals in the CA algorithm. In our settings, a time step in the CA model is 0.29 while in the SF model is 0.02. Hence, we have $N_{tc} < N_{ts}$.

```
for c = 1 to N_c do
    for e = 1 to N_e do
        Compute distance to exit e;
        Check if cell c is an exit area cell of exit e (EA_e);
        if c ∈ EA_e then // Put c in En_e
        end
    end
end
Place randomly persons on the domain;
Set state of occupied cell equal 1. Otherwise 0;
no_c = 0;
for t = 1 to N_tc do
    for e = 1 to N_e do
        Find cells in En_e that their states are 1;
        Count OD of exit e;
    end
    Set states of all cells equal 0;
    for i = 1 to N do
        for e = 1 to N_e do
            Compute PS of exit e;
        end
        Select the exit that is the highest PS;
        Find PPs;
        Choose randomly one cell in the PPs;
    end
    Check if conflicts arise;
    while there are conflicts do
        Find cells which have conflicts;
        for cf = 1 to N_cf do
            Find persons who want to move to conflict cell cf;
            Choose randomly one person to move to this cell.
            Others stay their old cell;
        end
    end
    for i_1 = 1 to N do
        Update position of person i_1;
        Set state of cell which person i_1 occupies equal 1;
        Check if person i_1 is out of the room;
        if person i_1 is out of the room then // no_c = no_c + 1;
        end
    end
end
```

Algorithm 1: CA pseudo code

```
Random x_i(0) on the domain; Choose v_i(0) randomly;
no_s = 0;
for t = 1 to N_ts do
    for e = 1 to N_e do
        OD_e = 0;
        for n_1 = 1 to N do
            Check if person n_1 is in the exit area of exit e (A_e);
            if person n_1 ∈ A_e then // OD_e = OD_e + 1;
            end
        end
    end
    for i = 1 to N do
        for e = 1 to N_e do
            Compute distance from person i' s position to exit e;
            Compute PS of exit e;
        end
        Select the exit that is the highest PS;
        Compute f_i^d;
        f_i^soc = 0; f_i^phy = 0; f_i^w = 0; f_i^tw = 0;
        for j = 1 to N do
            if j ≠ i then // Compute d_ij;
                // f_i^soc = f_i^soc + f_ij^soc
                if r_ij ≥ d_ij then // f_i^phy = f_i^phy + f_ij^phy;
                end
            end
        end
        for w = 1 to N_w do
            Compute d_iw // f_i^w = f_i^w + f_iw
            if r_i ≥ d_iw then // f_i^tw = f_i^tw + f_iw^tw;
            end
        end
        Update position and velocity of person i;
        Check if person i is out of the room;
        if person i is out of the room then // no_s = no_s + 1;
        end
    end
end
```

Algorithm 2: SF pseudo code

1.5 Conclusions

In this chapters basic exit selections and human behaviour in emergency situations were embedded in the cellular automata and the social force model. Thus, we simulated evacuation processes in a multiple exits room with and without obstacles. The exit selection model was used to determine the evacuation route of individuals. It incorporates the consideration of the distance, the occupant density (OD), the pedestrians' impatience degree and the smoke density around an exit area in a simulation domain with a smoke source. Through simple mathematical models, human behaviour in emergency situation, i.e. the unadventurous effect, the inertial effect, the group effect,the smoke spreading effect, the flow with the stream effect and the obstacle effect were demonstrated. These effects were implemented in the CA and the SF models and their numerical results were compared. In most of the experiments, the CA and SF models yielded similar results, except for the flow with the stream effect. Considering this effect all occupants were able to evacuate within the given period of time in the SF model. This is because the movements of pedestrians in each time step of the SF model are not limited to neighbouring cells as in the CA model. Therefore, the chance that an individual traces their old paths is less in the SF model compared to the CA model. Since the time step to update individuals' positions of the SF model is relatively smaller than of the CA model, individuals' positions are updated more frequently in the SF model than in the CA model. Thus, the possibility that pedestrians in the SF model find others in their limited visibility, move with others and leave the room is larger than in the CA model.

Arching phenomena were evident at the exits and were observed in both the CA and the SF models. In many studies the occupant density of each exit (OD) is higher in the SF model than in the CA model.

In no effect, different panic levels and different numbers of pedestrians versus evacuation time and computation time are studied. The CA and SF models can represent the *faster is slower effect*. An increasing number of pedestrians in the simulation leads to a longer evacuation time in both the CA and the SF models. In all simulations, the computation times of the SF model are relatively larger than those of the CA model. With an increasing number of individuals to be simulated, the costs increases linearly in the CA model and quadratically in the SF model.

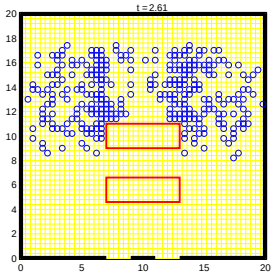

(a) CA, $t = 2.61s$

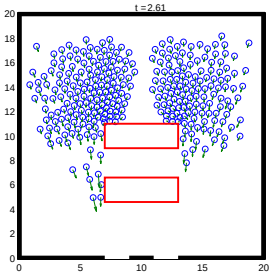

(e) SF, $t = 2.61s$

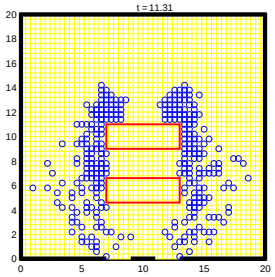

(b) CA, $t = 11.31s$

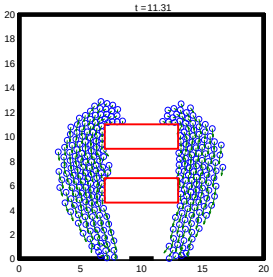

(f) SF, $t = 11.31s$

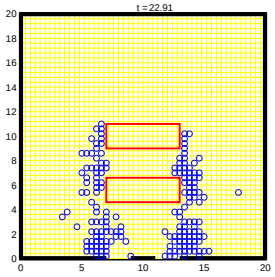

(c) CA, $t = 22.91s$

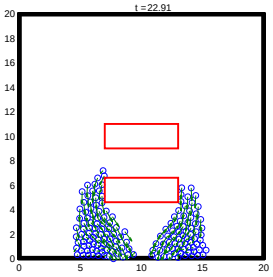

(g) SF, $t = 22.91s$

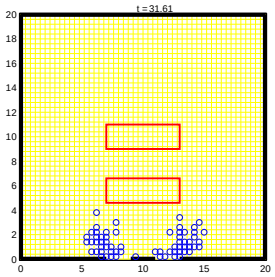

(d) CA, $t = 31.61s$

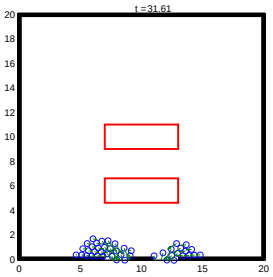

(h) SF, $t = 31.61s$

Figure 1.49: Comparison of the individuals' movements in a room with rectangular obstacles arranged parallel to exits of the CA and SF models.

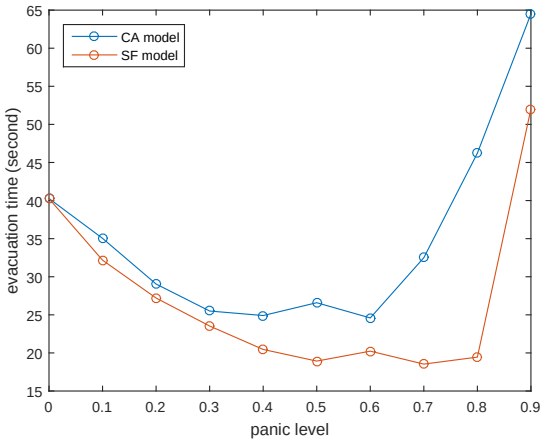

Figure 1.50: Panic level versus average evacuation time plot of the CA model and the SF model.

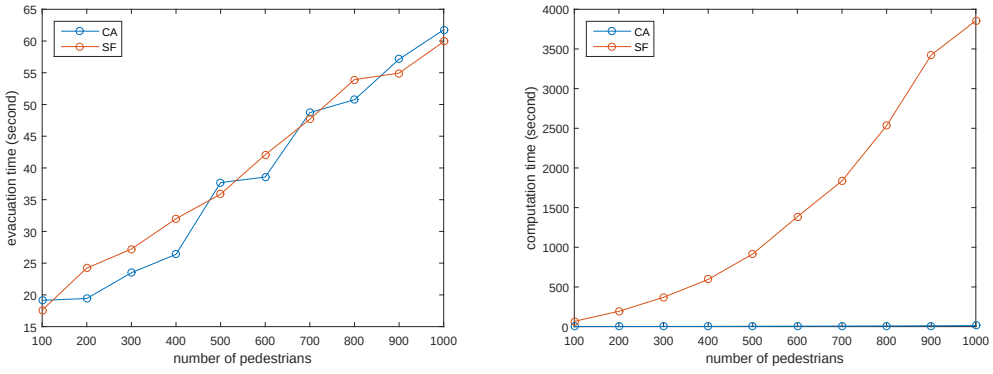

(a) Evacuation time

(b) Computation time

Figure 1.51: Plots of evacuation times and computation times of the CA, SF models with different number of pedestrians in the simulation.

Chapter 2

Local visibility model for pedestrian flow: a hierarchy of models and particle methods

In this chapter, we couple the microscopic social force model with the local visibility model first. In a second step, we derive the related mean field equation. Then, the hydrodynamic equations and their qualitative analysis are presented. The associated scalar model is proposed and finally, the numerical methods and numerical results are shown and the conclusions are made.

2.1 Microscopic social force model

A microscopic social force model without boundary force for pedestrian crowd is considered [35]. In our model, the pedestrians are assumed to have a global knowledge about the physical setting but their perception of density is limited by their visual field. The movement direction of a pedestrian results from a compromise between the shortest path and the way with the least pedestrian density in his visual field. Therefore, the microscopic social force model including the local visibility model [9, 17] together with the shortest path in two dimensions with location $x_i \in \mathbb{R}^2$ and velocity $v_i \in \mathbb{R}^2$ is described by the following equations

$$dx_i = v_i dt, \tag{2.1}$$

$$dv_i = D(x_i, v_i, \rho(x_i))dt + \sum_{i \neq j} U(x_i, x_j, v_i, v_j)dt, \tag{2.2}$$

where the desired force is given by

$$D(x_i, v_i, \rho(x_i)) = \frac{1}{\tau}[v^d \nu(x_i) - v_i]. \tag{2.3}$$

Here, τ is the relaxation time, v^d is the desired speed and $\nu(x_i) = \nu_0(x_i) + \nu_1(\rho(x_i))$ with

$$\nu_0(x_i) = -\frac{\nabla T(x_i)}{|\nabla T(x_i)|}. \tag{2.4}$$

T is given by the solution of the Eikonal equation

$$|\nabla T(x)| = \frac{1}{F(x)}, \quad x \in \Omega,$$

with boundary condition

$$T(x) = 0, \quad x \in \Gamma_0,$$

where Γ_0 stands for initial front or area in the domain where the pedestrians want to reach. $F(x)$ is a moving speed of front. It is set to 1 for walkable areas and set to 0.0001 for areas obstructed by obstacles [53]. Equation (2.4) is interpreted as the unit vector pointing in the direction of shortest path towards the target. The direction with the minimum pedestrian density in the visual view of pedestrian i is defined as in [9, 17], i.e.

$$\nu_1(\rho(x_i)) = \eta \mu_m(\rho(x_i)), \tag{2.5}$$

$$\mu_m(\rho(x_i)) = \min_{\xi \in M}[\xi \cdot \nabla \rho(x_i)], \tag{2.6}$$

$$M = \{\ \xi = \cos\alpha i + \sin\alpha j | \alpha \in R_v\}\ , \tag{2.7}$$

$$R_v = [\gamma - \theta_v, \gamma + \theta_v], \quad \gamma = \arctan(\frac{\nu_{02}(x_i)}{\nu_{01}(x_i)}), \tag{2.8}$$

where R_v is the visual range interval in which the pedestrian chooses the direction of motion. γ is the angle identifying the direction of ν_0, $\nu_0 = (\nu_{01}, \nu_{02})$. θ_v is the maximum visibility angle of the individual in average. M is the domain of the path directions on R_v. $\mu_m(\rho(x_i))$ represents the direction that points to the minimal pedestrian density. It yields the position ξ in M where the dot product with the density gradient at x_i is minimal. η is a positive small parameter introduced to model a corrective term which is related to the attraction towards the small density gradients. The interaction force U consists of the repulsive social force and the physical interaction force, i.e.

$$U(x_i, x_j, v_i, v_j) = f_{ij}^{soc}(t) H(r_{ij} - d_{ij}) + f_{ij}^{phy}(t), \tag{2.9}$$

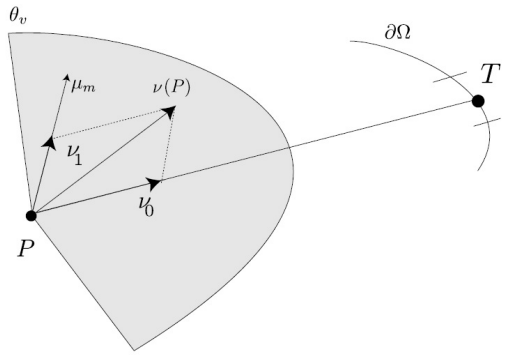

Figure 2.1: Direction of motion in the visual range [9].

where $H(r_{ij} - d_{ij})$ denotes the Heaviside function. $f_{ij}^{soc}(t)$ is the repulsive social force that is illustrated as

$$f_{ij}^{soc}(t) = A_i \exp\left(\frac{r_{ij} - d_{ij}}{B_i}\right) n_{ij}\left(\lambda_i + (1 - \lambda_i)\frac{1 + \cos(\varphi_{ij})}{2}\right), \tag{2.10}$$

where $A_i, B_i, r_{ij}, d_{ij}, \lambda_i$ and $\cos\varphi_{ij}$ are explained in the same way as in equation (1.23). $f_{ij}^{ph}(t)$ reflects the physical interaction force and is expressed by

$$f_{ij}^{ph}(t) = k_n H(r_{ij} - d_{ij}) n_{ij} + k_t H(r_{ij} - d_{ij}) \Delta v_{ji}^t t_{ij}, \tag{2.11}$$

where k_n, k_t, v_{ij}^t and t_{ij} are defined in the same way as in equation (1.24).

2.2 Mean field and macroscopic limits

2.2.1 Mean field equation

To analyze the limit of a large number of particles N, the amplitude of the interaction potential is scaled with a factor $\frac{1}{N}$ using the assumption of the *weak coupling scaling*. Therefore, the scaled microscopic model is written as

$$dx_i = v_i dt, \tag{2.12}$$

$$dv_i = D(x_i, v_i, \rho_i)dt + \frac{1}{N}\sum_{i \neq j} U(x_i, x_j, v_i, v_j)dt. \tag{2.13}$$

The derivation of the mean field kinetic model from the particle system (2.12-2.13) is as follows. Let $f^{(N)}(x_i, v_i, t)$ be the N-particle probability density

function. The time evolution of $f^{(N)}$ can be written according to the following Liouville equation

$$\frac{\partial f^{(N)}}{\partial t} + \sum_{i=1}^{N}[\mathrm{div}_{x_i}(\dot{x_i} f^{(N)}) + \mathrm{div}_{v_i}(\dot{v_i} f^{(N)})] = 0, \tag{2.14}$$

where x_i and v_i are specified through (2.12-2.13). The one particle distribution function $f^{(1)}$ is expressed as

$$f^{(1)}(x_1, v_1, t) = \int f^{(N)} dx_2 ... dx_N dv_2 ... dv_N.$$

We integrate equation (2.14) over $d\Omega_1$, $d\Omega_1 = dx_2 ... dx_N dv_2 ... dv_N$ and restrict our study to the case of $f^{(1)}$. Then one achieves

$$\frac{\partial f^{(1)}}{\partial t} + \int \mathrm{div}_{x_1}(v_1 f^{(N)}) d\Omega_1 + \int \mathrm{div}_{v_1}(\dot{v_1} f^{(N)}) d\Omega_1 = 0.$$

The spatial divergence term reduces to $v_1 \cdot \nabla_{x_1} f^{(1)}$, while we obtain two contributions for the velocity divergence term:

$$\mathrm{div}_{v_1}[D(x_1, v_1, \rho(x_1)) f^{(1)}] \quad \text{and} \quad \mathrm{div}_{v_1} \int \frac{1}{N} \sum_{j \neq 1} U(x_1, x_j, v_1, v_j) f^{(N)} d\Omega_1.$$

Since particles are indistinguishable, the second term can be written as

$$\frac{N-1}{N} \mathrm{div}_{v_1} \int U(x_1, x_2, v_1, v_2) f^{(2)}(x_1, x_2, v_1, v_2, t) dx_2 dv_2.$$

Here, $f^{(2)}$ is the two particle probability function

$$f^{(2)}(x_1, x_2, v_1, v_2, t) = \int f^{(N)} dx_3 ... dx_N dv_3 ... dv_N.$$

With the assumption of the factorization

$$f^{(2)}(x_1, x_2, v_1, v_2, t) = f^{(1)}(x_1, v_1, t) f^{(1)}(x_2, v_2, t),$$

we attain the second term of the velocity divergence as

$$\frac{N-1}{N} \mathrm{div}_{v_1} \int U(x_1, x_2, v_1, v_2) f^{(1)}(x_2, v_2, t) dx_2 dv_2 f^{(1)}(x_1, v_1, t). \tag{2.15}$$

Since $\rho(x,t) = \int f(x, v, t) dv$, equation (2.15) can be written as

$$\frac{N-1}{N} \mathrm{div}_{v_1} \int U(x_1, x_2, v_1, v_2) \rho(x_2, t) dx_2 f^{(1)}(x_1, v_1, t).$$

Replacing $f^{(1)}$ with f and setting $N \to \infty$, the mean field equation is obtained

$$\frac{\partial f}{\partial t} + v \cdot \nabla_x f + Pf = 0, \tag{2.16}$$

where

$$Pf = \nabla_v \cdot (D(x, v, \rho(x)) f) + \nabla_v \cdot (\int U(x, y, v, w) \rho(y, t) dy f).$$

2.2.2 Hydrodynamic model

Starting from the mean field equation (2.16), we can derive the macroscopic quantities. We integrate equation (2.16) against v and vdv and assume that the fluctuation terms are negligible, i.e. the velocity distribution is monokinetic: $f(x,v,t) = \rho(x,t)\delta(v-u(x,t))$, where δ is the Dirac delta function. The following macroscopic system results:

$$\frac{\partial \rho}{\partial t} + \nabla_x \cdot (\rho u) = 0, \tag{2.17}$$

$$\frac{\partial u}{\partial t} + (u \cdot \nabla_x)u = \widetilde{D}(x,u,\rho) + \widetilde{U}(x,u,\rho), \tag{2.18}$$

with

$$\widetilde{U}(x,u,\rho) = \int U(x,w,u(x),u(w))\rho(w)dw,$$
$$\widetilde{D}(x,u,\rho) = \frac{1}{\tau}[v^d(\nu_0(x) + \nu_1(\rho(x))) - u],$$

where

$$\begin{aligned} \nu_0(x) &= -\frac{\nabla T(x)}{|\nabla T(x)|}, \quad \nu_1(\rho(x)) = \eta\mu(\rho(x)), \\ \mu(\rho(x)) &= \min_{\xi \in M}[\xi \cdot \nabla\rho(x)], \\ M &= \{\xi = \cos\alpha i + \sin\alpha j | \alpha \in R_v\}, \\ R_v &= [\gamma - \theta_v, \gamma + \theta_v], \quad \gamma = \arctan(\frac{\nu_{02}(x)}{\nu_{01}(x)}). \end{aligned} \tag{2.19}$$

Hydrodynamic limits for similar equations have been derived in the references [13, 16] for the case of swarming, in the reference [30] for material flow problems and in the reference [29] for pedestrian flows with optimal path. Now let us consider a qualitative analysis of the system of partial differential equations (2.17-2.18). First, we give a definition of a system of partial differential equations (PDEs). Then we analyze the derived macroscopic system (2.17-2.18).

Definition 2.2.1. [9] A system of PDEs in two dimensions is given by

$$\partial_t(Q) + \partial_x B(Q) + \partial_y G(Q) = 0 \in \mathbb{R}^+ \times \mathbb{R}^2,$$
$$Q(0,\cdot) = Q_0 \in \mathbb{R}^n,$$

$Q \in \mathbb{R}^n$ and $(x,y) \in \mathbb{R}^2$. The PDEs system is called a (strictly) hyperbolic system, if all eigenvalues of $\delta_1 B'(Q) + \delta_2 G'(Q)$ are real (and distinct) for all $\delta_1, \delta_2 \in \mathbb{R}$ and $Q \in \mathbb{R}^n$.

The macroscopic system (2.17-2.18) in two dimensions can be rewritten as

$$\partial_t \rho + \partial_x(\rho u_x) + \partial_y(\rho u_y) = 0, \tag{2.20}$$
$$\partial_t u_x + u_x \partial_x(u_x) + u_y \partial_y(u_x) = A_1(\rho, u_x), \tag{2.21}$$
$$\partial_t u_y + u_x \partial_x(u_y) + u_y \partial_y(u_y) = A_2(\rho, u_y), \tag{2.22}$$

where $u = (u_x, u_y)$ and

$$A_1(\rho, u_x) = \frac{1}{\tau}[v^d(\nu_{0x} + \nu_{1x}) - u_x] + \int U_x \rho(w) dw,$$
$$A_2(\rho, u_y) = \frac{1}{\tau}[v^d(\nu_{0y} + \nu_{1y}) - u_y] + \int U_y \rho(w) dw,$$

where $\nu_0 = (\nu_{0x}, \nu_{0y}), \nu_1 = (\nu_{1x}, \nu_{1y})$ and $U = (U_x, U_y)$. Now we write the system (2.17-2.18) in the conservation form as

$$\partial_t(Q) + \partial_x B(Q) + \partial_y G(Q) = A,$$

where Q represents the conservative variables, B and G are the fluxes in the two space dimension, and A is considered as the source term. These are given by

$$Q = \begin{pmatrix} q_1 \\ q_2 \\ q_3 \end{pmatrix} = \begin{pmatrix} \rho \\ u_x \\ u_y \end{pmatrix}, \quad B(Q) = \begin{pmatrix} q_1 q_2 \\ q_2^2 \\ q_2 q_3 \end{pmatrix} = \begin{pmatrix} \rho u_x \\ (u_x)^2 \\ u_x u_y \end{pmatrix},$$
$$G(Q) = \begin{pmatrix} q_1 q_3 \\ q_2 q_3 \\ q_3^2 \end{pmatrix} = \begin{pmatrix} \rho u_y \\ u_x u_y \\ (u_y)^2 \end{pmatrix}, \quad A = \begin{pmatrix} 0 \\ A_1(\rho, u_x) \\ A_2(\rho, u_y) \end{pmatrix}.$$

In the next step we write the system in the general quasi-linear form and set the source term to zero. Then we obtain the homogeneous PDEs as

$$\partial_t(Q) + K(Q)\partial_x Q + M(Q)\partial_y Q = 0,$$

where the flux Jacobian matrices $K(Q)$ and $B(Q)$ are recieved from the partial derivative of the fluxes given by

$$K(Q) = \frac{\partial B(Q)}{\partial Q} = \begin{pmatrix} q_2 & q_1 & 0 \\ 0 & 2q_2 & 0 \\ 0 & q_3 & q_2 \end{pmatrix} = \begin{pmatrix} u_x & \rho & 0 \\ 0 & 2u_x & 0 \\ 0 & u_y & u_x \end{pmatrix},$$
$$M(Q) = \frac{\partial G(Q)}{\partial Q} = \begin{pmatrix} q_3 & 0 & q_1 \\ 0 & q_3 & q_2 \\ 0 & 0 & 2q_3 \end{pmatrix} = \begin{pmatrix} u_y & 0 & \rho \\ 0 & u_y & u_x \\ 0 & 0 & 2u_y \end{pmatrix}.$$

The eigenvalues of matrix K are found by solving the characteristic equation

$$|K(Q) - \lambda I| = 0,$$

which gives $\lambda_{1K} = \lambda_{2K} = u_x$, $\lambda_{3K} = 2u_x$. The corresponding eigenvectors are $\chi_{1K} = \begin{pmatrix} 1 \\ 0 \\ 1 \end{pmatrix}$, $\chi_{2K} = \begin{pmatrix} 0 \\ 1 \\ 0 \end{pmatrix}$, $\chi_{3K} = \begin{pmatrix} \rho \\ u_x \\ u_y \end{pmatrix}$.

For matrix $M(Q)$, we solve

$$|M(Q) - \lambda I| = 0,$$

which yields $\lambda_{1M} = \lambda_{2M} = u_y$, $\lambda_{3M} = 2u_y$. The corresponding eigenvectors are $\chi_{1M} = \begin{pmatrix} 1 \\ 1 \\ 0 \end{pmatrix}$, $\chi_{2M} = \begin{pmatrix} 0 \\ 0 \\ 1 \end{pmatrix}$, $\chi_{3M} = \begin{pmatrix} \rho \\ u_x \\ u_y \end{pmatrix}$.

In order to check if the system is (strictly) hyperbolic or not, we consider the combined Jacobian matrices which satisfy the definition 2.2.1. Let $\delta_1, \delta_2 \in \mathbb{R}$, then we have

$$\begin{aligned} J(Q) &= \delta_1 B'(Q) + \delta_2 G'(Q) \\ &= \begin{pmatrix} \delta_1 u_x + \delta_2 u_y & \delta_1 \rho & \delta_2 \rho \\ 0 & 2\delta_1 u_x + \delta_2 u_y & \delta_2 u_x \\ 0 & \delta_1 u_y & \delta_1 u_x + 2\delta_2 u_y \end{pmatrix} \end{aligned}$$

.

The eigenvalues of the combined Jacobian matrices are found to be
$\lambda_{1J} = \lambda_{2J} = \delta_1 u_x + \delta_2 u_y = \widetilde{u}, \quad \lambda_{3J} = 2(\delta_1 u_x + \delta_2 u_y) = 2\widetilde{u},$
while their corresponding eigenvectors are

$$\chi_{1J} = \begin{pmatrix} 1 \\ -\delta_2 \\ \delta_1 \end{pmatrix}, \quad \chi_{2J} = \begin{pmatrix} 0 \\ 1 \\ 1 \end{pmatrix}, \quad \chi_{3J} = \begin{pmatrix} \rho \\ u_x \\ u_y \end{pmatrix}.$$

The three eigenvalues of the combined Jacobian matrices are real. Two of the eigenvalues are equal. However, we can find linearly independent eigenvectors. Hence the crowd model (2.17-2.18) is a nonlinear hyperbolic PDEs. Since we have repeated eigenvalues, the model is not strictly hyperbolic. In addition, the system preserves its isotropic nature as seen from its eigenvalues. One of them is always greater than the velocity of the corresponding state in both velocity directions. It means that information from all directions affects the pedestrian's motion (isotropic property) [9].

2.2.3 The Scalar Model

To obtain the scalar model, we proceed in a similar way as in reference [30]. Starting from the hydrodynamic momentum equation (2.18), we assume that

the interaction potential U depends only on x. Neglecting the anisotropic term in the repulsive social force $(\lambda_i + (1-\lambda_i)\frac{1+\cos\varphi_{ij}}{2})$, the sliding friction force $(k_t H(r_{ij} - d_{ij})\Delta v_{ji}^t t_{ij})$, the inertial term and the time changes, one obtains

$$\widetilde{D}(x, u, \rho) = -U * \rho, \tag{2.23}$$

where

$$U * \rho = \int U(x, w)\rho(w)dw,$$
$$\widetilde{D}(x, u, \rho) = \frac{1}{\tau}[v^d(\nu_0(x) + \nu_1(\rho(x))) - u],$$

Solving equation (2.23) for u gives us

$$u = v^d(\nu_0(x) + \nu_1(\rho(x))) + \tau U * \rho.$$

The result u is used to close the continuity equation (2.17). This provides us the scalar equation

$$\frac{\partial \rho}{\partial t} + \nabla_x \cdot (\rho v^d(\nu_0(x) + \nu_1(\rho(x)))) + \nabla_x \cdot ((\tau U * \rho)\rho) = 0. \tag{2.24}$$

2.3 Numerical Methods

This section is devoted to numerical methods that are used on the microscopic equations (2.1-2.2 and 2.12-2.13) as well as on the hydrodynamic limit (2.17-2.18) and on the scalar model (2.24).

2.3.1 Microscopic simulation

The microscopic equations are solved numerically by using the explicit Euler method with fixed time step 0.02. The computational domain is discretized into cells. Each cell has the same area with a size of $0.5m \times 0.5m$ and is represented by its centre. The macroscopic quantities ρ, u are evaluated at these cell centres. The local particle density of each cell is the number of particles in that cell divided by N_{max}, where N_{max} is the maximum number of pedestrians in one cell. u is the average velocity of the pedestrians in the cell. The density gradient in equation (2.6) is approximated by the forward difference. In the case that the forward difference cannot be applied, if, for example, the density cell is near a boundary, we apply the backward difference.

2.3.2 Macroscopic simulation

We consider the hydrodynamic equations (2.17-2.18) in a Lagrangian formulation:

$$\frac{dx}{dt} = u, \tag{2.25}$$

$$\frac{d\rho}{dt} = -\rho\frac{\partial u}{\partial x}, \tag{2.26}$$

$$\frac{du}{dt} = \widetilde{D}(\rho, T, u) + \widetilde{U}(\rho, u), \tag{2.27}$$

where $\frac{d}{dt} = \partial_t + u \cdot \nabla_x$. We evaluate these quantities at the particle location and approximate the spatial derivative of u by a corrective smoothed particle method (CSPM) [15]. In two dimensions, the particle approximations for the derivative of $u^{(1)}$ with respect to $x^{(1)}$ at point i, where $u = (u^{(1)}, u^{(2)})$ and $x = (x^{(1)}, x^{(2)})$, is given by

$$\frac{du_i^{(1)}}{dx^{(1)}} = \frac{\sum_{j=1}^{Nb} \frac{m_j}{\rho_j}(u_j^{(1)} - u_i^{(1)})\frac{\partial W_{ij}}{\partial x_j^{(1)}}}{\sum_{j=1}^{Nb} \frac{m_j}{\rho_j}(x_j^{(1)} - x_i^{(1)})\frac{\partial W_{ij}}{\partial x_j^{(1)}}}. \tag{2.28}$$

The first derivative of $u^{(2)}$ with respect to $x^{(2)}$ of particle i is obtained in a similar way illustrated as

$$\frac{du_i^{(2)}}{dx^{(2)}} = \frac{\sum_{j=1}^{Nb} \frac{m_j}{\rho_j}(u_j^{(2)} - u_i^{(2)})\frac{\partial W_{ij}}{\partial x_j^{(2)}}}{\sum_{j=1}^{Nb} \frac{m_j}{\rho_j}(x_j^{(2)} - x_i^{(2)})\frac{\partial W_{ij}}{\partial x_j^{(2)}}},$$

where $u(x_i) = u_i = (u_i^{(1)}, u_i^{(2)})$, $x_i = (x_i^{(1)}, x_i^{(2)})$ and $x_j = (x_j^{(1)}, x_j^{(2)})$. $W_{ij} = W(x_j - x_i, h)$ is the smoothing function whose support domain is determined by the smoothing length h. Nb is the number of particles in the support domain. m_j and ρ_j are the mass and density of particle j. The following cubic spline function is applied as the smoothing function in our numerical experiments [57]:

$$W_{ij} = \frac{15}{7\pi h^2}\begin{cases} \frac{2}{3} - \vartheta^2 + \frac{1}{2}\vartheta^3 & , \quad 0 \le \vartheta < 1, \\ \frac{1}{6}(2-\vartheta)^3 & , \quad 1 \le \vartheta < 2, \\ 0 & , \quad \vartheta \ge 2, \end{cases} \tag{2.29}$$

where $\vartheta = \frac{|x_j - x_i|}{h}$. A smoothed particle hydrodynamics (SPH) method [50] is applied to calculate the spatial derivative of the density ρ in equation (2.19)

as follows:

$$\frac{\partial \rho_i}{\partial x} = \sum_{j=1}^{Nb} m_j \frac{\partial W_{ij}}{\partial x_i}. \tag{2.30}$$

The integral over the interaction force is computed by a straight-forward integration rule:

$$\widetilde{U}(\rho, u) = \sum_j U(x, x_j, u(x), u_j)\rho_j dV_j, \tag{2.31}$$

where dV_j is the local area around particle j which is determined by a nearest neighbor search. It is obvious that certain macroscopic computations have some similarities with the microscopic ones. The difference constitutes in the way of evaluating the interaction term. In the microscopic model we calculate

$$\frac{1}{N}\sum_j U(x, x_j, v, v_j)$$

instead of (2.31). If the value of ρ_j and dV_j are equal, we employ

$$1 = \int \rho(x)dx = \sum_j \rho_j dV_j$$

Obvoiusly, both similutions are equivalent to each other. However, in the macroscopic context the particles are not physical particles as in the microscopic case. They play the role of discretization points. If the real number of particles are large, it does not mean that the number of macroscopic particles has to be increased in the same way. Furthermore, the macroscopic equations that are regarded here are derived under the assumption of a mono-kinetic distribution function. Hence, they are not able capture all microscopic patterns.

Finally, the scalar model (2.24)

$$\frac{\partial \rho}{\partial t} + \nabla_x(a\rho) = 0,$$

with

$$a = v^d(\nu_0(x) + \nu_1(x)) + \tau U * \rho,$$

is solved with the particle method as well. We consider it in a Lagrangian description and write it as

$$\frac{dx}{dt} = a,$$
$$\frac{d\rho}{dt} = -\rho\frac{\partial a}{\partial x}.$$

The approximation of the spatial derivative of a and ρ in the local visibility model (2.19) uses the same method as in the hydrodynamic model, i.e. a CSPM method for the spatial derivative of a and a SPH method for the spatial derivative of ρ. An explicit time integration is used to solve the hydrodynamic and scalar models with the constant time step $\Delta t = 0.02$. In all simulations, the Eikonal equation is coupled to the flow simulation and is solved numerically by a fast marching method [79] with step size $0.1m$. Details of this method have already been described in chapter 1, section 1.3.1.

2.4 Numerical Results

In this section we investigate numerical examples. First we point out the difference between the microscopic social force that is coupled with the local visibility model (LV) and the microscopic social force that is coupled with the shortest path (SP). Then the numerical experiments on the microscopic equation (2.12-2.13) as well as the hydrodynamic equations (2.17-2.18) and scalar limit (2.24), which are coupled to the local visibility model, are presented.

The modeling area is carried out on a corridor of size $10m \times 20m$. The visual angle of a pedestrian is set to 170°, i.e. $\theta_v = 85°$, as reported in [7, 73, 85]. The angles of the test directions of a pedestrian's visual field are in R_v given by

$$R_v = \{\gamma - \theta_v, ..., \gamma - 2\theta_a, \gamma - \theta_a, \gamma, \gamma + \theta_a, \gamma + 2\theta_a, ..., \gamma + \theta_v\},$$

where $\theta_a = 5°$. The computations are performed on a ASUS Intel Core i3-2350M, 2.3GHz. All programs are implemented in MATLAB.

2.4.1 Local visibility model (LV) versus shortest path (SP)

We perform simulations of the microscopic model that is equipped with the LV path and compare numerical results with the microscopic model that is

coupled with the SP path. Considering the microscopic model with shortest path, we solve

$$\begin{aligned} dx_i &= v_i dt, \\ dv_i &= \widehat{D}(x_i, v_i)dt + \sum_{i \neq j} U(x_i, x_j, v_i, v_j)dt, \end{aligned} \tag{2.32}$$

where

$$\widehat{D}(x_i, v_i) = \frac{1}{\tau}[v^d \nu_0(x_i) - v_i].$$

The interaction force U is defined as usual in equation (2.9). The difference between the LV and SP paths lies in the movement direction. In the SP path it is given by $\nu_0(x)$, while in the LV path it is defined by $\nu_0(x) + \nu_1(x)$, where $\nu_0(x)$ gives the direction towards shortest path to the destination and $\nu_1(x)$ provides the direction with the mininum density gradient.

Two numerical experiments are investigated. In the first experiment, we arrange 120 individuals orderly with distance $0.42m$ away from each other. These pedestrians are marked with red color. 28 individuals are placed behind the red people with a distance of $1m$ from each others and labeled with blue colour, see Figure 2.2-2.3. When the simulation begins, they move towards an exit which is on the right and marked with a red straight line. The microscopic and its scaling models with LV and SP paths are conducted and their results are compared.

As a second example, we set 227 pedestrians standing orderly on the left side of the corridor at initial state. When the simulation starts, they move to the exit which is on the right side. These people are labeled with red colour. 200 blue pedestrians are randomly distributed in front of the red pedestrians at the beginning and do not move during the simulation run, see Figure 2.4. The scaled microscopic models with LV and SP path are employed in this test.

Figure 2.2 shows movements of the pedestrians with LV path on the one hand and with SP path on the other hand in the first experiment of the microscopic models. For the scaled microscopic models these movements are presented in Figure 2.3. It is obvious that for the SP path, both for scaling and for no scaling models, the movements of individuals are in order compared to the LV path. The positions of most of the people in the scaled models, both considering the SP and the LV path, are quite close to each

other, especially when they move near to the exit. This is due to the effect of scaling the interaction forces in the models. It is noted that the setting parameters are the same for scaling and for no scaling models. Therefore, the interaction strength (A_i), the normal constant (k_n) and tangential constant (k_t) in the scaling models are smaller than in the no scaling models. They are reduced by N in the scaled models. This results that pedestrians are closed to each other in the scaling models.

The time evolution of pedestrians' movements for the second experiment is demonstrated in Figure 2.4. Considering the LV path, the moves of red pedestrians are disorder, particularly when they pass through regions where blue pedestrians stand. Patterns of motions of the pedestrians are not in order compared to the simulation with the SP path. Considering the SP path, we observe that red pedestrians still move orderly, even if they have passed through a dense crowd. In this case the pedestrians' movement direction does not take the pedestrians' density factor into account.

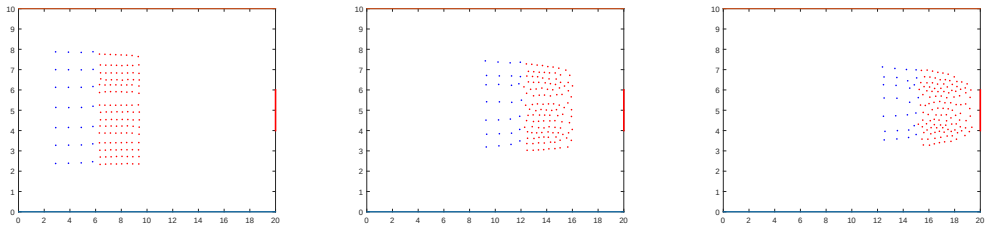

(a) LV, $t = 2s$ (b) LV, $t = 6s$ (c) LV, $t = 8s$

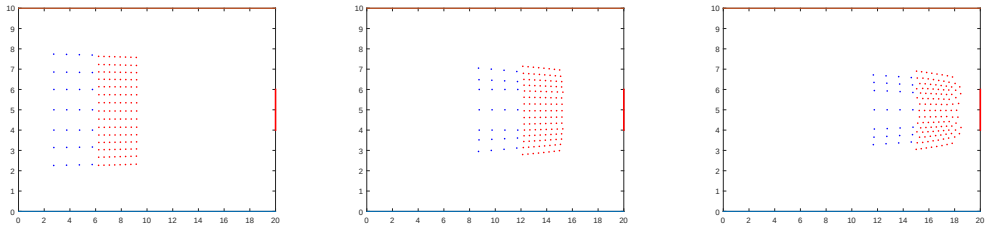

(d) SP, $t = 2s$ (e) SP, $t = 6s$ (f) SP, $t = 8s$

Figure 2.2: Comparison of the local visibility model (LV) and the shortest path (SP) included into the microscopic model.

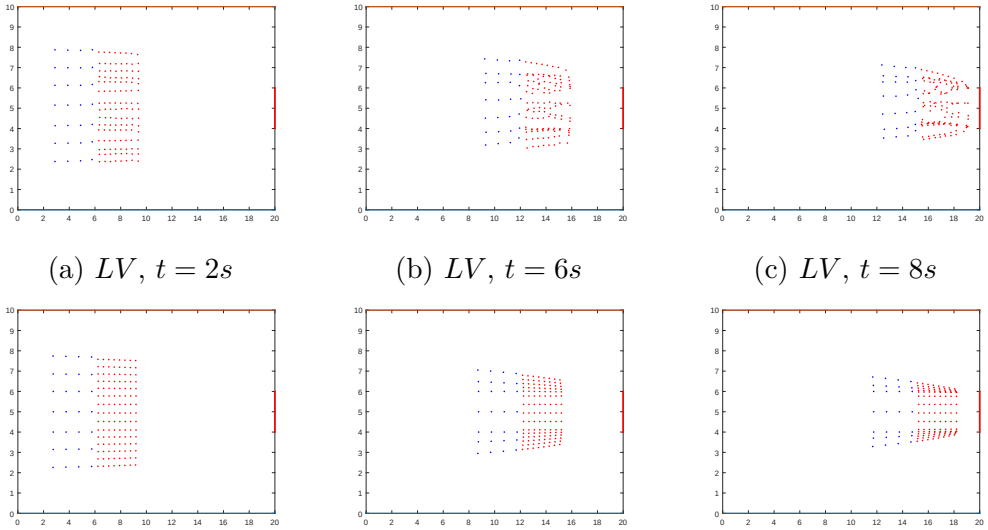

(a) LV, $t = 2s$ (b) LV, $t = 6s$ (c) LV, $t = 8s$

(d) SP, $t = 2s$ (e) SP, $t = 6s$ (f) SP, $t = 8s$

Figure 2.3: Comparison of the local visibility model (LV) and the shortest path (SP) included into the *scaled* microscopic model.

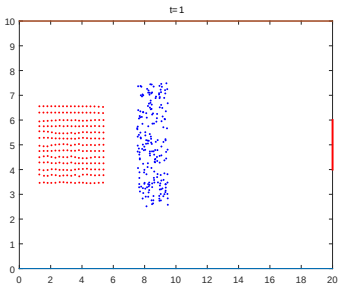

(a) LV, $t = 1s$

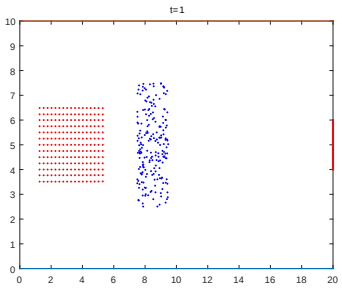

(e) SP, $t = 1s$

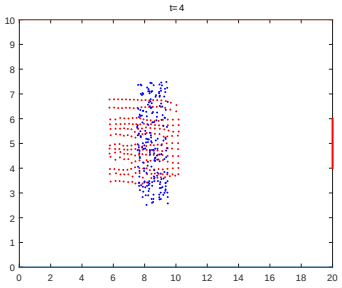

(b) LV, $t = 4s$

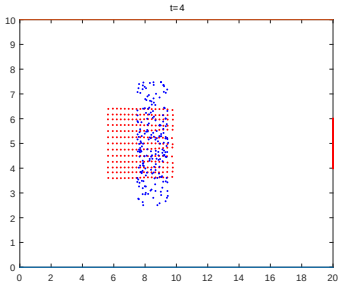

(f) SP, $t = 4s$

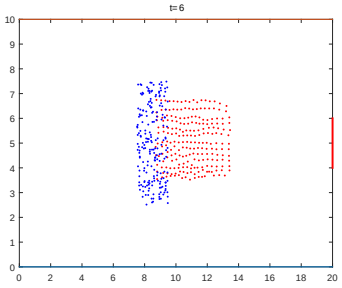

(c) LV, $t = 6s$

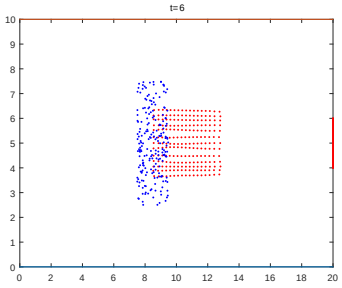

(g) SP, $t = 6s$

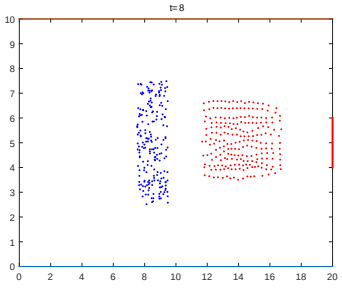

(d) LV, $t = 8s$

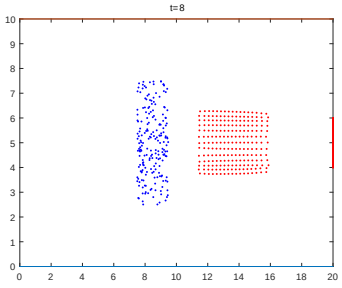

(h) SP, $t = 8s$

Figure 2.4: Local visibility model (LV) versus shortest path (SP) included into the *scaled* microscopic model.

2.4.2 Numerical results for microscopic, hydrodynamic and scalar equations with local visibility model

In these experiments, the modeling area is carried out on a corridor of size $(10m \times 20m)$ with a $2m \times 2m$ rectangular obstacle in the middle. Two exits with $2m$ width are on the right of the corridor, see Figure 2.5.

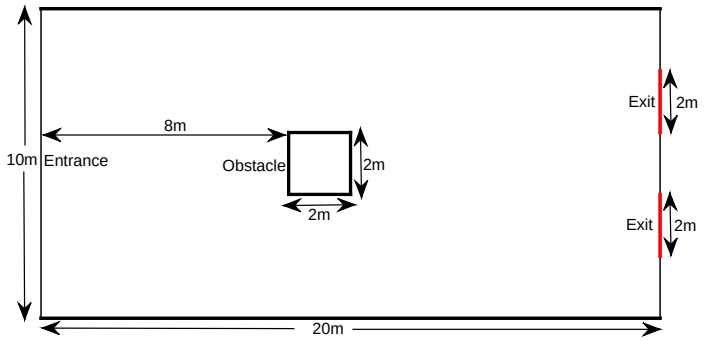

Figure 2.5: The modeling area for numerical experiments with a rectangular obstacle.

We determine that pedestrians enter the corridor from the left boundary and leave on the right through two exits. On the inflow boundary we prescribe by the following boundary conditions

$$\rho = \begin{cases} 2.5\dfrac{t}{5} & \text{if} \quad 0 \leq t \leq 5, \\ -\dfrac{2.5}{5}(t-10) & \text{if} \quad 5 \leq t \leq 10, \\ 0 & \text{else}, \end{cases} \tag{2.33}$$

In microscopic model, we discretize the domain into cells. Each cell has a size of $0.5m \times 0.5m$. The density of each cell is obtained by

$$\rho = \frac{N_a}{N_{max}},$$

where N_a is the actual number of pedestrians in the cell and N_{max} is the maximum number of pedestrians in each cell. In every $0.3s$, ρN_{max} pedestrians are initiated randomly in the cells containing the left boundary, where ρ is defined as in (2.33).

In hydrodynamic and scalar models, we generate particles every $0.3s$ on the left boundary which have a distance of $0.5cm$ from the top and bottom walls. Each particle is also placed with a distance of $2.1 \times r_i$ to each other so that they do not interact at the initial stages. Here r_i is the interaction radius of pedestrian i. The computation time for a simulation of the microscopic, hydrodynamic and scalar model is set to $25s$. The parameters that are used in our simulations are shown in Table 2.1.

Parameter	Value		Equation
	micro	hydro & scalar	
v^d	1.5	1.5	(2.3)
τ	0.5	0.5	(2.3)
η	0.05	0.05	(2.5)
θ_v	85°	85°	(2.8)
A_i	20	0.002	(2.10)
B_i	0.2	0.2	(2.10)
λ_i	0.61	0.61	(2.10)
r_{ij}	0.4	0.4	(2.9-2.11)
k_n	20	0.002	(2.11)
k_t	20	0.002	(2.11)
m_j	-	1	(2.28), (2.30)
h	-	0.4	(2.29)

Table 2.1: Parameters for microscopic, hydrodynamic and scalar simulations.

Table 2.2 shows the comparison of the computation times for the microscopic model with a different number of particles per cell. The computation times for the hydrodynamic and scalar models with 805 particles are displayed in Table 2.3. Comparing Table 2.2 and Table 2.3, it is obvious that the computation times in the macroscopic models are smaller than in the microscopic model when 2 or more particles per cell are used in the microscopic simulations. This comparison demonstrates the advantage of using the particle methods combined with the macroscopic models. In the case that the number of real microscopic particles in the system is very large, the benefit of using the meshfree macroscopic approach over the microscopic simulation is remarkable.

The comparisons of density at $t = 10s$ along the cuts $y = 7.5m$ and $x = 7.5m$ considering the microscopic, hydrodynamic and scalar models are

illustrated in Figure 2.6(a) and Figure 2.6(c). In Figure 2.6(b) and Figure 2.6(d) the densities along the cuts $y = 7.5m$ and $x = 7.5m$ at time $t = 10$, determined from microscopic model for different number of particles per cell, are compared. The macroscopic models provide a good approximation to microscopic model, especially when the number of particles per cell is large in the microscopic simulation.

The time evolution of the particles' movements for microscopic, hydrodynamic and scalar models is demonstrated in Figure 2.7. All three models show similar behaviour. The comparison of the particles' movements in corridors with rectangular obstacle and circular obstacle considering the hydrodynamic model is displayed in Figure 2.9.

N_{max}	Run Time (hour)	#Particles
1	1.0400	793
2	3.9223	1637
3	7.9868	2457
4	14.1023	3324
5	20.7598	4108

Table 2.2: Microscopic model: Maximal particles per cell N_{max}, computation time for $t = 25s$ and total number of pedestrians.

Model	Run Time (hour)	#Particles
Hydrodynamic	2.1046	805
Scalar	2.3687	805

Table 2.3: Hydrodynamic and scalar models: computation time for $t = 25s$ and total number of particles.

2.5 Conclusions

We have derived a hierarchy of models for pedestrian flow so far. It ranges from a social force model coupled to a local visibility model to macroscopic models including interaction forces and a local visibility term. The macroscopic systems are based Lagrangian formulation and solved numerically with particle methods. The numerical results of macroscopic models are similar

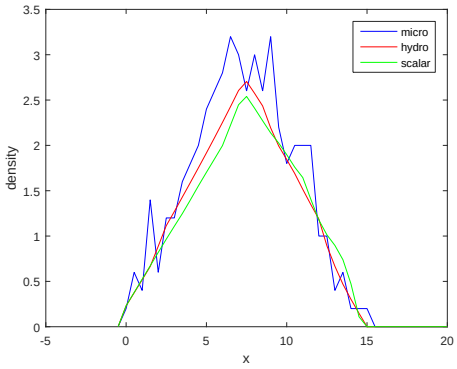

(a) cuty7.5-comparison

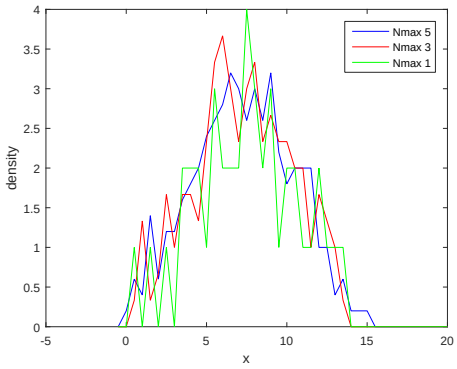

(b) cuty7.5-microscopic

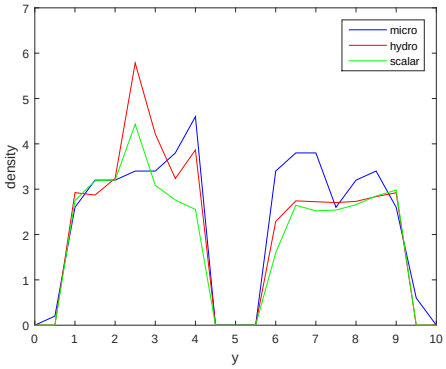

(c) cutx7.5-comparison

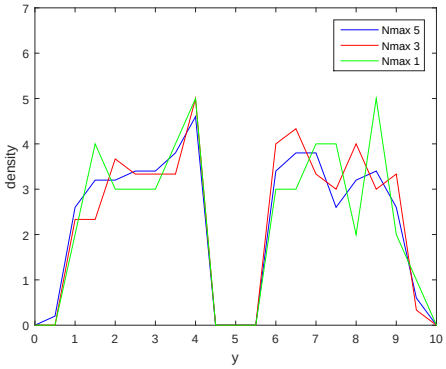

(d) cutx7.5-microscopic

Figure 2.6: Density at $t = 10s$ along $y = 7.5m$ and $x = 7.5m$ for the microscopic, hydrodynamic and scalar model.

to the results in the microscopic models and provide a good approximation to the microscopic problem when there is a large number of particles in the microscopic simulation.

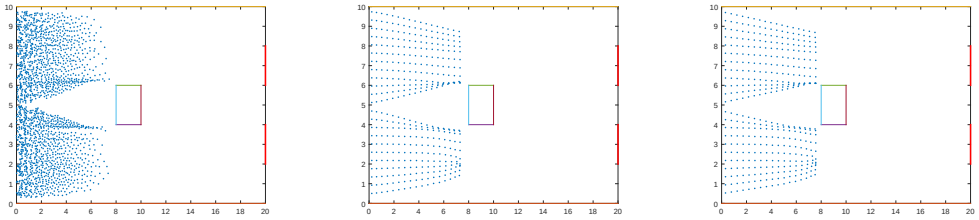

(a) Micro, $t = 5s$ (e) Hydro, $t = 5s$ (i) Scalar, $t = 5s$

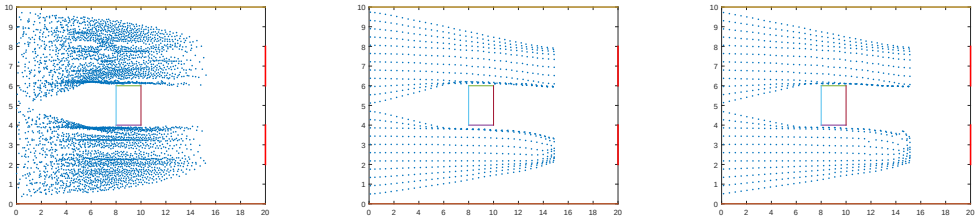

(b) Micro, $t = 10s$ (f) Hydro, $t = 10s$ (j) Scalar, $t = 10s$

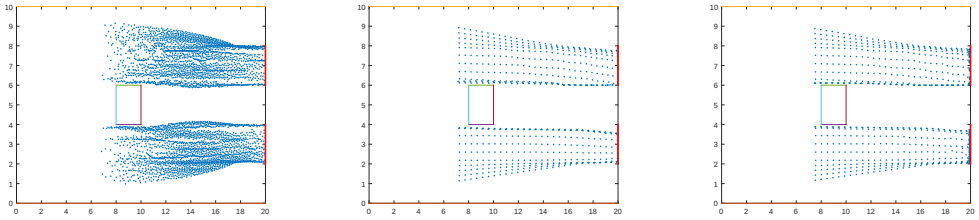

(c) Micro, $t = 15s$ (g) Hydro, $t = 15s$ (k) Scalar, $t = 15s$

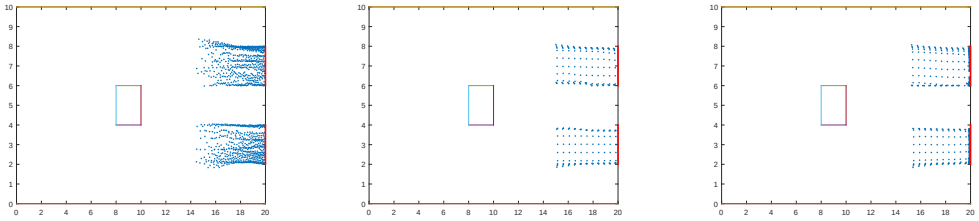

(d) Micro, $t = 20s$ (h) Hydro, $t = 20s$ (l) Scalar, $t = 20s$

Figure 2.7: Distribution of particles for microscopic ($N_{max} = 5$), hydrodynamic and scalar models at different times.

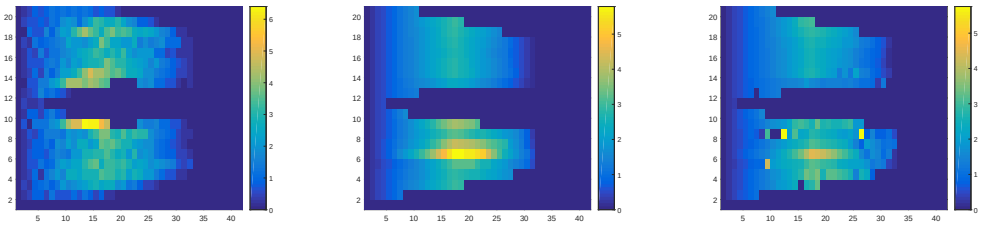

(a) Microscopic (b) Hydrodynamic (c) Scalar

Figure 2.8: Density of microscopic ($N_{max} = 5$), hydrodynamic and scalar models at $t = 10s$.

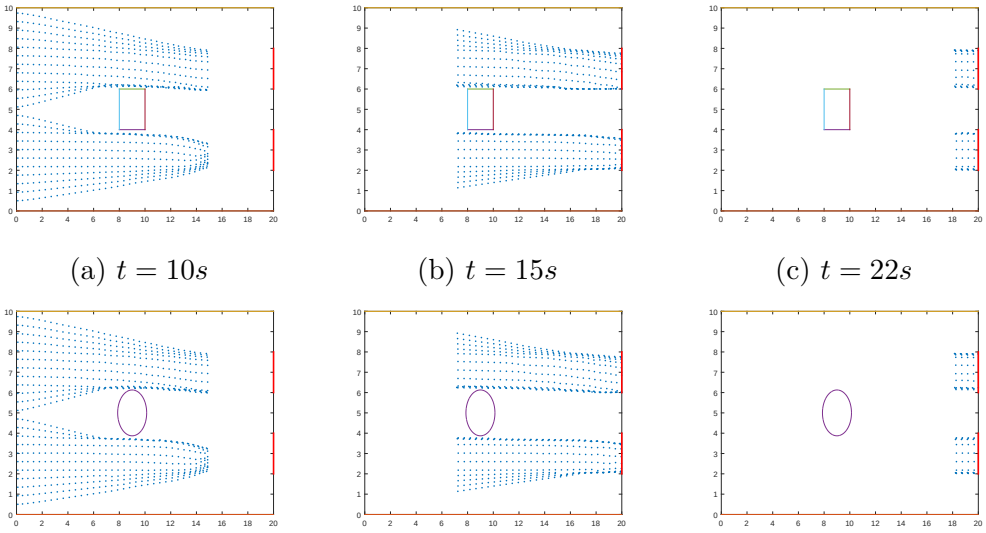

(a) $t = 10s$ (b) $t = 15s$ (c) $t = 22s$

(d) $t = 10s$ (e) $t = 15s$ (f) $t = 22s$

Figure 2.9: Comparison of rectangular and circular obstacles considering the hydrodynamic model at $t = 10s$, $t = 15s$ and $t = 22s$.

Bibliography

[1] K. Abe. Human science of panic. *Brain Pub. Co., Tokyo*, 1986.

[2] S. Ahmed, S. Bak, J. Mclaughlin, and D. Renzi. A third order accurate fast marching method for the eikonal equation in two dimensions. *Society for Industrial and Applied Mathematics.SIAM J. SCI. COMPUT, 33(5)*, pages 2402–2420, 2011.

[3] L.E. Aik and T.W. Choon. Simulating evacuations with obstacles using a modified dynamic cellular automata model. *Hindawi Publishing Corporation*, 2012.

[4] R. Alizadeh. A dynamic cellular automaton model for evacuation process with obstacles. *Safety Science 49*, pages 315–323, 2011.

[5] S.J. Alnasur. New models for crowd dynamics and control. *Virginia Polytechnic Institute and State University*, 2006.

[6] G. Antonini. A discrete choice modeling framework for pedestrian walking behavior with application to human tracking in video sequences. *PhD. Thesis*, 2005.

[7] G. Antonini, M. Bierlaire, and M. Weber. Discrete choice models of pedestrian walking behavior. *Transportation Research Part B 40*, pages 667–687, 2006.

[8] K.S. Babu and N. Srinivasacharyulu. Numerical study of convection-diffusion problem in two-dimensional space. *IJRRAS, 5(2)*, 2010.

[9] N. Bellomo and C. Dogbé. On the modelling crowd dynamics from scaling to hyperbolic macroscopic models. *Mathematical Models and Methods in Applied Sciences*, pages 1327–1345, 2008.

[10] C. Burstedde. Simulation of pedestrian dynamics using a two-dimensional cellular automaton. *Physica A: Statistical Mechanics and its Applications, 295(3-4)*, pages 507–525, 2001.

[11] C. Burstedde, A. Kirchner, K. Klauck, A. Schadschneider, and J. Zittartz. Cellular automaton approach to pedestrian dynamics - applications. *Pedestrian and Evacuation Dynamics (Springer 2001)*, page 87, 2001.

[12] S.C. Cao, W.G. Song, X.D. Liu, and N. Mu. Simulation of pedestrian evacuation in a room under fire emergency. *Procedia Engineering 71. Published by Elsevier Ltd.*, pages 403–409, 2014.

[13] J.A. Carrillo, M.R. D'Orsogna, and V. Panferov. Double milling in self-propelled swarms from kinetic theory. *Kinetic and related models 2*, pages 363–378, 2009.

[14] T.F. Chan. Stability analysis of finite difference schemes for the advection diffusion equation. *SIAM Journal of Numerical Analysis 21*, pages 272–283, 1984.

[15] J.K. Chen, J.E. Beraun, and T.C. Carney. A corrective smoothed particle method for boundary value problems in heat conduction. *Internat. J. Numer. Methods Engrg 46*, pages 231–252, 1999.

[16] Y. Chuang, M.R. DOrsogna, D. Marthaler, A.L. Bertozzi, and L.S. Chayes. State transitions and the continuum limit for a 2d interacting, self-propelled particle system. *Physica D 232*, pages 33–47, 2007.

[17] V. Coscia and C. Canavesio. First-order macroscopic modelling of human crowd dynamics. *Math. Mod. Meth. Appl. Sci. 18*, pages 1217–1247, 2008.

[18] M. Dehghan and R. Salehi. A boundary-only meshless method for numerical solution of the eikonal equation. *Comput. Mech*, pages 283–294, 2011.

[19] T. Deschamps and L.D. Cohen. Fast extraction of tubular and tree 3d surfaces with front propagation methods. *Pattern Recognition. 16th International Conference*, pages 731–734, 2002.

[20] C. Dogbe. On the modelling of crowd dynamics by generalized kinetic models. *J. Math. Anal. Appl. 387*, pages 512–532, 2012.

[21] F. Durupinar, N. Pelechano, J.M. Allbeck, U. Gudukbay, and N.I. Badler. How the ocean personality model affects the perception of crowds. *IEEE Computer Graphics Appl.*, pages 22–31, 2011.

[22] P.J. Erdelsky. A general theorem on dominant diagonal matrices. *Linear Algebra and Its Applications 1. American Elsevier Publishing Company, Inc.*, pages 203–209, 1968.

[23] G.B. Ermentrout and L. Edlestein-Keshet. Cellular automata approaches to biological modeling. *J. Theoret. Biol. 160*, pages 97–133, 1993.

[24] R. Etikyala. Pedestrian flow models. *PhD thesis, Technical University of Kaiserslautern*, page 53, 2014.

[25] Z. Fang, W. Song, J. Zhang, and H. Wu. Experiment and modeling of exit-selecting behaviors during a building evacuation. *Physica A 389*, pages 815–824, 2010.

[26] C.A.J. Fletcher. Computational techniques for fluid dynamics 1. *Springer*, 1990.

[27] G.E. Forsyth and W. R. Wasow. Finite difference methods for partial differential equations. *Wiley*, 1960.

[28] R.A. Gingold and J.J. Monaghan. Smoothed particle hydrodynamics: Theory and application to non-spherical stars. *Monthly Notices Roy. Astronom. Soc. 181*, pages 375–389, 1977.

[29] S. Göttlich, A. Klar, E. Ragavendar, and S. Tiwari. Particle methods for pedestrian flow models: from microscopic to non-local continuum models. *Math. Models Methods Appl. Sci. 24, 2503*, 2014.

[30] S. Göttlich, A. Klar, E. Ragavendar, and S. Tiwari. Complex material flow problems: a multi-scale model hierarchy and particle methods. *Engineering Mathematics, 92(1)*, pages 15–29, 2015.

[31] P.A. Gremaud and C.M. Kuster. Computational study of fast methods for the eikonal equation. *SIAM J. Sci. Comput., 27(6)*, pages 1803–1816, 2006.

[32] D. Helbing. A fluid-dynamic model for the movement of pedestrians. *Complex Systems. 6*, pages 391–415, 1992.

[33] D. Helbing, L. Buzna, A. Johansson, and T. Werner. Self-organized pedestrian crowd dynamics: Experiments, simulations, and design solutions. *Transportation Science*, pages 1–24, 2005.

[34] D. Helbing, I.J. Farkas, P. Molnár, and T. Vicsek. Simulation of pedestrian crowds in normal and evacuation situations. *Pedestrian and Evacuation Dynamics. Springer, Berlin, Germany*, pages 21–58, 2002.

[35] D. Helbing, I.J. Farkas, P. Molnár, and T. Vicsek. Simulation of pedestrian crowds in normal and evacuation situations. *Pedestrian and Evacuation Dynamics, Publisher: Springer, Editors*, pages 21–58, 2002.

[36] D. Helbing, I.J. Farkas, and T. Vicsek. Freezing by heating in a driven mesoscopic system. *Physical Rev. Lett. 84*, pages 1240–1243, 2000.

[37] D. Helbing and A. Johansson. Pedestrian, crowd, and evacuation dynamics. *Encyclopedia of Complexity and Systems Science 16*, pages 6476–6495, 2013.

[38] D. Helbing, A. Johansson, J. Mathiesen, M.H. Jensen, and Hansen A. Analytical approach to continuous and intermittent bottleneck flows. *Phys. Rev. Lett. 97, 168001*, 2006.

[39] D. Helbing and P. Molnár. A social force model for pedestrian dynamics. *Phys. Rev. E51*, pages 4282–4286, 1995.

[40] D. Helbing, P. Molnár, I.J. Farkas, and K. Bolay. Self-organizing pedestrian movement,. *Environment and Planning B28*, pages 361–383, 2001.

[41] D. Helbing and T. Vicsek. Simulating dynamical features of escape panic. *Macmillan Magazines Ltd. Nature*, 2000.

[42] S. Heliövaara. Computational models for human behavior in fire evacuations. *M.Sc. Thesis, Department of Engineering Physics and Mathematics, Helsinki University of Technology*, 2007.

[43] L.F. Henderson. On the fluid mechanic of human crowd motion. *Transp. Research 8*, pages 509–515, 1975.

[44] L. Huang, S.C. Wong, M. Zhang, C. Shu, and W.H.K. Lam. Revisiting hughes dynamic continuum model for pedestrian flow and the development of an efficient solution algorithm. *Transportation Research Part B 43*, pages 127–141, 2009.

[45] R.L. Hughes. A continuum theory for the flow of pedestrians. *Transportation Research Part B: Methodological, 36(6)*, pages 507–535, 2002.

[46] R.L. Hughes. The flow of human crowds. *Annu. Rev. Fluid Mech, 35*, pages 169–182, 2003.

[47] W.K. Jeong and R.T. Whitaker. A fast eikonal equation solver for parallel system. *SIAM conference on Computational Science and Engineering*, 2007.

[48] Y. Jiang and P. Zhang. Modeling and simulation of pedestrian flow through hydrodynamics. *Procedia Engineering 31*, pages 1039–1044, 2012.

[49] Y. Jiang, P. Zhangb, S.C. Wong, and R. Liu. A higher-order macroscopic model for pedestrian flows. *Physica A: Statistical Mechanics and its Applications, 389(21)*, pages 4623–4635, 2010.

[50] Monaghan J.J. Smoothed particle hydrodynamics. *Rep. Prog. Phys. 68*, pages 1703–1759, 2005.

[51] N.R. Johnson. Panic at the who concert stampede: An empirical assessment. *Social Problems, 34(4)*, pages 362–373, 1987.

[52] R. Kimmel and J.A. Sethian. Optimal algorithm for shape from shading and path planning. *Journal of Mathematical Imaging and Vision 14: Kluwer Academic Publishers. Manufactured in The Netherlands.*, pages 237–244, 2001.

[53] T. Kretz, A. Groess, S. Hengst, L. Kautzsch, A. Pohlmann, and P. Vortisch. Quickest paths in simulations of pedestrians. *Advances in Complex Systems 14(5)*, pages 733–759, 2011.

[54] J.C. Latombe. Robot motion planning. *The Springer International Series in Engineering and Computer Science, 124*, 1991.

[55] P.D. Lax and R.D. Richtmyer. Survey of the stability of linear finite difference equations. *Comm. Pure Appl. Math.9*, pages 267–293, 1956.

[56] P. Lino, G. Maione, and B. Maione. Modeling and simulation of crowd egress dynamics in a discrete event environment. *18th IEEE International Conference on Control Applications Part of 2009 IEEE Multiconference on Systems and Control Saint Petersburg, Russia*, 2009.

[57] M.B. Liu and G.R. Liu. Restoring particle consistency in smoothed particle hydrodynamics. *Applied numerical mathematics 56*, pages 19–36, 2006.

[58] L.B. Lucy. Numerical approach to testing the fission hypothesis. *Astronom. J. 82*, pages 1013–1024, 1977.

[59] S. Maerivoet and B.D. Moor. Cellular automatamodels of road traffic. *Physics Reports, 419(1)*, pages 1–64, 2005.

[60] I.M. Mitchellt and S. Sastry. Continuous path planning with multiple constraints. *Proceedings of the 42nd IEEE Conference on Decision and Control Maui, Hawaii USA*, 2003.

[61] R. Monneau. Introduction to the fast marching method. *https://hal.archives-ouvertes.fr/hal-00530910*, 2010.

[62] G.E. Mulholland. Smoke production and properties. *The SFPE Handbook of Fire Protection Engineering, second ed.*, pages 217–227, 1995.

[63] K. Nagel and M. Schreckenberg. A cellular automata model for freeway traffic. *J. Phys. I. 2(12)*, pages 2221–2229, 1992.

[64] A. Nakayama, K. Hasebe, and Y. Sugiyama. Instability of pedestrian flow and phase structure in two-dimensional optimal velocity model. *Phys. Rev. E.71. 036121*, 2005.

[65] A. Nakayama and Y. Sugiyama. Two-dimensional optimal velocity model for pedestrians and biological motion. *AIP Conference Proceedings, 661(1)*, page 107, 2003.

[66] J.V. Neumann and A.W. Burks. Theory of self-reproduction automata. *University of Illinois Press, Urbana*, 1966.

[67] K. Nishinari, A. Kirchner, A. Namazi, and A. Schadschneider. Extended floor field ca model for evacuation dynamics. *IEICE Transactions on Information and Systems E87d*, pages 726–732, 2001.

[68] C. Nitzsche. Cellular automata modeling for pedestrian dynamics. *Bachelor Thesis*, 2013.

[69] S. Okazaki. A study of simulation model for pedestrian movement with evacuation and queuing. *Part 1: Pedestrian Movement by the Application on of Magnetic Models. Trans. of A.I.J., 35(283)*, pages 111–119, 1979.

[70] F. Ozel. Time pressure and stress as a factor during emergency egress. *Safety Science, 38(2)*, pages 95–107, 2001.

[71] X. Pan. Computational modeling of human and social behaviors for emergency egress analysis. *Dissertation, Stanford University*, 2006.

[72] Y. Peizhong, W. Xin, and L. Tao. Agent-based simulation of fire emergency evacuation with fire and human interaction model. *Safety Science 49*, pages 1130–1141, 2011.

[73] Th. Robin, G. Antonini, M. Bierlaire, and J. Cruz. Specification, estimation and validation of a pedestrian walking behavior model. *Transportation Research Part B 43*, pages 36–56, 2009.

[74] E. Rouy and A. Tourin. A viscosity solutions approach to shape from shading. *SIAM J. NUMER. ANAL., 29(3)*, pages 867–884, 1992.

[75] A. Schadschneider, A. Kirchner, and K. Nishinari. Ca approach to collective phenomena in pedestrian dynamics. *The series lecture notes in computer science, 2493*, pages 239–248, 2002.

[76] A. Schadschneider, W. Klingsch, H. Klüpfel, T Kretz, C. Rogsch, and A. Seyfried. Evacuation dynamics: Empirical results, modeling and applications. *Encyclopedia of Complexity and System Science, B. Meyers (Ed.) (Springer, Berlin)*, 2008.

[77] J.A. Sethian. Advancing interfaces: Level set and fast marching methods. *Proceedings of the National Acadenamic of Sciences*, 1995.

[78] J.A. Sethian. A fast marching level set method for monotonically advancing fronts. *Proceedings of the National Acadenamic of Sciences*, 1995.

[79] J.A. Sethian. Fast marching methods. *University of California, Berkeley 94720*, 1998.

[80] J.A. Sethian. Fast marching methods and level set methods for propagating interfaces. *University of California, Berkeley 94720*, 1998.

[81] L. Shaobo, Y. Lizhong, F. Tingyong, and L. Jian. Evacuation from a classroom considering the occupant density around exits. *Physica A: Statistical Mechanics and its Applications, 388(9)*, pages 1921–1928, 2009.

[82] J.M. Stockie. The mathematics of atmospheric dispersion modelling. *Society for Industrial and Applied Mathematics, 53(2)*, pages 349–372, 2011.

[83] J.C Strikwerda. Finite difference schemes and partial differential equations (1st ed.). *Chapman & Hall, New York*, pages 26–222, 1989.

[84] P.C. Tissera, M. Printista, and M.L. Errecalde. Evacuation simulations using cellular automata. *JCS&T, 7(1)*, 2007.

[85] A. Turner. Analysing the visual dynamics of spatial morphology. *Environment and Planning B: Planning and Design, 30*, pages 657–676, 2003.

[86] A. Varas, M.D. Cornejoa, D. Mainemera, B. Toledob, J. Rogana, V. Munöza, and J.A. Valdiviaa. Cellular automaton model for evacuation process with obstacles. *Physica A: Statistical Mechanics and its Applications, 382(2)*, pages 631–642, 2007.

[87] F. Venuti, L. Bruno, and N. Bellomo. Crowd dynamics on a moving platform: Mathematical modelling and application to lively footbridges. *Mathematical and Computer Modelling 45*, pages 252–269, 2007.

[88] W.G. Weng, T. Chen, H.Y. Yuan, and W.C. Fan. Cellular automata simulation of pedestrian counter flow with different walk velocities. *Phys. Rev. E 74 036102*, 2006.

[89] S. Wolfram. Cellular automata fluids: basic theory. *J. Statist. Phys. 45*, pages 471–526, 1986.

[90] Z. Xiaoping, L. Wei, and G. Chao. Simulation of evacuation processes in a square with a partition wall using a cellular automaton model for pedestrian dynamics. *Physica A: Statistical Mechanics and its Applications, 389(11)*, pages 2177–2188, 2010.

[91] D. Xie, Z. Gao, X. Zhao, and D.Z. Wang. Agitated behavior and elastic characteristics of pedestrians in an alternative floor field model for pedestrian dynamics. *Physica A: Statistical Mechanics and its Applications, 391(7)*, pages 2390–2400, 2012.

[92] K. Yamamoto, S. Kokubo, and K. Nishinari. Simulation for pedestrian dynamics by real-coded cellular automata (rca). *Physica A: Statistical Mechanics and its Applications, 379(2)*, pages 654–660, 2007.

[93] L.Z. Yang, W.F. Fang, R. Huang, and Z.H. Deng. Occupant evacuation model based on cellular automata in fire. *Chinese Sci. Bull. 47(17)*, pages 1484–1488, 2002.

[94] G.R. Yong and H.H. Jun. Logit-based exit choice model of evacuation in rooms with internal obstacles and multiple exits. *Chin. Phys. B, 19(3)*, 2010.

[95] W. Yuan and K.H. Tan. An evacuation model using cellular automata. *Physica A: Statistical Mechanics and its Applications, 384(2)*, pages 549–566, 2007.

[96] W. Yuan and K.H. Tan. A model for simulation of crowd behaviour in the evacuation from a smoke-filled compartment. *Physica A: Statistical Mechanics and its Applications, 390(2324)*, pages 4210–4218, 2011.

[97] Z. Zainuddin and L.E. Aik. Intelligent exit-selection behaviors during a room evacuation. *CHIN. PHYS. LETT., 29(1)*, 2012.

[98] X. Zheng, T. Zhong, and M. Liu. Modeling crowd evacuation of a building based on seven methodological approaches. *Building and Environment, 44(3)*, pages 437–445, 2009.

[99] Y. Zheng, B. Jia, X. Li, H. Fei, and N. Zhu. Study of exit choice with fire based on cellular automaton. *The Seventh Advanced Forum on Transportation of China*, pages 103–107, 2011.

[100] Y. Zheng, B. Jia, X.G. Li, and N. Zhu. Evacuation dynamics with fire spreading based on cellular automaton. *Physica A: Statistical Mechanics and its Applications, 390(1819)*, pages 3147–3156, 2011.

[101] K. Zia and A. Ferscha. A simulation study of exit choice based on effective throughput of an exit area in a multi-exit evacuation situation. *2009 13th IEEE/ACM International Symposium on Distributed Simulation and Real Time Applications*, 2009.